Hochschule für Angewandte Wissenschaften Hamburg
Hamburg University of Applied Sciences

Diploma thesis

Department of Automotive and Aerospace Engineering

Development of a tool for preliminary calculations of performance and loads on a wind turbine rotor, and utilization of this tool to achieve a rotor-strength-optimized power curve

Rune Pedersen

27. June 2011

Hamburg University of Applied Sciences
Faculty of Engineering and Computer Science
Department of Automotive and Aerospace Engineering
Berliner Tor 9
20099 Hamburg
Germany

Author: Rune Pedersen
Date of submission: 27.06.2011

1. Examiner Prof. Dr. Martin Wagner
2. Examiner Prof. Dr. Detlef Schulze

Secrecy Agreement

This Diploma thesis, written within the Examination Regulations of Hamburg University of Applied Sciences, is not subject for secrecy, as no firm or company submits the theme.

Statement

I assure that I independently and without help have written this Diploma thesis, and that I have used the referred sources and tools only. Passages containing words or sense from other works have been made clear through indication of the sources.

…….....

Place, date, signature

HAW Hamburg
Faculty of Automotive and Aerospace Engineering
Berliner Tor 9
20099 Hamburg
Germany

Diploma thesis: Development of a tool for preliminary calculations of performance and loads on a wind turbine rotor, and utilization of this tool to achieve a rotor-strength-optimized power curve.

Date of submission: 27.06.2011

Author: Rune Pedersen
1. Examiner: Prof. Dr. Martin Wagner
2. Examiner Prof. Dr. Detlef Schulze

Abstract:

In a time where the wind turbine industry draws ever closer of reaching the goal of developing a floating offshore wind turbine, capable of operating far away from the coastline, new possibilities might open in terms of controlling the energy production of wind turbines.

Because of the absence of human presence at such a location, the current restrictions laid upon the industry to limit the implications on humans in the form of noise would most likely be revoked. This in turn would make it possible to develop new philosophies of mating rotor and generator, so that the higher wind speeds ranges could be exploited to a higher degree than today.

This work will investigate how much reserve of solidity an existing horizontal axis wind turbine rotor, equipped with an variable pitch system, has at wind speeds above its reference value.

To do this, a computational tool for calculating preliminary results of performance and loads on such a rotor will be developed, so that the results of different wind speeds and power settings can be compared to the results of the reference wind speed and power output.

Utilizing this tool, it will further be strived to develop an improved power curve, from an energy point of view, with the rotor strength as the limiting factor.

Table of contents

Table of Figures

Table Overview

Abbreviations:

AoA	Angle of Attack
BEM	Blade Element Momentum
CFD	Computational Fluid Dynamics
CoG	Center of Gravity
FMI	First Moment of Inertia
GW	Giga Watt
GWh	Giga Watt hours
HAWT	Horizontal Axis Wind Turbine
MW	Mega Watt
PMI	Product Moment of Inertia
SC	Shear Center
SMI	Second Moment of Inertia
VAWT	Vertical Axis Wind Turbine

Nomenclature

a	Speed of sound / Axial induction factor
a'	Angular induction factor
$a(r)$	Area of the airfoil, dependent on blade radius
$A(s)$	Area of the elapsed distance s
A	X-gradient of a linear function
A_0	Area value for the linear function
$A_{be,i}$	Area of a given blade element
$A_{blade,AE}$	Area of the inner part oft he blade
$A_{blade,HA}$	Area of the blade hub-attachment cross section
A_{FS}	Area of the front spar
A_{Fr}	Area of a part of the structure
A_{LF}	Area of the lower flange
A_{RS}	Area of the rear spar
A_{Rotor}	Rotor area
A_{Sum}	Overall Area of the walls of the torque box
$A_{Sum,X}$	Calculation value for the overall x-coordinate of the CoG
$A_{Sum,Z}$	Calculation value for the overall z-coordinate of the CoG
A_{TB}	Area of the torque box
A_{UF}	Area of the upper flange
$A_{x,LF}$	X-gradient of the linear function of the lower flange
$A_{x,UF}$	X-gradient of the linear function of the upper flange
α	Angle of attack
α_i	Initial AoA
$\alpha_{i,be1}$	Initial AoA for the 1st blade element for the 1st run
$\alpha_{be,max}$	AoA for the blade element with dT_{max}
β	Local relative airfoil flow angle
β_i	Initial relative flow angle
$\beta_{i,be1}$	β_i for the 1st blade element for the 1st run
$\beta_{be,max}$	Relative flow angle for the blade element with dT_{max}
β_{PG}	Correction factor according to the Prandl-Glauert-Rule
B	Number of blades / Y-gradient of a linear function

c	Local length of chord
$c\left(r_{S,AE}\right)$	Chord length at the first blade element t
$c\left(r_{Blade}\right)$	Chord length at the last blade element
$\Delta 0{,}5c_{TF}$	Deviation for the 0,5c point for $F_{thrust,bs}$
$\Delta 0{,}5c_{SF}$	Deviation for the 0,5c point for $F_{G,Shear,bs}$
$\Delta 0{,}5c_{x}$	Deviation for the 0,5 chord-line
C	Constant in a linear function
c_D	Local Drag coefficient
$c_{d,c}$=	Corrected drag coefficient
c_{FS}	Position of front spar along the chord line
c_{RS}	Position of rear spar along the chord line
c_{gen}	Constant for the load torque function
c_L	Local Lift coefficient
$c_{l,c}$ =	Corrected lift coefficient
c_m	Local Moment coefficient
$c_{m,c}$=	Corrected moment coefficient
C_P	Power coefficient
$C_{P,betz}$	Maximum Possible efficiency from Betz Theory
c_e	Chord-length near the end, before the elliptical drop
c_s	Chord-length at the beginning of the effective blade
$C_{x,LF}$	Constant of the linear function of the lower flange
$C_{x,UF}$	Constant of the linear function of the upper flange
d	The shortest distance between a point and a linear function
da	Area linearization factor
d_{FS}	Shortest distance between front spar and the overall CoG
d_{LF}	Shortest distance between l. flange and the overall CoG
d_{RS}	Shortest distance between rear spar and the overall CoG
d_{UF}	Shortest distance between u. flange and the overall CoG
dF_{thrust}	Blade element thrust force
$dF_{thrust,Aero}$	Local axial force from Blade Element Theory
$dF_{thrust,MT}$	Local axial force from Momentum Theory
dF_{torque}	Blade element torque force
$dM_{thrust,bs}$	Thrust moment integration value of a blade segment

$dM_{Torsion}$	Blade element torsional moment
dP	Local power
dr_{be}	Width of each blade element
$d_{SC,thrust}$	Arm from thrust force-line to SC
$d_{SC,torque}$	Arm from torque force-line to SC
$d_{SC,weight}$	Arm from weight force-line to SC
dT	Local angular torque
dT_{bs}	Torque integration value of a blade segment
dT_{Aero}	Local angular torque from Blade Element Theory
dT_{MT}	Local angular torque from Momentum Theory
ε_b	Bending strain
ε_t	Torsion strain
e_x	Distance between X_{TB} and the x-coordinate of the SC
EI	Blade bending rigidity
$f_A(r)$	Area of the inner part oft he blade
$f_{c1}(r)$	Function of constant chord length
$f_{c2}(r)$	Function of chord length at the blade tip
$f_{c,i}(r_{be,i})$	Chord-length of the applicable blade element
$F_{c,AP}$	Inertia force from the inner part oft he blade
F_{Drag}	Local drag force
F_{Lift}	Local lift force
F_{thrust}	Local thrust force
$F_{thrust,bs}$	Overall thrust force of a blade segment
F_{torque}	Local torque force
$F_{torque,bs}$	Overall torque force of a blade segment
E_k	Kinetic energy available to the rotor
F	Force
F_{cF}	Inertia force
$F_{cF,bs}$	Inertia force of a blade segment
$F_{G,Normal,bs}$	Normal force of a blade segment due to gravity
$F_{G,Shear,bs}$	Shear force of a blade segment due to gravity
F_{wt}	Actio/reactio force from the airstream
g	Coupling coefficient
γ	Pitch angle

γ_i	Initial pitch angle
$\gamma_{be,i}$	Pitch angle for a given blade element
γ_{be-1}	Pitch angle reached for the previous blade element
$\gamma_{i,be1}$	Initial pitch angle for the 1st blade element for the 1st run
$\gamma_{be,imax}$	Pitch angle for the blade element with dT_{max}
λ_r	Local tip speed ratio
ϕ	Rotor Blade angle in rotor plane
g	Gravitational acceleration = 9,81 m/s^2
h_{FS}	Height of front spar
h_{RS}	Height of rear spar
I_X	Total SMI with respect to the x-axis
$I_{X,FS}$	SMI of the front spar with respect to the x-axis
$I_{X,LF}$	SMI of the lower flange with respect to the x-axis
$I_{X,RS}$	SMI of the rear spar with respect to the x-axis
$I_{X,UF}$	SMI of the upper flange with respect to the x-axis
I_Z	Total SMI with respect to the z-axis
$I_{Z,FS}$	SMI of the front spar with respect to the z-axis
$I_{Z,LF}$	SMI of the lower flange with respect to the z-axis
$I_{Z,RS}$	SMI of the rear spar with respect to the z-axis
$I_{Z,UF}$	SMI of the upper flange with respect to the z-axis
kg	Kilogram
l	Total length of Torque Box wall being calculated
l_{LF}	Length of lower flange
l_{UF}	Length of upper flange
ω	Wake rotoational speed
Ω	Blade rotational speed
m	Meter / mass of the air
m_{bs}	Mass of a blade segment
m_{blade}	Total mass of the blade
m_{AE}	Mass of the aerodynamically effective part of the blade
m_{AP}	Mass of the aerodynamically passive part of the blade
$m_{r,AE}$	Mass of the effective part of the blade relative to total mass
$\dot{m}$	Massflow of the air
M	Mach number

M_b	Bending moment
M_t	Torsion moment
$M_{Torsion,bs}$	Torsional load from a blade segment
$M_{Torsion,SF}$	Torsion moment from shear forces
$M_{thrust,bs}$	Total moment from thrust of a blade segment
$M_{SF,bs}$	Shear force bending moment of a blade segment
M_X	Total bending moment about the x-axis
M_Z	Total bending moment about the z-axis
n	Total normal flow in the torque box
n_{BE}	Number of blade elements
n_{yx}	Normal flow in the torque box due to moments
n_{yz}	Normal flow in the torque box due to moments
n_{yy}	Normal flow in the torque box due to normal forces
N	Newton
η_{gear}	Gearbox efficiency
η_e	Generator efficiency
P	Power
P_e	Generator output power
P_{dr}	Submitted de-rated power from user
P_{gear}	Transmission output power
P_L	Power not captured by the wind turbine
P_O	Power output from the wind turbine rotor
P_T	Total available power to the rotor
P_{wt}	Extracted power from the wind turbine
p	Static pressure
p_1	Static pressure far upstream
p_2	Static pressure at rotor entry
p_3	Static pressure at rotor exit
p_4	Static pressure far downstream
q	Total shear flow in the torque box
q_0	Constant shear flow in a closed structural cell
q_1	Basic shear flow in the structure
q_s	Total shear flow due to shear force
q_T	Total shear flow due to torsion moment

Q_{Hub}	Loss due to proximity of hub
Q_{Tip}	loss due to proximity of blade tip
Q_{Total}	Total loss due to proximity of hub and blade tip
Q_X	Total shear force in the x-direction
Q_Z	Total shear force in the z-direction
r	Local blade radius
rev_{min}	Rotor revolutions
R	Specific gas constant for air, 287 [J/(kg*K)]
$r_{be,1}$	Radius to the middle of the first blade element
$r_{be,i}$	Radius to the middle of a random blade element
r_{be-1}	Radius to the middle of the previous blade element
r_{blade}	Blade radius
r_{bs}	Radius to the current blade section
$r_{cross,s}$	Radius of the circular part of the blade attached to the hub
$\overline{r}_{bs}$	CoG of a blade segment
$\overline{r}_{blade,AE}$	CoG of the aerodynamically effective blade
$\overline{r}_{AP}$	CoG of the inner part of the blade
r_E	Radius to the start of the tip geometry
$r_{r,E}$	Relative distance to the end of the constant chord
$r_{r,H}$	Relative distance to the start of the blade
r_H	Hub radius
$r_{r,S}$	Relative distance to the outer, active part of the blade
$r_{S,AE}$	Distance to the outer, active part of the blade
r_X	Radius to force outside the current blade element
s	Seconds / Variable for the FMI
s_{fs}	Position of the front spar relative to chord-length
s_{rs}	Position of the rear spar relative to chord-length
$S_X(s)$	FMI, parallel to the z-axis
$S_Z(s)$	First Moment of Inertia (FMI), parallel to the x-axis
t	Time / Thickness of the structure
t_{FS}	Thickness of the front spar
$t_{fs,max}$	Maximum thickness of the front spar
$t_{fs,min}$	Minimum thickness of the front spar
t_{LF}	Thickness of the lower flange

$t_{lf,max}$	Maximum thickness of the lower flange
$t_{lf,min}$	Minimum thickness of the lower flange
t_{RS}	Thickness of the rear spar
$t_{rs,max}$	Maximum thickness of the rear spar
$t_{rs,min}$	Minimum thickness of the rear spar
t_{UF}	Thickness of the upper flange
$t_{uf,max}$	Maximum thickness of the upper flange
$t_{uf,min}$	Minimum thickness of the upper flange
T	Orbital period / Total torsion moment
T_{load}	Torque from gears and generator
T_{Total}	Total torque of the rotor
v	Wind Speed
$v_{eq,fr}$	Equivalent full-rate wind speed
V_{AP}	Volume of the inner part of the blade
V_{AE}	Volume oft he outer part oft he blade
v_1	Undisturbed wind speed
v_2	Wind speed at rotor entry
v_3	Wind speed at rotor exit
v_4	Wind speed far down wind
v_r	Local resultant wind-speed
v_{wt}	Average wind speed in the rotor
x	X-value of the structure at the point being calculated
x_0	X-value of the starting point, with relation to X_{TB}
x_1	X-coordinate
Δx	Difference in x-value of the elapsed distance
$\bar{x}(s)$	CoG of the elapsed distance *s* in x-direction
x_r	X-Coordinate of the CoG to a part of the structure
z_0	Z-value of the starting point, with relation to Z_{TB}
Δz	Difference in z-value of the elapsed distance
$\bar{z}(s)$	CoG of the elapsed distance *s* in z-direction
z_r	Z-Coordinate of the CoG to a part of the structure
$x_{S,FS}$	X-value of the CoG of the front spar
$x_{S,LF}$	X-value of the CoG of the lower flange
$x_{S,RS}$	X-value of the CoG of the rear spar

X_{TB}	Overall x-coordinate of the torque box CoG
$x_{S,UF}$	X-value of the CoG of the upper flange
y_1	Y-coordinate
y_{LF}	Approximate function of lower flange
y_{UF}	Approximate function of upper flange
$\psi_{be,i}$	Twist angle for the current blade element
ψ_{i-1}	Twist angle for the previous blade element
$\psi_{be,imax}$	Twist with respect to “iMax_Position”
z	Z-value of the structure at the point being calculated
$z_{S,FS}$	Z-value of the CoG of the front spar
$z_{S,LF}$	Z-value of the CoG of the lower flange
$z_{S,RS}$	Z-value of the CoG of the rear spar
Z_{TB}	Overall z-coordinate of the torque box CoG
$z_{S,UF}$	Z-value of the CoG of the upper flange
ρ	Density of the air
ρ_{blade}	Overall density of the blade
$\rho_{blade,AE}$	Density of the aerodynamically effective blade
κ	Heat capacity ratio, 1,4 [-]
σ	Tension
$\sigma_{V,F}$	Change of shape hypothesis
$\sigma_{V,N}$	Normal stress hypothesis
$\sigma_{V,S}$	Shear stress hypothesis
σ_y	Overall normal stress
σ_{yz}	Normal stress in the torque box from moments
σ_{yx}	Normal stress in the torque box from moments
σ'	Local solidity
$\tau_{x,z}$	Overall shear stress

1 Introduction

1.1 The wind turbine industry

In a world with an ever increasing consume of energy, we face a challenging future to both meet this energy demand, and at the same time keep the environmental implications to a minimum. Through several incidents of extreme weather the latest years, and a quite dramatic global rise in temperature, have we been reminded of the grim consequences of the extensive use of fossil fuel as energy source. Although the absolute proof that these changes in climate are human caused has not yet been confirmed, more and more scientists and people in general supports this theory, and think we in any case need to think of new ways to create a sustainable way of living. This subject is one our times defining issues, and the solution of which is by many considered as crucial for the future of both the human race and the earth as a whole.

One of the most promising and also most technical mature solutions to our energy problem seems today to be the use of wind turbines to harvest the renewable, kinetic energy from the wind. Even though many people question the effectiveness of wind turbines and the costs associated with getting these operational, the international demand for reducing CO_2 emissions has led to about 175,000MW installed power in the form of wind turbines worldwide as of June 2010, and an impressive 1,900,000MW being estimated by 2020 [1]. The list over the 10 countries in the world with the most installed wind power are displayed in Figure 1.1, with the amount of actual installed capacity in MW as of June 2010:

Wind Power Worldwide June 2010

Position	Country	Total capacity June 2010 [MW]	Added capacity June 2010 [MW]	Total capacity end 2009 [MW]
1	USA	**36.300**	1.200	35.159
2	China	**33.800**	7.800	26.010
3	Germany	**26.400**	660	25.777
4	Spain	**19.500**	400	19.149
5	India	**12.100**	1.200	10.925
6	Italy	**5.300**	450	4.850
7	France	**5.000**	500	4.521
8	United Kingdom	**4.600**	500	4.092
9	Portugal	**3.800**	230	3.535
10	Denmark	**3.700**	190	3.497
	Rest of the World	**24.500**	2.870	21.698
Total		**175.000**	**16.000**	**159.213**

© WWEA 2010

Figure 1.1: Overview installed wind power worldwide, June 2010 [1]

These optimistic numbers are mainly based on the growth rates of annual installed MW of wind power the last years, as well as funding programs from the governments, but naturally has the technological development in the industry also been taken into consideration.

Although the knowledge and also actual deployment of wind mills and wind turbines as a source of mechanical and electrical power is several centuries old, it is first in the last few decades that this technology has become mature and effective enough to be an important contribution to the energy production industry. As some of the largest and most advanced wind turbine designs today clock in at power capacities in the 5 – 10 MW class, it is not only the cleanness of the technology which makes it interesting anymore, but because it has started to become a competitive part of the industry.

As a result of the increasing power output from new wind turbines, the cost per GWh is dropping. The oil prices on the other hand are steadily increasing due to increasing demand and drop in discoveries of new oilfields [2], which in turn have led to big investments in wind turbine projects across the globe – especially countries like China, Mexico and Brazil [3]. However, despite the increasing scarcity of oil due to higher consumptions of growing economies like China and India, the oil price has not yet risen as much as feared, and this continues to challenge the wind turbine producers and operators to convince the stakeholders of the potential in their projects.

1.2 Floating Offshore Wind Turbines

The next important milestone for the industry, which is anxiously awaited by governments and the whole energy sector, would be when a floating offshore wind turbine is available. This would open up the areas with the best possible conditions for wind energy production – the open oceans far off the coastline, where the wind speeds are stronger and more consistent. A bonus of such locations would also be that the conflict between the industry and the public, which today is one of the greatest issues when planning new wind turbine parks, practically would be eliminated.

Since the first offshore wind turbine became operational in Denmark in 1991, there was registered 2396 MW installed offshore wind power in Europe alone as of June 2010, with United Kingdom, Denmark and the Netherlands as the three leading countries [4]. Even though there are a few concepts for a fully floating wind turbine, and some promising pioneer projects are under testing at the time this work is written, all of the actual producing offshore wind turbines are mounted on towers, which are fixed to and supported by the seabed.

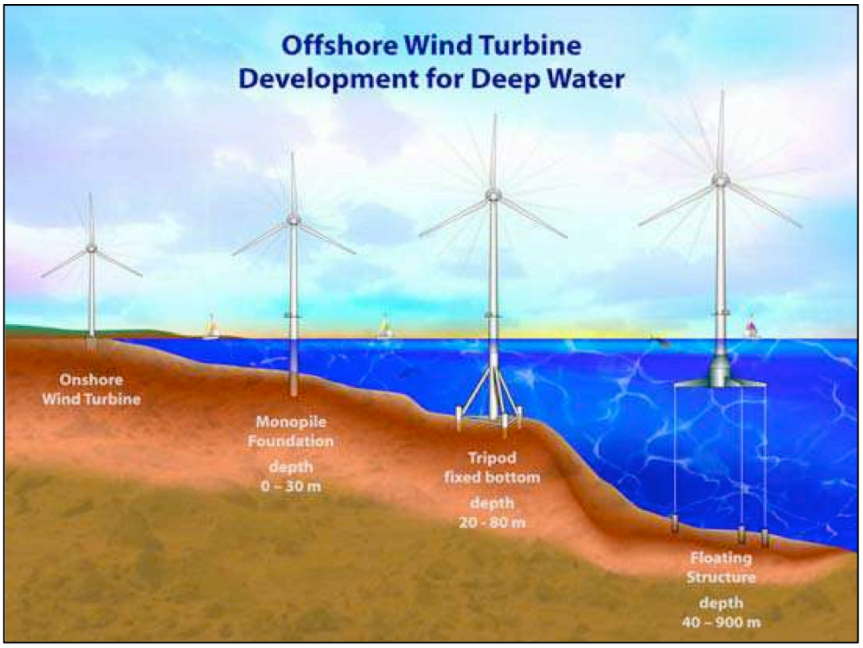

Figure 1.2: Onshore and Offshore Wind Turbine Tower Concepts [4]

Figure 1.2 shows that water depths up to 80m are the limit of today's operational technology. Even though this makes wind energy extraction possible in many suitable locations as e.g. the Skagerrak and North Sea, it is clear that it is first with the realization of the floating wind turbine that the full potential of wind turbines can be exploited.

The main reasons why still no finished solutions for a floating wind turbine is available, is the complexity of the system, and the funding needed to successfully execute and land such a comprehensive project. The combination of designing a floating structure robust enough to withstand the rough conditions of the windy waters of an ideal location, and to calculate the interactions of the dynamic loads from the sea and the wind, makes it a challenging piece of engineering.

One example of how much potential offshore wind energy could have, and also which expectations many experts place upon the technology, is a report from the Department of Interior in the U.S. dated April 2009. This states that the estimated recoverable energy potential in offshore wind power in the U.S. could be enough to cover the power consumption of as much as 53 million households (1000 – 1500TWh) [5].

1.3 Issues and Objectives

This work will look upon the potential to control the energy production of an offshore Horizontal Axis Wind Turbine (HAWT) equipped with a blade variable pitch system more favorably with respect to energy production, once the deep water floating wind turbine concept is a fact. More accurately will the wind speed range above the reference value be investigated, an area which today is flat rated for two reasons: The limitation of the generator, and to not exceed the legal noise levels which regulate the industry.

By writing a program, which can calculate preliminary results of power output from the rotor and loads on the blades at different wind speeds and efficiency settings, it is the goal to define a power curve limited only by the solidity of the rotor. The main objective is to prove that the rotors of existing wind turbines have the possibility to generate more power than the maximum output they produce today, without exceeding their limitations of solidity. In order to validate the theories and the results from the calculation program, the calculations will be executed for an existing example wind turbine, of which as much technical information as possible is to be obtained.

For such a power curve to actually be implemented into the industry, in addition to new regulations regarding the noise emitted by the rotor, also the philosophy of sizing a wind turbine system would have to be different than today. This will be investigated in this work, and the different aspects of the engineering in need of attention, highlighted.

2 Theory

2.1 Wind turbine types

As mentioned in the introduction, the actual calculations and investigations of this work will concentrate on HAWT's. However, a short introduction to the major types of wind turbines will be given.

All wind turbines function in the way that they extract the kinetic energy available in the wind and convert this to either mechanical or electrical power, and there are two main groups of layouts, which all types can be sorted in, even though some designs may be more of a combination of the two. These two groups are the already mentioned HAWT's, and Vertical Axis Wind Turbines (VAWT's).

2.1.1 Vertical Axis Wind Turbines (VAWT)

The VAWT has, as the name reveals, a vertical axis and they are actually the oldest subgroup of wind turbines [6]. The main advantages of these types are the simplicity of the axle, gearbox and generator arrangement and that they do not need a yaw system to turn into the wind. This is particularly favorable on days with frequent changes in wind directions, as no time is lost for the rotor to swivel.

The advantage of no need for yaw control is on the other hand also the main reason why the VAWT's cannot compete with modern HAWT's – as one half of the rotor at all times is turning in the opposite direction of the wind. This disadvantage has however been repressed in modern designs of VAWT's, as they not only function by the means of aerodynamic drag anymore, but also aerodynamic lift [6]. This is particularly prominent in the Darrieus-Rotor, which has a quite complex rotor shape, and still may have potential to be developed [6]. The advanced rotor of this design also increases the overall cost of the wind turbine, which therefore loses some of its initial advantage in simplicity to HAWT's.

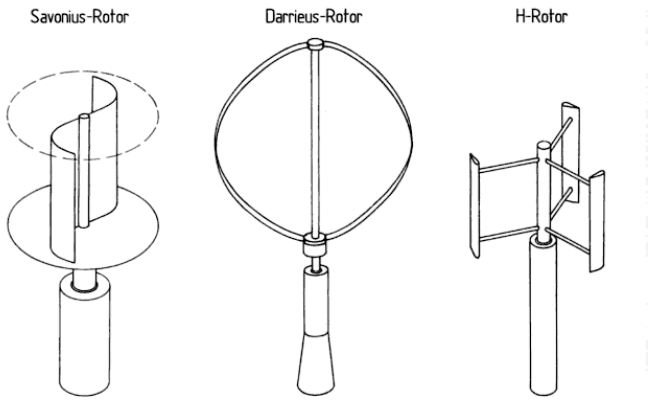

Figure 2.1: Main types of vertical axis wind turbines [6]

2.1.2 Horizontal Axis Wind Turbines (HAWT)

The HAWT consists typically of a vertical tower with the gears and generator sitting on top of the tower, and connected to the rotor through a horizontal axis. At the bottom of the tower is usually the electrical equipment for the interface with the electrical grid. With the rotor spinning in the vertical plane, the HAWT has not the disadvantage of spinning partly against the wind direction like the VAWT's. Uneven wind speeds over the rotor disc through the proximity to the tower and ground, however, causes this design to face operational cons with regards to efficiency and loads.

The HAWT is by far the most common type of wind turbines today. Many creative design proposals of HAWT and VAWT subgroups have been tested and investigated in the course of history, and most of them have had some theoretical advantages, which made them worth putting to the test. This evolutionary process has shown that the HAWT seems to be the design with the most potential, and which gives the most profit over time. Even though the costs of manufacturing and erecting a HAWT almost always are higher than the case is for a VAWT, the combination of power output and reliability has made the HAWT the preferred design.

One of the most difficult thresholds for the producers of wind turbines to overcome, when it comes to gain investments and acceptance in the power production industry, is to achieve a sheer power output that is interesting for investors and the public. As modern HAWT's most likely always will have a higher efficiency than VAWT's, because of the VAWT's natural need to turn against the wind, the HAWT's are the design that will be able to achieve the highest power production.

Figure 2.2: Offshore HAWT's [@consumerenergyreport.com]

When looking at large operational wind turbines connected to the public electricity net, one will further observe that the majority of these have 3 blades, as can be seen in Figure 2.2. The significance of the number of blades on a rotor will be explained in more detail later in connection with Figure 2.8, but one crucial reason for this is the reduced cyclic load on the rotor, rotor attachment and tower, due to the distribution of the blades over the disk. In difference to a 2- or 4-bladed rotor, the nature of the 3-bladed rotor eliminates the scenario of one blade passing through the top of the disk, where the wind is strongest, simultaneously as another passes the bottom, where the wind speed is lowest due to the proximity of the tower and the ground, and thus preventing a cyclic bending of the rotor axle. A graph of a similar phenomenon in the yaw-plane, the cyclic variation of the yaw moment for different numbers of blades, is shown in Figure 2.3. In this case, however, is the 4-bladed rotor the best performer, due to its symmetry. This is exactly because two of the rotor blades of the 4-bladed rotor are located in the 3 o'clock and 9 o'clock positions at the same time, and due to the same elevation of these two positions are the wind speed at these two positions typically the same.

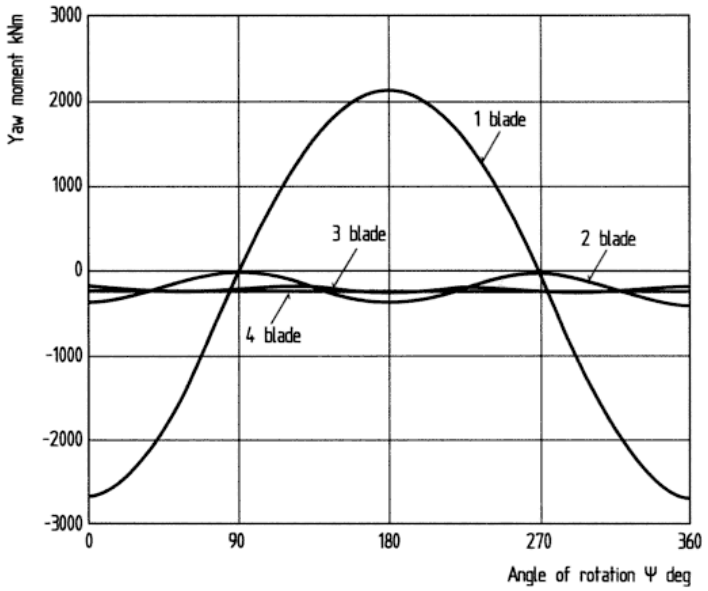

Figure 2.3: Cyclic yaw moment for different numbers of blades [6]

The most modern wind turbines of the 3-Bladed layout is actually not very far from reaching the absolute theoretical limit of energy extraction effectiveness from the wind, called the Betz Limit, which will be discussed later. Additionally, as the know-how regarding composite materials is making steady progress and enables ever-larger rotors to be built, both the increasing possible energy production of a wind turbine and the direct related sinking cost per GWh, turn more and more skeptics into believing in this technology.

2.2 Energy extraction

As mentioned under 2.1, the energy production of a wind turbine happens when the rotor captures the kinetic energy in the wind and converts it into another form of energy, which can be commercially utilized.

Here the theory of the energy extraction of the rotor will be shown. The next equations are derived from [6]:

Defining the Rotor Area:

$$A_{Rotor} = \pi r_{blade}^2 \quad \textbf{(2.1)}$$

A_{Rotor} Rotor area [m^2]

r_{blade} Blade radius [m]

The kinetic energy of the wind available to the rotor is:

$$E_k = \frac{1}{2} m v^2 \quad \textbf{(2.2)}$$

E_k Kinetic energy available to the rotor [J]

m Mass of the air [kg]

v Wind speed [m/s]

The total power available to the rotor can be expressed as:

$$P_T = \frac{E_k}{t} \quad \textbf{(2.3)}$$

P_T Total available power to the rotor [W]

t Time [s]

Or expressed with the massflow of the air:

$$\dot{m} = \rho A_{rotor} v \quad \textbf{(2.4)}$$

$\dot{m}$ Massflow of the air [kg/s]

ρ Density of the air [kg/m^3]

$$P_T = \frac{1}{2} \dot{m} v^2 \quad \textbf{(2.5)}$$

By combining (2.1), (2.4) and (2.5):

$$P_T = \frac{1}{2}\rho\pi r_{blade}^2 v^3 \quad \textbf{(2.6)}$$

An important observation of (2.6) is that the available power to the rotor grows with the cube of the wind speed, and the square of the blade radius, which underlines the importance of the location of the wind turbine, and the size of the rotor.

The wind turbine effectiveness is hence defined as:

$$C_P = \frac{P_O}{P_T} \quad \textbf{(2.7)}$$

C_P Power coefficient of the wind turbine rotor [-]

P_O Power output from the wind turbine rotor [MW]

Finally the power output from the rotor that is transmitted to the gear can be expressed as:

$$P_O = C_P P_T = C_P \frac{1}{2}\rho\pi r_{blade}^2 v^3 \quad \textbf{(2.8)}$$

2.2.1 Betz Limit – the theoretical limit of wind turbine effectiveness

As with all efficiencies, also the C_P value can initially by definition not be more than 1. According to the theory of Betz Limit however, it turns out that the best possible efficiency of wind turbines is considerably less than 1.

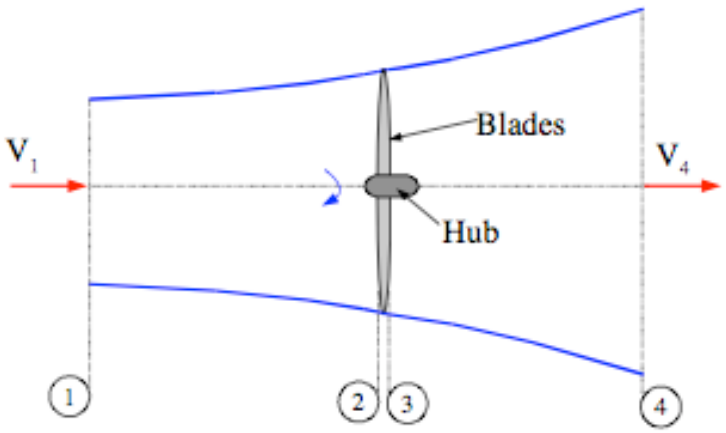

Figure 2.4: Control planes when calculating performance on a HAWT [7]

On the basis on Figure 2.4, the theory of Betz Limit can be derived as follows [8]:

$$P_O = P_T - P_L = \frac{1}{2}\dot{m}(v_2^2 - v_3^2) \quad \textbf{(2.9)}$$

P_L Power from P_T not captured by the wind turbine [MW]

Or expressed as the total force, F_{wt}, which act upon the wind turbine as a result of the incoming and the outgoing wind:

$$F_{wt} = \dot{m}(v_2 - v_3) \quad \textbf{(2.10)}$$

Knowing that power is force multiplied with velocity and by introducing a new variable, v_{wt}, for the wind velocity exactly at the wind turbine, between stations 2 and 3 in Figure 2.4, the power extracted by the wind turbine can be described as follows:

$$P_{wt} = v_{wt}F_{wt} = v_{wt}\dot{m}(v_2 - v_3) \quad \textbf{(2.11)}$$

P_{wt} Extracted power from the wind turbine [MW]

Now, as P_{wt} must be equal to P_O, it's possible to equate these, and solve for the unknown v_{wt}:

$$P_{wt} = P_O = \dot{m}v_{wt}(v_2 - v_3) = \frac{1}{2}\dot{m}(v_2^2 - v_3^2) \quad \textbf{(2.12)}$$

$$v_{wt} = \frac{1}{2}\frac{\dot{m}(v_2 - v_3)(v_2 + v_3)}{\dot{m}(v_2 - v_3)} = \frac{1}{2}(v_2 + v_3) \quad \textbf{(2.13)}$$

This shows that the wind speed exactly at the wind turbine is the geometrical average between the speeds at stations 2 and 3.

Using this, it is possible to expand on (2.9):

$$P_O = \frac{1}{2}\dot{m}(v_2^2 - v_3^2) = \frac{1}{2}\rho A_{rotor}v_{wt}(v_2^2 - v_3^2) = \frac{1}{4}\rho A_{rotor}(v_2 + v_3)(v_2^2 - v_3^2) \quad \textbf{(2.14)}$$

$$\mathrm{P_O} = \frac{1}{4}\rho \mathrm{A_{rotor}} \mathrm{v_2^3}\left(1 + \left(\frac{\mathrm{v_3}}{\mathrm{v_2}}\right) - \left(\frac{\mathrm{v_3}}{\mathrm{v_2}}\right)^2 - \left(\frac{\mathrm{v_3}}{\mathrm{v_2}}\right)^3\right) \quad \textbf{(2.15)}$$

By differentiation of (2.15) with respect to (v_3/v_2), and by equating this to nil, the max/min of (2.15) can be identified. The result is a function with (v_3/v_2) as the horizontal axis, and C_P as the vertical axis, where the maximum C_P value occurs by v_3/v_2=1/3 as shown in Figure 2.5:

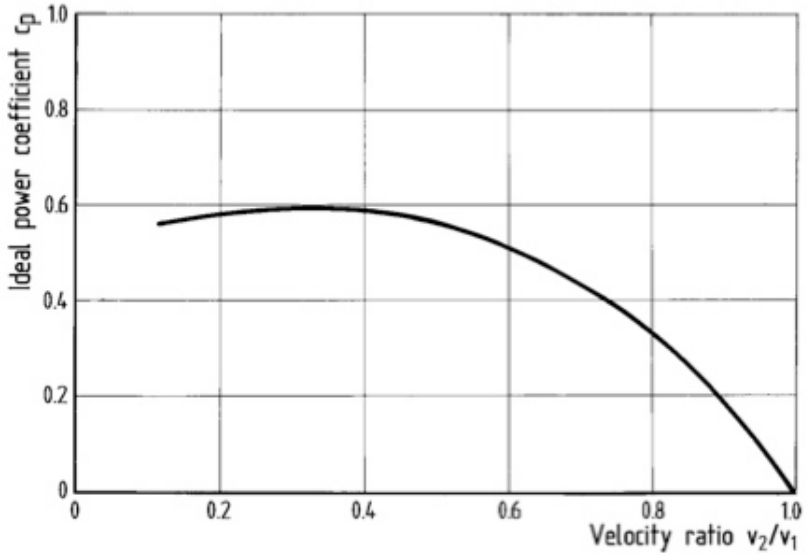

Figure 2.5: C_P over v_3/v_2 - the Theory of Betz Limit [6]

$$C_{P_{Betz}}\left(\frac{v_3}{v_2}=\frac{1}{3}\right)=\frac{16}{27}=0,593 \qquad \textbf{(2.16)}$$

$C_{P_{Betz}}$ The maximum possible C_P value according to Betz Limit

This maximum, called the Betz Limit, is not a thermodynamic limit, but a mechanical one [8]. As the most modern wind turbines today reach C_P values of more than 0,5, it is clear that the most potential in future designs probably lay in reaching the bests locations where strong, consistent wind is available, and to further develop the material technology which would allow ever bigger rotors to be built.

2.3 Blade Element Momentum Theory

To be able to analytically calculate the performance of a wind turbine rotor, it is necessary to have a way of transforming the complex aerodynamic processes that take place in conjunction with the energy extraction between the air and the rotor into a concrete and manageable set of mathematical equations. The most advanced and accurate way of doing this would be to create a 3d mesh of the rotor, and to simulate the airflow by using a Computational Fluid Dynamics (CFD) program. Such a program is however quite expensive, and also requires training to be operated correctly, and as this opportunity was not available to the author for this work, another solution had to be found.

Because of the high prices of obtaining license of CFD programs and the corresponding high performance computers, plus the extensive effort of training the employees to be able to use this software, this technology has not yet become the industry standard in the wind turbine industry in terms of actual application. There exists namely another method of calculating performance of wind turbine rotors, which by comparison to the CFD method is much less complicated, quicker and cheaper, and which also delivers quite accurate results – called the Blade Element Momentum Theory (BEM).

The BEM Theory is based upon the equation of two different approaches of calculating the results of the interaction between rotor and air. One of these, the Momentum Theory, describes the momentum balances of the airstream before and after the rotor. The other, the Blade Element Theory, calculates the forces generated due to lift and drag from the airfoil of the blades. The results are achieved by equating these two theories and iterative calculating new start values, which eventually approach the correct final values.

One of the theories, the Blade Element Theory, relies on two basic assumptions, which are simplifications compared to the real world: [7]

1. There are no aerodynamic interactions between the blade elements
2. The forces on the blade elements are solely determined by the lift and drag coefficients

Due to the simplicity of this theory, the results are by far not as rich and full as the case is with the CFD method, which delivers information regarding pressure distribution, local temperature and density etc.

The results of the BEM Theory only consist of information regarding the relevant angles and speeds of the blades and the wind, the lift and drag coefficients and finally the forces and moments, which act upon the rotor. This is however enough to perform a complete sizing of the rotor and coupled with a few corrections that have been developed over the years, leads to quite satisfying results.

The actual execution of this method is done by dividing the rotor blade into elements, and carrying out the calculating process for each element, applying the simplification that the speeds and angles induced by rotor and wind are

constant over each element. By calculating the relevant values for each element in one point in the middle of the element, and finally integrating over the whole blade, the resulting forces and moments are determined.

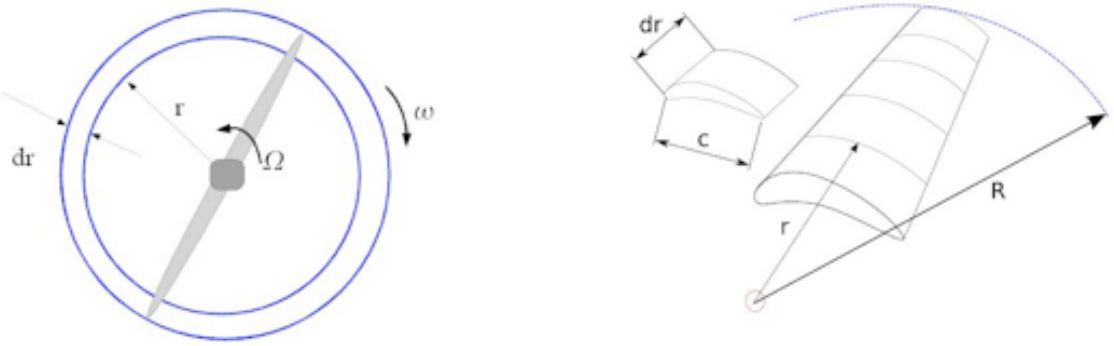

Figure 2.6: Details to the Blade Element Method [7]

The following equations and procedures explaining the BEM Theory are derived from [7]. The derivation will however not be shown in its entirety - for more details see Appendix A.

Referring to Figure 2.4 the following assumptions are made for the Momentum Theory:

$$v_2 = v_3 \tag{2.17}$$

And:

$$p_1 = p_4 \tag{2.18}$$

Further, the following definitions are utilized:

$$a = \frac{v_1 - v_2}{v_1} \tag{2.19}$$

a Axial induction factor [-]

And:

$$a' = \frac{\omega}{2\Omega} \tag{2.20}$$

a´ Angular induction factor [-]

ω Wake rotational speed [s^{-1}]

Ω Blade rotational speed [s^{-1}]

The blade rotational speed is further defined as:

$$\Omega = \frac{2\pi}{T} \tag{2.21}$$

T Orbital period [s]

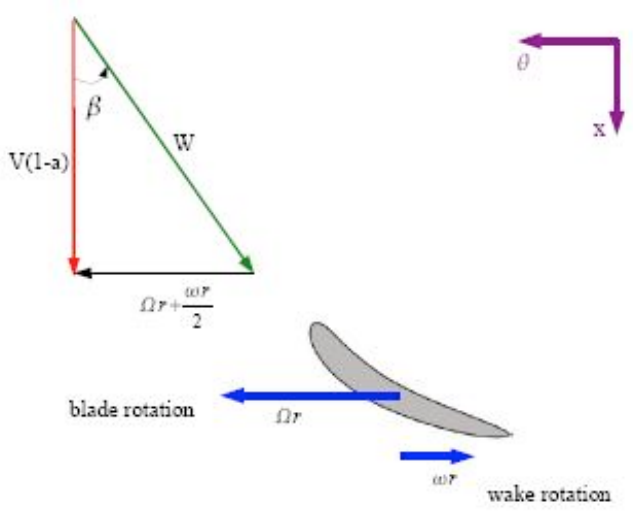

Figure 2.7: Resulting speeds and angles [7]

Out of this, the following relationships emerge:

$$dF_{Thrust,MT} = Q_{Total}\rho v_1^2\left[4a\left(1-a\right)\right]\pi r dr \tag{2.22}$$

$dF_{thrust,MT}$ Local axial force from Momentum Theory [N/m]

Q_{Total} Local total loss due to proximity of hub and tip [-]

r Local radius to hub [m]

$$dT_{MT} = Q_{Total}\rho v_1 4a'\left(1-a\right)\Omega r^3\pi dr \tag{2.23}$$

dT_{MT} Local angular torque from Momentum Theory [N]

$$dF_{Thrust,Aero} = \sigma'\pi\rho\frac{v_1^2\left(1-a\right)^2}{\cos^2\beta}\left(c_l\sin\beta + c_d\cos\beta\right)r dr \tag{2.24}$$

$dF_{thrust,Aero}$ Local axial force from Blade Element Theory [N/m]

β Local relative inflow angle [rad]

c_l Local lift coefficient [-]

c_d Local drag coefficient [-]

σ' Local solidity [-]

$$dT_{Aero} = \sigma' \pi \rho \frac{v_1^2 (1-a)^2}{\cos^2 \beta} \left(c_l \cos\beta - c_d \sin\beta \right) r^2 dr \quad \textbf{(2.25)}$$

dT_{Aero} Local angular torque from Blade Element Theory [N]

The local total loss, Q_{Total}, is defined as:

$$Q_{Total} = Q_{Hub} \cdot Q_{Tip} \quad \textbf{(2.26)}$$

Q_{Hub} and Q_{Tip} are further defined as:

$$Q_{Hub} = \frac{\pi}{2} \cos^{-1} \left[\exp^{\left\{ -1 \left(\frac{B/2[1-r_{r,S}/r]}{(r_{r,S}/r)\cos\beta} \right) \right\}} \right] \quad \textbf{(2.27)}$$

$r_{S,AE}$ Distance from the center of the rotor to the point where the aerodynamically active part of the blade starts.

$$Q_{Tip} = \frac{\pi}{2} \cos^{-1} \left[\exp^{\left\{ -1 \left(\frac{B/2[1-r/r_{Blade}]}{(r/r_{Blade})\cos\beta} \right) \right\}} \right] \quad \textbf{(2.28)}$$

These corrections to the original BEM Theory, which include the losses due to the proximity of the hub and the rotor at any given spot along the blade radius, are derived from the Prandl Theory [9]. The losses are added to the Momentum Theory, and can be compared to the effect of induced drag for an airplane. By applying these, the deficit from the Blade Element Theory, which assumes that there is no interaction between the blade elements, can be reduced.

The local solidity σ' is a dimension which at any given length along the blade radius describes how much of the disc´s circumference is occupied by the rotor. In this way, not only one blade is included in the calculations, but the whole rotor:

$$\sigma' = \frac{Bc}{2\pi r} \quad \textbf{(2.29)}$$

B Number of blades [-]

C Local length of chord [m]

Finally, the equations (2.21) and (2.23), as well as (2.22) and (2.24) can be equated, and the BEM Theory has been reduced into two equations:

$$\frac{a}{(1-a)} = \frac{\sigma'(c_l \sin\beta + c_d \cos\beta)}{4Q_{Total} \cos^2\beta} \quad \textbf{(2.30)}$$

$$\frac{a'}{(1-a)} = \frac{\sigma'(c_l \cos\beta - c_d \sin\beta)}{4Q_{Total}\lambda_r \cos^2\beta} \quad \textbf{(2.31)}$$

Hereby λ_r is the local tip-speed ratio, which describes the relationship between the local rotational speed and the wind speed:

$$\lambda_r = \frac{\Omega r}{v_1} \quad \textbf{(2.32)}$$

λ_r Local tip speed ratio [-]

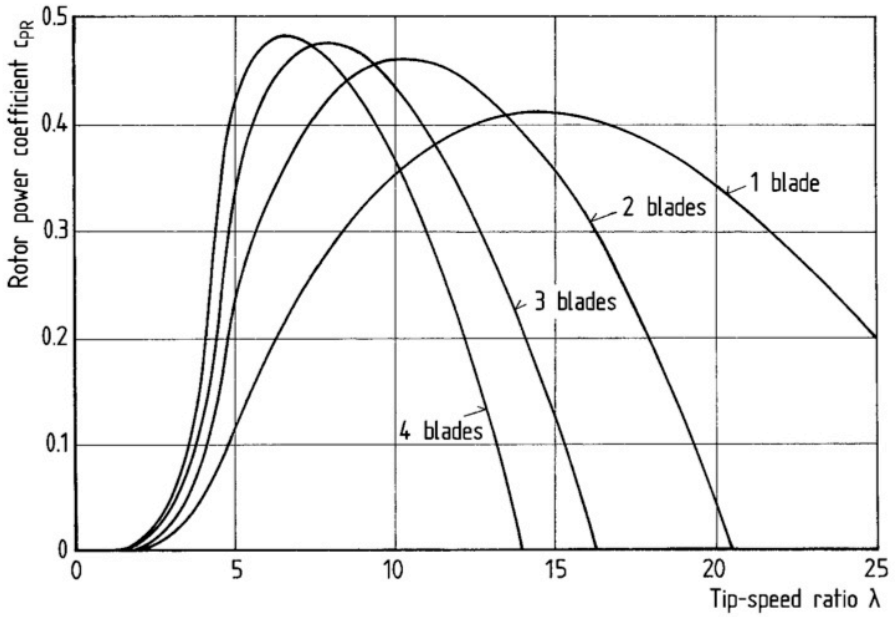

Figure 2.8: Connection between no. of blades, tip speed and efficiency [6]

Figure 2.8 displays the connection between the number of blades on the rotor, the tip speed ratio and the resulting efficiency for rotors with blades set at a fixed pitch. This underlines the importance of including these factors during the preliminary sizing of the wind turbine. It can here further be recognized that the optimum tip speed ratio drops with increasing numbers of blades. This explains why rotors equipped with many blades are better suited for installations where a lot of torque is needed, as e.g. water pumps, and why fewer blades are better when a faster rotation is wanted, as e.g. in electrical power production. Referring to (2.35), it is obvious that the torque *dT* must increase when Ω drops for a given value of *dP*. This fact is also the reason why rotors with many blades have a much better start-up torque than rotors with fewer blades, which means that they easier start turning and generating power.

2.3.1 Utilization of the BEM Theory results

Out of these results, which apply to one particular blade element, it is possible to calculate the overall results for the power output of the rotor when all of the blade elements have been determined. This is possible through numerical integration over the blade radius, and it is therefore obvious that the more blade elements the rotor blade is divided into, the more accurate will the results be. To determine how many blade elements to use, one has to weigh the need for accurate results up against the possibility of managing the amount of data, which is generated consequently.

The numerical integration can be carried out by the means of for example the Simpson´s Formula, or the Trapezoid Method [10].

$$\int_a^b f(x)dx \approx \left(y_0 + 4y_1 + 2y_2 + 4y_3 + ... + 2y_{n-2} + 4y_{n-1} + y_n\right)\frac{h}{3} \tag{2.33}$$

Simpson´s Formula

$$\int_a^b f(x)dx \approx \left(\frac{1}{2}y_0 + y_1 + y_2 + ... + y_{n-1} + \frac{1}{2}y_n\right)h \tag{2.34}$$

Trapezoid Method

Numeric integration is carried out extensively throughout this work, and out of these two alternatives, the Trapezoid Method has been chosen.

The power contribution of one rotor annulus is:

$$dP = \Omega dT \tag{2.35}$$

dT Local angular torque [N]

dP Local power [N/s]

On the basis of (2.34) the power output of the whole rotor can be described as follows:

$$P_0 = \int_{r_H}^{r_{blade}} dP\,dr = \int_{r_H}^{r_{blade}} \Omega\,dT\,dr \tag{2.36}$$

Out of the BEM calculations has now the road to one of the objectives for this work been explained – to calculate the power output from a given wind turbine. It will later be shown how these equations and methods are implemented to the calculation program.

2.4 The Power Curve

By repeating the BEM-Method iteration for a number of wind speeds, and for each of these producing a result for (2.35), one has the foundation to graphically represent the data as a function. This function is known as a power curve, and it is maybe the best and most concise way to describe the performance and operational wind speed range of the wind turbine.

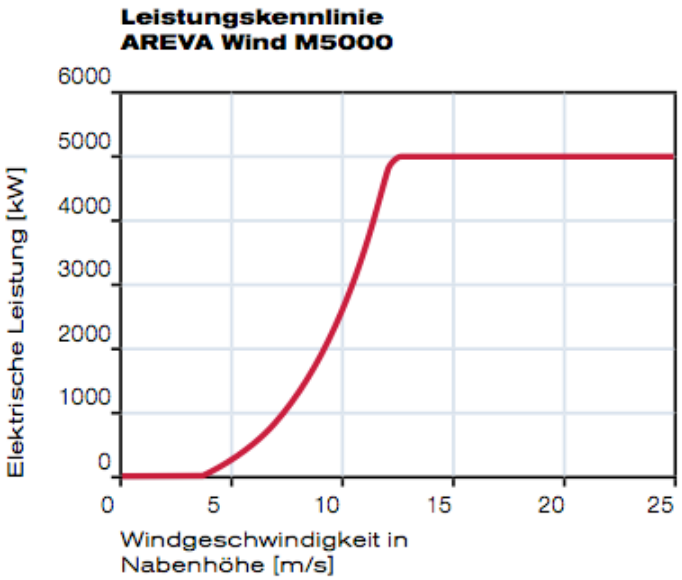

Figure 2.9: Example Power Curve [@areva-wind.com]

In Figure 2.9 it is easy to recognize the different areas of operation for this particular wind turbine: From 0m/s wind to about 4m/s there is no energy production, between 4m/s and up to about 12m/s there is a steep increase in power output, and over about 12m/s to the maximum operational wind speed the output from the wind turbine is flat-rated. Whereas the C_P value is kept at maximum by the variable pitch system in the area of the exponential growth of power production, the C_P value is rapidly decreasing in the flat-rated area, due to the dramatic increase in available kinetic energy in the wind. This constant power output is governed by the variable pitch system, which turns the blades more unfavorably as the wind increases.

The transition between the exponential curve and the flat-rated line is the design point for the wind turbine, where it is designed to operate optimally. This is a typical power curve for a wind turbine equipped with a variable pitch system, and as mentioned in the introduction, the sort of power curve this work aims to improve in the flat-rated area.

2.5 Theory for structural calculations

2.5.1 Definitions and equations to the rotor blade load calculations

Before starting to define the load cases and corresponding equations, the geometry and layout of a rotor blade segment and its construction will be represented more thoroughly:

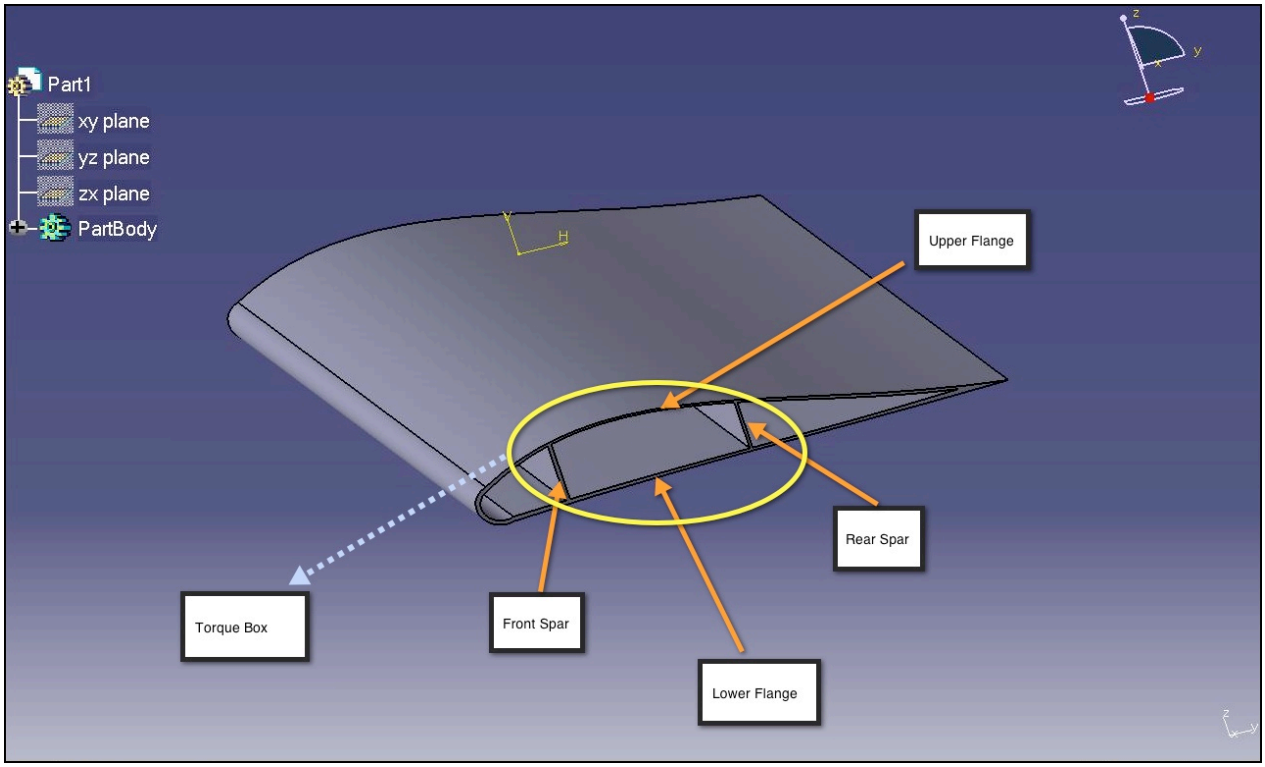

Figure 2.10: Torque Box of the Rotor Blade

Referring to Figure 2.10, it is evident that the construction of the rotor blade in this work is based upon the construction manner that is the standard in the aircraft industry for aircraft wings. This structure is based upon the fact that the upper and lower flanges together with the two vertical beams, the front and rear spars, form the load bearing element in an airfoil – the torque box. Not all wind turbine rotor blades apply to this type of construction, but as the torque box can be simplified to that of an unsymmetrical rectangle without too much inaccuracy, this makes it less complicated to calculate the loads on the airfoil than if the more complex front and rear parts had been considered as loadbearing.

The calculations in this work are done at each blade element, which in turn is strained by the forces and loads generated by the rest of the blade located outside, or further away from the hub. In this way the current blade element is considered a fixed bearing that has to absorb all of the loads from the part of

the blade located in the direction of the tip, relative to the blade element. The loadings on a blade element, with all the primary load sources that are taken into account in this work, are shown in Figure 2.11.

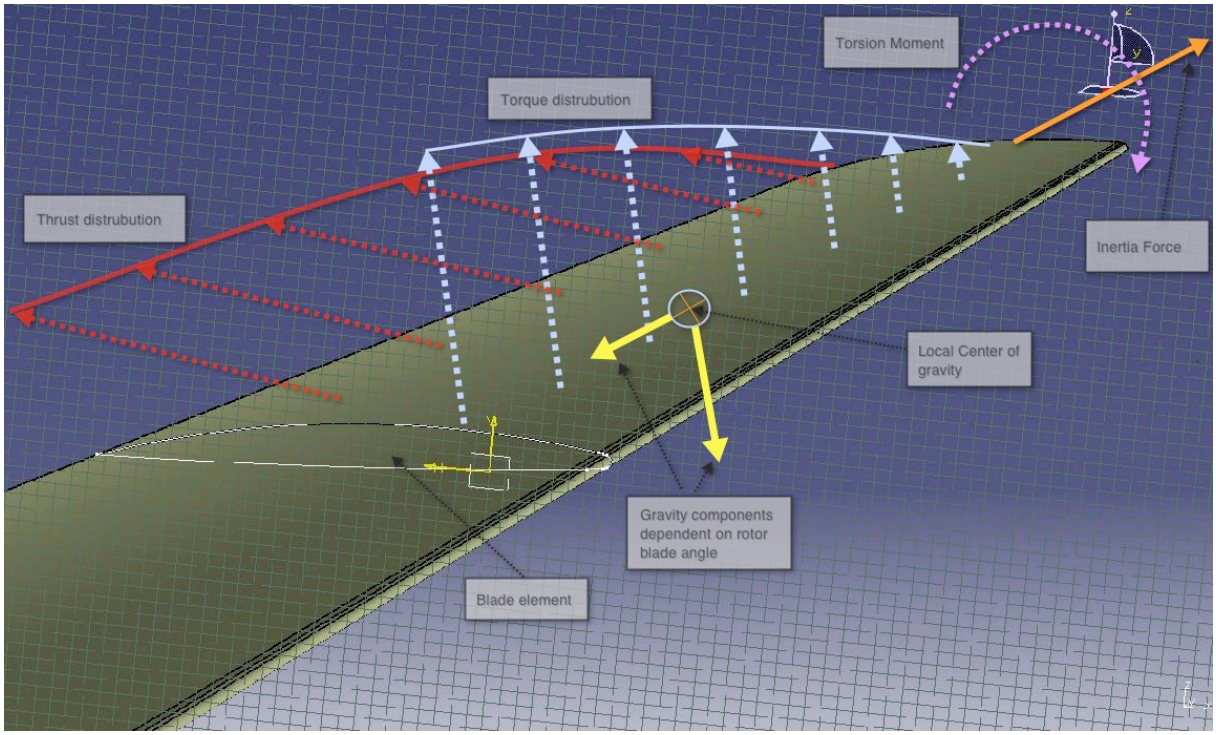

Figure 2.11: Loading on a blade element

2.5.2 Load cases for the wind turbine rotor

The wind turbine rotor is a highly complex part, which obviously is crucial for the success of the whole wind turbine. On the one hand it should be as light and aerodynamically effective as possible to achieve the wanted power output as affordable as possible. On the other hand however, it also has to be robust and able to withstand all of the strain it will face during its operational life. These two requirements are difficult to combine, and compromises have to be made as a result. The desire to keep these compromises as minor as possible and thusly design ever more effective rotors is the reason for the wind turbine industry´s dependence on further research and development in the field of material technology.

As Figure 2.11 shows, there are several overlapping loads which together result in the combined strain on a rotor blade. Each of these load cases will now be introduced and discussed.

2.5.2.1 Loads due to Gravity

As the rotor turns, the constant gravitational pull on the blades causes a cyclic load on them. While a blade at the twelve o'clock position is strained by the gravitation as a compressing load, a blade in the opposite six o'clock position is being stretched, and "feels" a tensional stress act upon it. In the three- and nine o'clock positions, the loads from the gravitational pull are pure shear forces, which strain the blades as tangential forces and bending moments. Anywhere between these four mentioned positions, the loads from gravitation are combinations of tensional/compressional stress and shear stress plus bending moments. These relationships can be expressed as follows:

Normal force of a blade segment:

$$F_{G,Normal,bs} = -m_{bs} g \cdot \cos\phi \tag{2.37}$$

$F_{G,Normal,bs}$ Normal force of a blade segment due to gravity [N]

m_{bs} Mass of the blade segment located in the direction of the tip, relative to the current blade element [kg]

ϕ Current blade angle in the rotation plane [rad]

Shear force of a blade segment:

$$F_{G,Shear,bs} = m_{bs} g \cdot \sin\phi \tag{2.38}$$

$F_{G,Shear,bs}$ Shear force of a blade segment due to gravity [N]

The rotor blade`s position in the rotor disc, ϕ, is defined as 0 at the twelve o'clock position, and moving positively in the clockwise direction when looking at the rotor from the downwind position. The gravity force, m_{bs} *x* g, is being calculated by integration of the area of the blade elements along the blade radius, and assuming that the density of the blade is constant [11]:

$$m_{bs} = \rho_{blade} \int_{r_{bs}}^{r_{blade}} a(r)\, dr \tag{2.39}$$

ρ_{blade} Overall density of the blade [kg/m^3]

r_{bs} Radius to the current blade section [m]

$a(r)$ Area of the airfoil, dependent on blade radius [m^2]

Further, the local center of gravity has to be determined, to be able to calculate the moment acting upon the blade element due to the shear force component of the blade segment weight. This is done in the following manner [11]:

$$\overline{r}_{bs} = \frac{\int_{r_{bs}}^{r_{blade}} a(r) \cdot r \, dr}{\int_{r_{bs}}^{r_{blade}} a(r) \, dr} \tag{2.40}$$

$\overline{r}_{bs}$ Center of gravity of the blade segment located in the direction of the tip, relative to the current blade element [m]

The moment on the blade element created by the shear force from the weight of the blade segment can consequently be calculated as follows:

$$M_{SF,bs} = F_{G_{Shear,bs}} \cdot \overline{r}_{bs} = \rho_{blade} \int_{r_{bs}}^{r_{blade}} a(r) dr \cdot g \cdot \sin\phi \cdot \left[\frac{\int_{r_{bs}}^{r_{blade}} a(r) \cdot r \, dr}{\int_{r_{bs}}^{r_{blade}} a(r) \, dr} \right] \tag{2.41}$$

$M_{SF,bs}$ Shear force bending moment of a blade segment [Nm]

2.5.2.2 Loads due to Inertia

As a result of the circular path of the blade, a centripetal force is created. This force is not influenced by the position of the blade in the rotor disc, when factors such as the proximity of the tower and the ground are omitted. The inertia force can therefore be considered as only dependent on the angular velocity. The general definition of a centripetal force is [11]:

$$F_{cF} = \frac{mv^2}{r} \tag{2.42}$$

F_{cF} Inertia force [N]

And by replacing the linear velocity, v, with the angular velocity, Ω:

$$F_{cF} = mr\Omega^2 \tag{2.43}$$

The approach to calculate the centripetal force is the same as described above, through integration of the results of each blade element, and by utilizing the derivations under the gravitational loads:

$$F_{cF,bs} = m_{bs} \cdot \overline{r}_{bs} \cdot \Omega^2 = \rho_{blade} \int_{r_{bs}}^{r_{blade}} a(r)\,dr \cdot \left[\frac{\int_{r_{bs}}^{r_{blade}} a(r) \cdot r\,dr}{\int_{r_{bs}}^{r_{blade}} a(r)\,dr} \right] \cdot \Omega^2 \qquad \textbf{(2.44)}$$

$F_{cF,bs}$ Centripetal force of the blade segment [N]

This centripetal force induces a pure normal force on the blade elements, which in turn strain the torque box as tensional stress.

2.5.2.3 Loads due to Torque

The loads on the rotor blades that occur due to torque are the only loads that originate from the wanted, beneficial utilization of the wind turbine. Because the torque is defined as the moment that drives the rotor to feed the generator, it works in the rotor plane. The resulting torque is influenced by both of the two main aerodynamic effects on an airfoil in a flow – lift and drag.

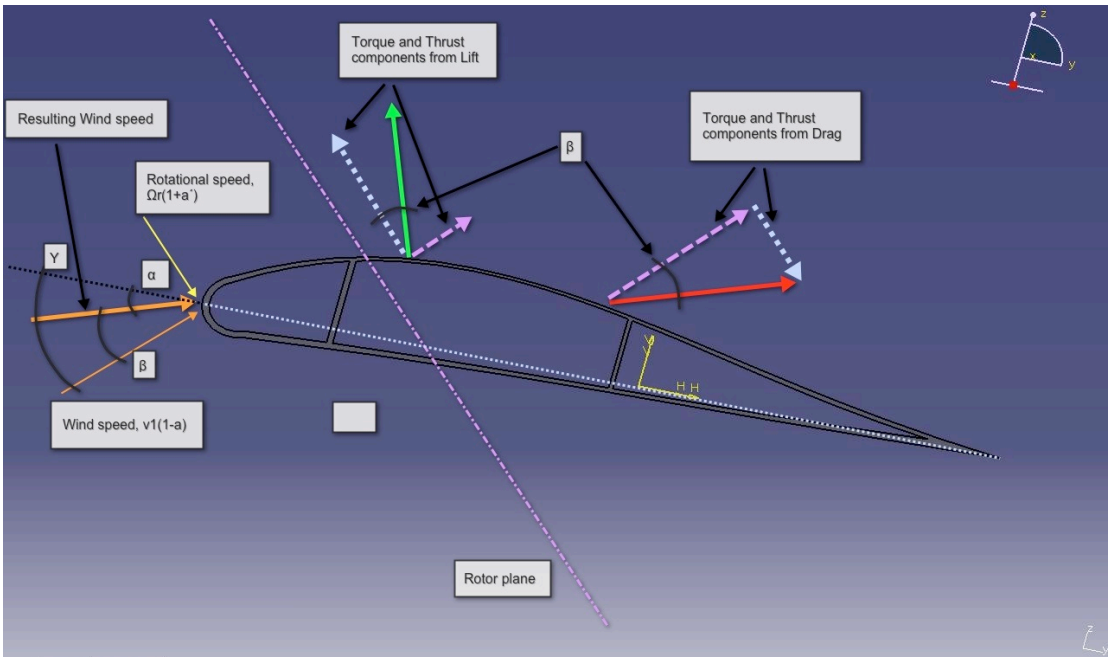

Figure 2.12: Torque and Thrust derived from Lift and Drag

Referring to Figure 2.12, it is evident that the resulting torque is influenced positively from the lift, and negatively from the drag of the airfoil. The angles shown in Figure 2.12 can be listed as follows [7]:

α Angle of attack (AoA)

β Relative flow angle

γ Pitch angle

Expressed as equations, the torque is defined as:

$$F_{torque} = F_{Lift}\cos(\beta) - F_{Drag}\sin(\beta) \quad \textbf{(2.45)}$$

F_{torque} Local torque force [N]

F_{Lift} Local lift force [N]

F_{Drag} Local drag force [N]

In the calculation program, the torque force is calculated in the BEM iteration as a variation of (2.25):

$$dF_{torque} = \frac{dT_{Aero}}{B \cdot r} = \sigma' \pi \rho \frac{v_1^2 (1-a)^2}{B \cdot \cos^2 \beta}\left(c_l \cos\beta - c_d \sin\beta\right) r\,dr \quad \textbf{(2.46)}$$

dF_{torque} Blade element torque force [N/m]

When considering a particular blade element in the same manner as under the gravitational and inertial loads, the loads from torque from the blade segment located in the direction of the tip relative to the blade element strain the blade element as a shear force and a bending moment:

$$F_{torque,bs} = \int_{r_{bs}}^{r_{blade}} dF_{torque}\,dr \quad \textbf{(2.47)}$$

$F_{torque,bs}$ Overall torque force of a blade segment [N]

To be able to calculate the correct moment from the torque on any given section of the blade, the torque values from the BEM iteration, dT_{MT} and dT_{Aero}, cannot simply be applied, as these refer to the rotor hub. The most transparent way of calculating this is to use the values for dF_{torque}, and to include the distance from the current blade element to the blade section in the integration procedure. When using the Trapezoid Method as described in (2.34), this can be executed in the following manner [11]:

$$dT_{bs} = \int_{r_{bs}}^{r_{blade}} dF_{torque} \cdot \frac{(r - r_{bs})}{(r_{blade} - r_{bs})}\,dr \quad \textbf{(2.48)}$$

dT_{bs} Torque integration value of a blade segment [N]

Now, by multiplying dT_{bs} with the width of the blade segment, the total torque of a blade segment relative to a given blade section can be determined:

$$T_{bs} = dT_{bs}(r_{blade} - r_{bs}) \quad \textbf{(2.49)}$$

T_{bs} Total torque of a blade segment on a blade section [Nm]

Note: Both $F_{torque,bs}$ and dT_{bs} could have been calculated by the use of dT_{MT} instead of dT_{Aero} , as these have reached the same value through the BEM iteration.

2.5.2.4 Loads due to Thrust

The loads from the thrust of a blade segment on a blade section can directly be compared to the loads from the torque, only that the thrust is located in the perpendicular plane to that of the torque. The thrust also originates from lift and drag, and strain a given blade section as a shear force and a bending moment.

Referring to Figure 2.12, the definition of the shear force derived from lift and drag is:

$$F_{thrust} = F_{Lift}\sin(\beta) + F_{Drag}\cos(\beta) \quad \textbf{(2.50)}$$

F_{thrust} Local thrust force [N]

From the BEM iteration, (2.24) can be used, slightly modified to be applicable for one blade:

$$dF_{thrust} = \frac{dF_{thrust,Aero}}{B}\sigma'\pi\rho\frac{v_1^2\left(1-a\right)^2}{B\cdot\cos^2\beta}\left(c_l\sin\beta + c_d\cos\beta\right)rdr \quad \textbf{(2.51)}$$

dF_{thrust} Blade element thrust force [N/m]

Analogue to (2.47), also the overall thrust force on a blade section from the outside located blade segment can be gained through integration:

$$F_{thrust,bs} = \int_{r_{bs}}^{r_{blade}} dF_{thrust}\,dr \quad \textbf{(2.52)}$$

$F_{thrust,bs}$ Overall thrust force of a blade segment [N]

The bending moment is calculated in the same manner as in (2.48), which allows the effective arm of the torque force of a blade segment in reference to the corresponding blade section to be included:

$$dM_{thrust,bs} = \int_{r_{bs}}^{r_{blade}} dF_{thrust} \cdot \frac{\left(r - r_{bs}\right)}{\left(r_{blade} - r_{bs}\right)} dr \quad \textbf{(2.53)}$$

$dM_{thrust,bs}$ Thrust bending moment integration value of a blade segment [N]

The bending moment around a given blade section can further be described as:

$$M_{thrust,bs} = dM_{thrust,bs}(r_{blade} - r_{bs}) \quad \textbf{(2.54)}$$

$M_{thrust,bs}$ Total moment from thrust of a blade segment on a blade section [Nm]

2.5.2.5 Loads due to Torsion

The last of the primary loads on a wind turbine rotor is caused by the twisting of the blade, which originates in the aerodynamic properties of the airfoil in question, as e.g. center of pressure and geometry. Similar to inertia, and in difference to the loads from thrust and torque, the torsional load is originally not included in the BEM iteration, and is calculated by including the moment coefficient, and using the values a, and a' to calculate the resulting flow velocity onto the respective blade element. This is done directly comparable to calculations for an aircraft wing, and the results from the BEM iteration do therefore not have to be divided by the number of blades of the rotor, as the equations already are configured for a blade.

The torsional moment around the quarter-line of the profile due to c_m is [12]:

$$dM_{Torsion} = c_m \frac{\rho}{2} v_r^2 c^2 \quad \textbf{(2.55)}$$

$dM_{Torsion}$ Blade element torsional moment [N]

c_m Blade element torsion coefficient [-]

v_r Local resultant wind-speed [m/s]

The local resultant wind-speed v_r is further calculated as follows:

$$v_r = \sqrt{\left(\left(v_1\left(1-a\right)\right)^2 + \left(\Omega r\left(1+a'\right)\right)^2\right)} \quad \textbf{(2.56)}$$

To calculate the overall torsional strain on a blade element from a blade segment, the blade element values are integrated over the blade radius in the applicable area:

$$M_{Torsion,bs} = \int_{r_{bs}}^{r_{blade}} dM_{Torsion}\, dr \quad \textbf{(2.57)}$$

$M_{Torsion,bs}$ Torsional load from a blade segment [Nm]

Additional torsion occurs if the resulting shear forces of the applicable blade segment do not have their force lines through the Shear Center (SC) of the torque box at the blade section to be calculated. If this is the case for all of the three shear forces included in this work, the additional torsion moment sums up as follows – without yet knowing the index for each of the forces:

$$M_{Torsion,SF} = \pm F_{torque,bs} \cdot d_{SC,torque} \pm F_{thrust,bs} \cdot d_{SC,thrust} \pm F_{G,Shear,bs} \cdot d_{SC,weight} \quad \textbf{(2.58)}$$

$M_{Torsion,SF}$	Torsion moment from shear forces [Nmm]
$d_{SC,torque}$	Arm from torque force-line to SC [mm]
$d_{SC,thrust}$	Arm from thrust force-line to SC [mm]
$d_{SC,weight}$	Arm from weight force-line to SC [mm]

2.5.3 Resulting Loads

Now, as the Loads on the wind turbine rotor and the blades have been identified following the BEM iteration, the rotational speed and the aerodynamic properties of the airfoil, the overall mechanical strain on the rotor blades can be studied on a more detailed level. The numeric integration of all of the load cases described under 2.5.2, have resulted in the knowledge of the combined, overall strain on the loadbearing torque box at any given blade segment, or blade element, from the hub to the rotor tip. Knowing the exact shape, size and thickness of the torque box at all of the blade elements, it is further possible to calculate the stress in the walls of the structure, and in that way obtaining a complete overview of the stress in the rotor blades. The approach of these calculations is obtained from the courses „Festigkeit Im Leichtbau 1 und 2”, and „Strukturkonstruktion“ (Calculations On Thin Structures 1 and 2, and Structural Design) [13], [14] and [15].

2.5.3.1 Torque Box geometry

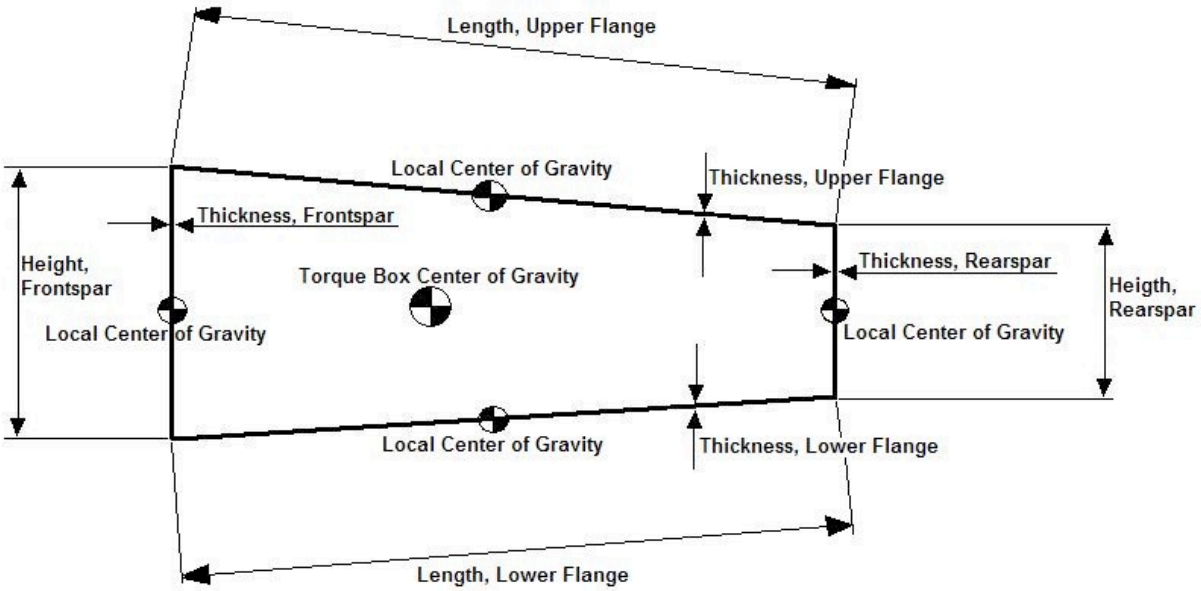

Figure 2.13: Torque Box Geometry

The geometry of the torque box is described through two functions that are approximations of the upper- and lower flanges, the position of the front- and rear spars as percent of the chord line, and the thicknesses of each of the sides in the torque box. Using the distance between the functions of the upper- and lower flanges at a given position of the chord, the heights of the front- and rear spars can be calculated. The lengths of the upper- and lower flanges are identified by calculating the coordinates of the four corner points in the torque box, and further simplifying the upper- and lower flanges to straight lines. In this manner, the upper- and lower flanges can be described as linear functions, and the angles and lengths can consequently be calculated by applying the rules for such functions.

$$h_{FS} = y_{UF}\left(c_{FS}\right) - y_{LF}\left(c_{FS}\right) \tag{2.59}$$

h_{FS} Height of front spar [mm]

$$h_{RS} = y_{UF}\left(c_{RS}\right) - y_{LF}\left(c_{RS}\right) \tag{2.60}$$

h_{RS} Height of rear spar [mm]

$$l_{UF} = \frac{abs\left(y_{UF}\left(c_{RS}\right) - y_{UF}\left(c_{FS}\right)\right)}{\sin\left(\arctan\left(\frac{abs\left(y_{UF}\left(c_{RS}\right) - y_{UF}\left(c_{FS}\right)\right)}{c_{RS} - c_{FS}}\right)\right)} \quad \textbf{(2.61)}$$

l_{UF} Length of upper flange [mm]
y_{UF} Approximate function of upper flange [mm]
c_{FS} Position of front spar along the chord line [mm]
c_{RS} Position of rear spar along the chord line [mm]

$$l_{LF} = \frac{y_{LF}\left(c_{RS}\right) - y_{LF}\left(c_{FS}\right)}{\sin\left(\arctan\left(\frac{y_{LF}\left(c_{RS}\right) - y_{LF}\left(c_{FS}\right)}{c_{RS} - c_{FS}}\right)\right)} \quad \textbf{(2.62)}$$

y_{LF} Approximate function of lower flange [mm]
l_{LF} Length of lower flange [mm]

Using a customary coordinate system for wings, with the plane of the airfoil profile consisting of the x- and z-axis, and the y-axis parallel to the length of the blade, the local Centers of Gravity (CoG) are calculated as follows:

Front spar:

$$x_{S,FS} = c_{FS} \quad \textbf{(2.63)}$$

$x_{S,FS}$ X-value of the CoG of the front spar [mm]

$$z_{S,FS} = y_{LF}\left(c_{FS}\right) + \frac{h_{FS}}{2} \quad \textbf{(2.64)}$$

$z_{S,FS}$ Z-value of the CoG of the front spar [mm]

Rear spar:

$$x_{S,RS} = c_{RS} \quad \textbf{(2.65)}$$

$x_{S,RS}$ X-value of the CoG of the rear spar [mm]

$$z_{S,RS} = y_{LF}\left(c_{RS}\right) + \frac{h_{RS}}{2} \quad \textbf{(2.66)}$$

$z_{S,RS}$ Z-value of the CoG of the rear spar [mm]

Upper flange:

$$x_{S,UF} = c_{FS} + \frac{\left(c_{RS} - c_{FS}\right)}{2} \tag{2.67}$$

$x_{S,UF}$ X-value of the CoG of the upper flange [mm]

$$z_{S,UF} = \left(\frac{y_{UF}\left(c_{RS}\right) - y_{UF}\left(c_{FS}\right)}{c_{RS} - c_{FS}}\right) \cdot \left(x_{S,UF} - c_{FS}\right) + y_{UF}\left(c_{FS}\right) \tag{2.68}$$

$z_{S,UF}$ Z-value of the CoG of the upper flange [mm]

Lower flange:

$$x_{S,LF} = c_{FS} + \frac{\left(c_{RS} - c_{FS}\right)}{2} \tag{2.69}$$

$x_{S,LF}$ X-value of the CoG of the lower flange [mm]

$$z_{S,LF} = \left(\frac{y_{LF}\left(c_{RS}\right) - y_{LF}\left(c_{FS}\right)}{c_{RS} - c_{FS}}\right) \cdot \left(x_{S,LF} - c_{FS}\right) + y_{LF}\left(c_{FS}\right) \tag{2.70}$$

$z_{S,LF}$ Z-value of the CoG of the lower flange [mm]

On the basis of the local CoG's, which now has been calculated, the overall CoG for the torque box can be obtained:

$$A_{Sum} = A_{UF} + A_{LF} + A_{FS} + A_{RS} = \left(l_{UF} \cdot t_{UF}\right) + \left(l_{LF} \cdot t_{LF}\right) + \left(h_{FS} \cdot t_{FS}\right) + \left(h_{RS} \cdot t_{RS}\right) \tag{2.71}$$

A_{Sum} Overall Area of the walls of the torque box [mm^2]
A_{UF} Area of the upper flange [mm^2]
A_{LF} Area of the lower flange [mm^2]
A_{FS} Area of the front spar [mm^2]
A_{RS} Area of the rear spar [mm^2]
t_{UF} Thickness of the upper flange [mm]
t_{FS} Thickness of the front spar [mm]
t_{LF} Thickness of the lower flange [mm]
t_{RS} Thickness of the rear spar [mm]

$$A_{Sum,X} = A_{UF} \cdot x_{S,UF} + A_{LF} \cdot x_{S,LF} + A_{FS} \cdot x_{S,FS} + A_{RS} \cdot x_{S,RS} \quad \textbf{(2.72)}$$

$A_{Sum,X}$ Calculation value for the overall x-coordinate of the CoG [m^3]

$$A_{Sum,Z} = A_{UF} \cdot z_{S,UF} + A_{LF} \cdot z_{S,LF} + A_{FS} \cdot z_{S,FS} + A_{RS} \cdot z_{S,RS} \quad \textbf{(2.73)}$$

$A_{Sum,Z}$ Calculation value for the overall z-coordinate of the CoG [m^3]

$$X_{TB} = \frac{A_{Sum,X}}{A_{Sum}} \quad \textbf{(2.74)}$$

X_{TB} Overall x-coordinate of the torque box CoG [m]

$$Z_{TB} = \frac{A_{Sum,Z}}{A_{Sum}} \quad \textbf{(2.75)}$$

Z_{TB} Overall z-coordinate of the torque box CoG [m]

With these values, it is now possible to calculate the Second Moments of Inertia (SMI), which are crucial for the stress calculations from the bending moments. Hereby, the SMI with index “x” describes the SMI that considers the structure’s distance from the x-axis, and increases proportionally with the z-value. Correspondingly, the SMI with the index “z” considers the structure’s distance from the z-axis, and increases proportionally with the x-value.

Keeping in mind that these calculations are preliminary, a few simplifications are made while determining the SMI’s: The torque box is considered a symmetrical rectangle, with the upper- and lower flanges parallel to the x-axis. In this way, the global coordinate system is kept the main coordinate system with regards to bending and displacement, and because of the symmetry, the Product Moment of Inertia (PMI), I_{XY}, is zero. For the final calculations of normal- and shear flows and stresses however, the actual angles of the upper and lower flanges are taken into consideration.

$$\begin{aligned} I_X &= I_{X,UF} + I_{X,FS} + I_{X,LF} + I_{X,RS} = \\ &\frac{1}{12} \cdot \left(\left(l_{UF} \cdot t_{UF}^3 \right) + \left(h_{FS}^3 \cdot t_{FS} \right) + \left(l_{LF} \cdot t_{LF}^3 \right) + \left(h_{RS}^3 \cdot t_{RS} \right) \right) + \\ &\left(\left(l_{UF} \cdot t_{UF} \right) \cdot \left(z_{S,UF} - Z_{TB} \right)^2 \right) + \left(\left(l_{LF} \cdot t_{LF} \right) \cdot \left(Z_{TB} - z_{S,LF} \right)^2 \right) + \\ &\left(\left(h_{FS} \cdot t_{FS} \right) \cdot \left(z_{S,FS} - Z_{TB} \right)^2 \right) + \left(\left(h_{RS} \cdot t_{RS} \right) \cdot \left(z_{S,RS} - Z_{TB} \right)^2 \right) \end{aligned} \quad \textbf{(2.76)}$$

I_X Total SMI with respect to the x-axis [mm^4]

$I_{X,UF}$ SMI of the upper flange with respect to the x-axis [mm^4]

$I_{X,FS}$ SMI of the front spar with respect to the x-axis [mm^4]

$I_{X,LF}$ SMI of the lower flange with respect to the x-axis [mm^4]

$I_{X,RS}$ SMI of the rear spar with respect to the x-axis [mm^4]

$$I_Z = I_{Z,UF} + I_{Z,FS} + I_{Z,LF} + I_{Z,RS} =$$
$$\frac{1}{12} \cdot \left(\left(l_{UF}^3 \cdot t_{UF} \right) + \left(h_{FS} \cdot t_{FS}^3 \right) + \left(l_{LF}^3 \cdot t_{LF} \right) + \left(h_{RS} \cdot t_{RS}^3 \right) \right) +$$
$$\left(\left(l_{UF} \cdot t_{UF} \right) \cdot \left(x_{S,UF} - X_{TB} \right)^2 \right) + \left(\left(l_{LF} \cdot t_{LF} \right) \cdot \left(X_{TB} - x_{S,LF} \right)^2 \right) + \quad \textbf{(2.77)}$$
$$\left(\left(h_{FS} \cdot t_{FS} \right) \cdot \left(x_{S,FS} - X_{TB} \right)^2 \right) + \left(\left(h_{RS} \cdot t_{RS} \right) \cdot \left(x_{S,RS} - X_{TB} \right)^2 \right)$$

I_Z Total SMI with respect to the z-axis [mm^4]

$I_{Z,UF}$ SMI of the upper flange with respect to the z-axis [mm^4]

$I_{Z,FS}$ SMI of the front spar with respect to the z-axis [mm^4]

$I_{Z,LF}$ SMI of the lower flange with respect to the z-axis [mm^4]

$I_{Z,RS}$ SMI of the rear spar with respect to the z-axis [mm^4]

Next, the shortest distances from the walls of the torque box to the overall CoG will be determined. These will be needed while calculating the SC, which directly influences the final shear flows in the torque box:

The shortest distance between a point and a linear function is defined as [10]:

$$d = \left| \frac{A x_1 + B y_1 + C}{\sqrt{\left(A^2 + B^2 \right)}} \right| \quad \textbf{(2.78)}$$

d The shortest distance between a point and a linear function [m]

A X-gradient of a linear function on the form: $Ax + By + C = 0$ [-]

B Y-gradient of a linear function on the form: $Ax + By + C = 0$ [-]

C Constant in a linear function on the form: $Ax + By + C = 0$ [m]

x_1 X-coordinate of the point [m]

y_1 Y-coordinate of the point [m]

For the front- and rear spars, the shortest distances are simple to determine, as they are parallel to the z-axis:

$$d_{FS} = X_{TB} - x_{S,FS} \quad \textbf{(2.79)}$$

d_{FS} Shortest distance between front spar and the overall CoG [m]

$$d_{RS} = X_{TB} - x_{S,RS} \quad \textbf{(2.80)}$$

d_{RS} Shortest distance between rear spar and the overall CoG [m]

For the upper and lower flanges, the necessary constants, A and C are calculated as follows:

$$A_{x,UF} = -\left(\frac{\left(y_{UF}\left(c_{RS}\right) - y_{UF}\left(c_{FS}\right)\right)}{\left(c_{RS} - c_{FS}\right)} \right) \quad \textbf{(2.81)}$$

$A_{x,UF}$ X-gradient of the linear function of the upper flange [-]

$$C_{x,UF} = -A_{x,UF} \cdot c_{FS} + y_{UF}\left(c_{FS}\right) \quad \textbf{(2.82)}$$

$C_{x,UF}$ Constant of the linear function of the upper flange [m]

$$A_{x,LF} = -\left(\frac{\left(y_{LF}\left(c_{RS}\right) - y_{LF}\left(c_{FS}\right)\right)}{\left(c_{RS} - c_{FS}\right)} \right) \quad \textbf{(2.83)}$$

$A_{x,LF}$ X-gradient of the linear function of the lower flange [-]

$$C_{x,LF} = -A_{x,LF} \cdot c_{FS} + y_{LF}\left(c_{FS}\right) \quad \textbf{(2.84)}$$

$C_{x,LF}$ Constant of the linear function of the lower flange [m]

The reason for the minuses at the start of the right hand side of these equations is that the functions originally were arranged on the form: $y = ax + b$, and that the x-gradient and the constant subsequently were moved to the other side. Because this form was the starting point, the value B in (2.78) is 1.

The results for the shortest distances from the upper and lower flanges to the overall CoG become:

$$d_{UF} = \left| \frac{-\left(\frac{\left(y_{UF}\left(c_{RS}\right) - y_{UF}\left(c_{FS}\right)\right)}{\left(c_{RS} - c_{FS}\right)}\right) \cdot X_{TB} + 1 \cdot Z_{TB} + \left(\left(\frac{\left(y_{UF}\left(c_{RS}\right) - y_{UF}\left(c_{FS}\right)\right)}{\left(c_{RS} - c_{FS}\right)}\right) \cdot c_{FS} + y_{UF}\left(c_{FS}\right)\right)}{\sqrt{\left(\left(-\left(\frac{\left(y_{UF}\left(c_{RS}\right) - y_{UF}\left(c_{FS}\right)\right)}{\left(c_{RS} - c_{FS}\right)}\right)\right)^2 + 1^2\right)}} \right| \quad \textbf{(2.85)}$$

$$d_{LF} = \left| \frac{-\left(\frac{\left(y_{LF}\left(c_{RS}\right) - y_{LF}\left(c_{FS}\right)\right)}{\left(c_{RS} - c_{FS}\right)}\right) \cdot X_{TB} + 1 \cdot Z_{TB} + \left(\left(\frac{\left(y_{LF}\left(c_{RS}\right) - y_{LF}\left(c_{FS}\right)\right)}{\left(c_{RS} - c_{FS}\right)}\right) \cdot c_{FS} + y_{LF}\left(c_{FS}\right)\right)}{\sqrt{\left(\left(-\left(\frac{\left(y_{LF}\left(c_{RS}\right) - y_{LF}\left(c_{FS}\right)\right)}{\left(c_{RS} - c_{FS}\right)}\right)\right)^2 + 1^2\right)}} \right| \quad \textbf{(2.86)}$$

d_{UF} Shortest distance between upper flange and the overall CoG [m]

d_{LF} Shortest distance between lower flange and the overall CoG [m]

2.5.3.2 Shear Flow

With each of the load cases and the applicable geometrical values for the torque box now known, the stress calculations can be carried into the final stage. This includes the shear- and normal flows, and finally the shear- and normal stress calculations.

The shear forces and torsion moments cause the resulting shear flow in the torque box on the given blade section. The geometrical constraints and definitions for the calculations are shown in Figure 2.14:

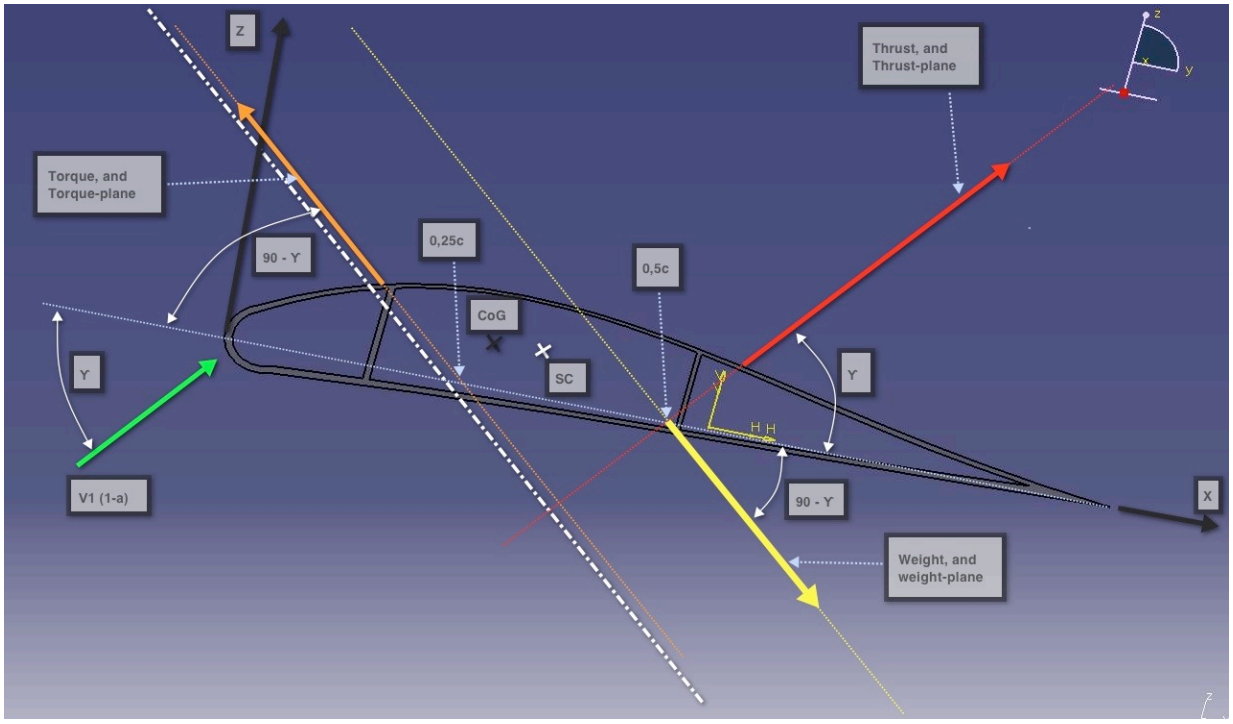

Figure 2.14: Constraints for shear flow calculations. Rotor angle: (181°;359°)

2.5.3.2.1 Shear Flow from Shear Force

The total shear flow in a closed structural cell due to shear force is:

$$q_S = q_1 + q_0 \tag{2.87}$$

q_s Total shear flow due to shear force [N/mm]
q_1 Basic shear flow in the structure [N/mm]
q_0 Constant shear flow in a closed structural cell [N/mm]

q_1 is further defined as [14]:

$$q_1 = \frac{Q_X \cdot S_Z(s)}{I_Z} + \frac{Q_Z \cdot S_X(s)}{I_X} = \frac{Q_X}{I_Z} \cdot \left(\int_0^S tx\,ds + \sum_{r=1}^{m} A_{Fr} \cdot x_r \right) + \frac{Q_Z}{I_X} \cdot \left(\int_0^S tz\,ds + \sum_{r=1}^{m} A_{Fr} \cdot z_r \right) \tag{2.88}$$

Q_X Total shear force in the x-direction [N]
Q_Z Total shear force in the z-direction [N]
$S_Z(s)$ First Moment of Inertia (FMI), parallel to the x-axis [mm^3]
$S_X(s)$ FMI, parallel to the z-axis [mm^3]
s Variable for the FMI, [mm]
t Thickness of the structure [mm]

A_{Fr} Area of a part of the structure [mm^2]

x_r The x-Coordinate of the CoG to a part of the structure [mm]

z_r The z-Coordinate of the CoG to a part of the structure [mm]

Q_X and Q_Z , the total shear forces in the x- and z-directions, are defined as:

$$Q_X = -F_{torque,bs} \cdot \cos(90° - \gamma) + F_{thrust,bs} \cdot \sin(90° - \gamma) - F_{G,Shear,bs} \cdot \cos(90° - \gamma) \quad \textbf{(2.89)}$$

$$Q_Z = -F_{torque,bs} \cdot \sin(90° - \gamma) - F_{thrust,bs} \cdot \cos(90° - \gamma) - F_{G,Shear,bs} \cdot \sin(90° - \gamma) \quad \textbf{(2.90)}$$

The index of the components in Q_Z is defined on the physiology that compression, which by definition delivers negative values for force flow and stress, occurs on the suction side of the blade.

Using a coordinate system with origin in the CoG of the torque box, and axes parallel to the axes in Figure 2.14, $S_Z(s)$ and $S_X(s)$ are defined as follows:

$$S_Z(s) = \bar{x}(s) \cdot A(s) = \left(\frac{\Delta x(l)}{2 \cdot l} \cdot s + x_0 \right) \cdot (s \cdot t) \quad \textbf{(2.91)}$$

$\bar{x}(s)$ CoG of the elapsed distance s in x-direction [mm]

$A(s)$ Area of the elapsed distance s [mm^2]

Δx Difference in x-value of the elapsed distance [mm]

l Total length of the side being calculated [mm]

x_0 X-value of the starting point, with relation to X_{TB} [mm]

$$S_X(s) = \bar{z}(s) \cdot A(s) = \left(\frac{\Delta z(l)}{2 \cdot l} \cdot s + z_0 \right) \cdot (s \cdot t) \quad \textbf{(2.92)}$$

$\bar{z}(s)$ CoG of the elapsed distance s in z-direction [mm]

Δz Difference in z-value of the elapsed distance [mm]

z_0 Z-value of the starting point, with relation to Z_{TB} [mm]

In practice, the basic shear flow is calculated individually for each of the walls in the torque box, separated through the four corner points. Point number 1 is here chosen to be at the top of the rear spar, and numbering counter-clockwise result in point number 4 being at the bottom of the rear spar. At the starting point at point 1, q_1 is defined as zero, and as (2.88) indicates, when moving to the front spar between point 2 and 3, the q_1-value at the end of the upper flange, or point 2, is added to the shear flow from the front spar. This is repeated for the lower

flange and rear spar, by adding the sum of q_1 from the previously calculated walls.

q_0 exists in the torque box because it is a closed cell. It is constant in the whole structure, and is defined as follows:

$$q_0 = -\frac{\oint \frac{q_1(s)}{t(s)} ds}{\oint \frac{ds}{t(s)}} \quad \textbf{(2.93)}$$

As (2.93) shows, q_0 is calculated on the basis of q_1, and is finally added to q_1, to deliver the q_s as described in (2.87).

2.5.3.2.2 Shear Flow from Torsion

The shear flow in a single-cell structure is defined through the 1st Bredt's Formula:

$$q_T = \frac{T}{2 \cdot A_{TB}} \quad \textbf{(2.94),}$$

q_T	Total shear flow due to torsion moment [N/mm]
T	Total torque moment [Nmm]
A_{TB}	Area of the torque box [mm^2]

The reason for the positive index in (2.94) is that a positive torsion moment from c_m, which triggers a "pitch-up" movement of the airfoil, is here compliant with a positive index from the "right-hand rule". In Figure 2.14, it is clear that the y-axis is pointing away from the viewer, and the "right-hand rule" defines consequently the positive rotation of the y-axis as clock-wise, which is in the same direction as the positive torsion moment.

Another factor, which has to be considered here, is that the resulting shear forces do not lie in the blade element plane, but somewhere towards the tip, as they are the resulting forces of the applicable blade segment. In this work, the quarter-line, or 0,25c is defined to be a straight line with no sweep. This results in, however, that the 0,5c line, which here is defined to intersect with the force-lines of thrust and weight in each blade element, has an angle from hub to tip. Because of this, the resulting shear forces from thrust and weight do not intersect the 0,5c point in the blade element to be calculated:

Referring to Figure 2.15, the following relationship emerge for the distance in x-direction between the 0,5c at the current blade element and 0,5c at another radius:

$$\Delta 0,5c_X = \left[\frac{\left(0,25\cdot\left(c\left(r_{S,AE}\right)-c\left(r_{Blade}\right)\right)\right)}{\left(r_{Blade}-r_{S,AE}\right)}\right]\cdot\left(r_X - r_{bs}\right) \qquad \textbf{(2.95)}$$

$\Delta 0,5c_X$ Distance in x-direction between the 0,5c point at the current blade element and the 0,5c point at radius r_X [mm]

$c\left(r_{S,AE}\right)$ Chord length at the first blade element [mm]

$c\left(r_{Blade}\right)$ Chord length at the last blade element [mm]

r_X Radius to the force outside the current blade element [mm]

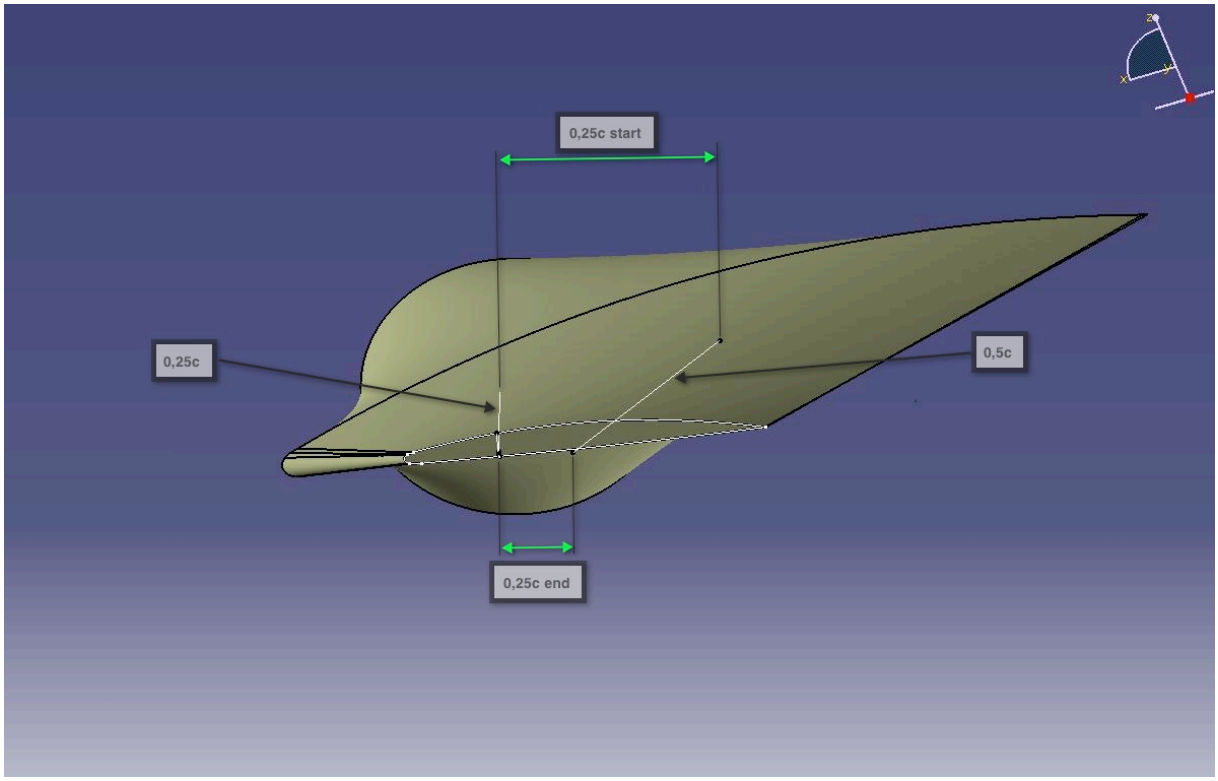

Figure 2.15: Quarter line and half-chord line

Now, a slight simplification compared to Figure 2.14 is introduced by defining the lines of force from torque, thrust and weight, so that they intersect the distances 0,25c and 0,5c level with the SC in the z-direction, instead of the chord line. In this way, only the force components in the z-direction contribute to the torsion. By using the same calculation method for distance between a point and a line as under 2.5.3.1 through (2.78), the result would have been more accurate, but in view of these calculations being preliminary, this simplification is found to be satisfactory.

Referring to Figure 2.14, and bearing in mind that $F_{G,Shear,bs}$ in this view is negative due to the rotor angle, the total torsion moment, T, adds up as follows:

$$T = M_{Torsion,bs} + M_{Torsion,SF}$$
$$= M_{Torsion,bs} + \begin{bmatrix} \left\{F_{torque,bs} \cdot \sin\left(90^\circ - \gamma\right) \cdot \left[\left(X_{TB} + e_x\right) - 0,25c\right]\right\} - \\ \left\{F_{G,Shear,bs} \cdot \sin\left(90^\circ - \gamma\right) \cdot \left[\left(0,5c - \Delta 0,5c_{SF}\right) - \left(X_{TB} + e_x\right)\right]\right\} - \\ \left\{F_{thrust,bs} \cdot \cos\left(90^\circ - \gamma\right) \cdot \left[\left(0,5c - \Delta 0,5c_{TF}\right) - \left(X_{TB} + e_x\right)\right]\right\} \end{bmatrix} \quad \textbf{(2.96)}$$

e_x Distance between X_{TB} and the x-coordinate of the SC [mm]

$\Delta 0,5c_{SF}$ Deviation for the 0,5c point for $F_{G,Shear,bs}$ [mm]

$\Delta 0,5c_{TF}$ Deviation for the 0,5c point for $F_{thrust,bs}$ [mm]

e_x is calculated by establishing the moment equilibrium about the torque box CoG:

$$e_x = \frac{\oint \left(q_s \cdot d\right) ds}{Q_Z} \quad \textbf{(2.97)}$$

d Distances from each wall to CoG, ref. (2.79), (2.80), (2.85) and (2.86) [mm]

The total shear flow in the torque box finally adds up to:

$$q = q_S + q_T \quad \textbf{(2.98)}$$

q Total shear flow in the torque box [N/mm]

The shear stress is now calculated directly on the basis of the shear flow, and the correspondingly wall thickness, t:

$$\tau_{x,z} = \frac{q}{t} \quad \textbf{(2.99)}$$

$\tau_{x,z}$ Overall shear stress [N/mm^2]

2.5.3.3 Normal Flow

Now the calculations for the normal flow in the torque box based on the loads presented under 2.5.2 shall be investigated. Whereas the shear flow works in the airfoil plane, the normal flow has direction parallel to the y-axis, or the radius of the blade. The loads, which cause the normal flow, are the normal forces from weight and inertia, and the moments around the x- and z-axis:

$$n = n_{yy} + n_{yx} + n_{yz} \tag{2.100}$$

n Total normal flow in the torque box [N/mm]

n_{yy} Normal flow in the torque box due to normal forces [N/mm]

n_{yx} Normal flow in the torque box due to moments about the x-axis [N/mm]

n_{yz} Normal flow in the torque box due to moments about the z-axis [N/mm]

The normal flow due to normal forces, n_{yy} , is distributed evenly in the torque box, and is calculated in the following manner:

$$n_{yy} = \frac{\left(F_{G,Normal,bs} + F_{cF,bs}\right)}{\left(l_{UF} + h_{FS} + l_{LF} + h_{RS}\right)} \tag{2.101}$$

n_{yx} is the normal flow due to bending moment about the x-axis, and the magnitude of this is directly proportional to the distance in z-direction to the x-axis:

$$n_{yx} = \sigma_{yx} \cdot t = \frac{M_X}{I_X} \cdot z \cdot t \tag{2.102}$$

σ_{yx} Normal stress in the torque box from moments about the x-axis [N/mm^2]

M_X Total bending moment about the x-axis [Nmm]

z Z-value of the structure at the point being calculated [mm]

t Thickness of the structure at the point being calculated [mm]

Except for the bending moment caused by the shear force from gravity, the other two components, thrust and torque, are delivered directly through the BEM-calculations and then prepared for each blade section through the methods shown under 2.5.2.3 and 2.5.2.4. As with the resulting shear forces in the shear flow calculations, the bending moments are converted into the airfoil coordinate system and summed. The indexes are also here determined by the fact that compression shall occur on the suction side of the blade:

$$M_X = -\left(M_{SF,bs} + T_{bs}\right) \cdot \sin\left(90° - \gamma\right) - M_{thrust,bs} \cdot \cos\left(90° - \gamma\right) \tag{2.103}$$

The same procedure is repeated for n_{yz}:

$$n_{yz} = \sigma_{yx} \cdot t = \frac{M_Z}{I_Z} \cdot x \cdot t \tag{2.104}$$

σ_{yz} Normal stress in the torque box from moments about the z-axis [N/mm^2]

M_Z Total bending moment about the z-axis [Nmm]

x X-value of the structure at the point being calculated [mm]

t Thickness of the structure at the point being calculated [mm]

$$M_Z = \left(T_{bs} + M_{SF,bs}\right) \cdot \cos\left(90° - \gamma\right) - M_{thrust,bs} \cdot \sin\left(90° - \gamma\right) \quad \textbf{(2.105)}$$

As with the shear stress, the normal stress is calculated by dividing the normal flow by the corresponding wall thickness, *t*:

$$\sigma_y = \frac{n_y}{t} \quad \textbf{(2.106)}$$

σ_y Overall normal stress [N/mm^2]

2.5.3.4 Comparative Stresses

Now, all of the primary load cases have been presented, and the theory of how they affect the structure, shown and derived. Finally, the overall strain on the structure at a given spot in the torque box in a given blade element will be calculated based on the resulting normal- and shear stresses. This type of strain is called comparative stress, and delivers a picture of the combined strain from normal- and shear stress. This can be calculated, based on different hypotheses. The hypotheses are models of the overall strain, where normal- and shear stress are emphasized differently, after what is considered to be the most critical type of strain [16]:

$$\sigma_{V,N} = 0,5 \cdot \left|\sigma_y\right| + 0,5 \cdot \sqrt{\left(\sigma_y^2 + 4\tau_{x,z}^2\right)} \quad \textbf{(2.107)}$$

$\sigma_{V,N}$ Normal stress hypothesis [N/mm^2]

$$\sigma_{V,S} = \sqrt{\left(\sigma_y^2 + 4\tau_{x,z}^2\right)} \quad \textbf{(2.108)}$$

$\sigma_{V,S}$ Shear stress hypothesis [N/mm^2]

$$\sigma_{V,F} = \sqrt{\left(\sigma_y^2 + 3\tau_{x,z}^2\right)} \quad \textbf{(2.109)}$$

$\sigma_{V,F}$ Change of shape hypothesis (Von Mieses) [N/mm^2]

3 Airfoils

3.1 Importance of airfoil data

As can be seen in the equations of the BEM Theory, it is crucial to have knowledge of the airfoil used for the blades in regards to the lift- and drag coefficients for this method to work. As the BEM Theory is calculated iteratively, it is further necessary to be able to calculate these coefficients using equations with regards to the AoA, because a database with intervals between the values would not be enough to feed the BEM equations during the iterative process. Especially near the end of the iteration are the changes in values small, and a seamless way of gathering the coefficients is needed to prevent the calculation program from crashing.

Information and data on airfoils are difficult to get access to, as they often are subject to secrecy and in some cases not available to the public to protect the interests of the inventor.

There is, however, much data to be obtained from some of the profiles which are no longer cutting edge, as e.g. the 4-digit NACA profiles, which were produced by NACA during the late 1920's and early 1930's. Some variants of these profiles are also still being used in the wind turbine industry today, and they are therefore a fitting alternative for this work. A NACA 4410 profile is subsequently chosen for this work.

In addition to the need for information about the aerodynamics of the airfoil, it is for this work also required to have information regarding the geometry, with reference to the structural solidity calculations, ref. 2.5.3. It is therefor decided to develop a NACA profile in an Excel spreadsheet, and let Excel calculate approximate functions for the upper- and lower sides of the airfoil. Based on these functions, it is possible to calculate the lengths of the upper- and lower flanges, the height of the front- and rear spar using their position in percentage of chord - as shown in (2.59) - (2.62) - and the area of the torque box through integration of the functions between the front- and rear spar. The area of the airfoil is obtained directly through numeric integration of the resulting coordinates from the equations in the spreadsheet. By norming the chord length to "1" in the calculations, it is further possible to determine the area of the airfoil by multiplying the normed area with the square of the actual chord length.

The procedures and equations related to the calculations of the NACA 4-digit profiles are shown in Appendix B [17].

The spreadsheet is originally set up variably with respect to the entry values for the NACA profiles, the four digits, and the results are thereby available when submitting the values of the applicable airfoil – here the 4410. The interval along the x-axis, or chord-line, is set to 0.005. Table 3-1 shows the entry values in the second column, and the resulting airfoil area from the numeric integration of the coordinates in the fourth column.

4-digit NACA-profiles			
Entry values			***Normed Area [m²]***
First digit:	4	(Max. camber in % of chord)	0,068801
Second digit:	4	(Pos. of max camber in 10-percent)	
Third & fourth digit:	10	(Max. thickness in percentage of chord)	***Scaled Area [m²]***
Constant x chord	5,3	(Chord-length)	1,932628145
Incidence angle α [Degree]	0		

Table 3.1: Entry values for the 4-digit NACA airfoil, and the resulting area

Out of the resulting coordinates for the camber line and the upper- and lower side, Excel generates a graph of the airfoil, and the approximate functions of the upper- and lower sides. These graph for the 4410 airfoil are shown in Figure 3.1:

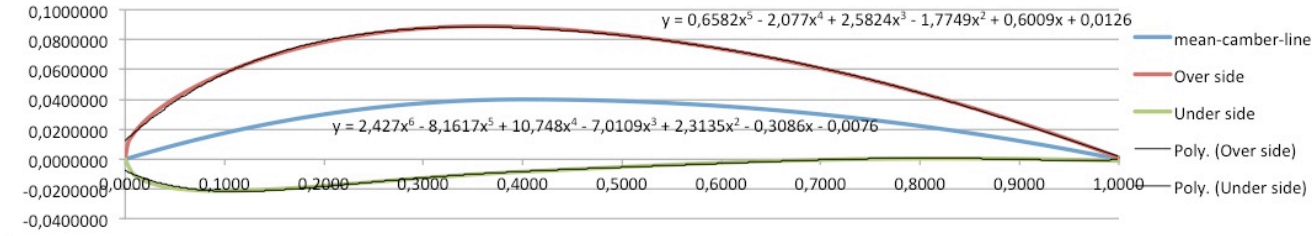

Figure 3.1: Graph and functions for the NACA 4410 airfoil

The results of the spreadsheet are listed below. The functions for the upper- and lower flanges are used extensively under 2.5.3.1 for the torque box geometry, and the airfoil area is used for the volume and density determination for the blades:

$$y_{UF}(c) = 0,6582c^5 - 2,077c^4 + 2,5824c^3 - 1,7749c^2 + 0,6009c + 0,0126 \quad \textbf{(3.1)}$$

$$y_{LF}(c) = 2,427c^6 - 8,1617c^5 + 10,748c^4 - 7,0109c^3 + 2,3135c^2 - 0,3086c - 0,0076 \quad \textbf{(3.2)}$$

$$a_{af}(c) = 0,068801 \cdot c^2 \quad \textbf{(3.3)}$$

$a_{af}(c)$ Airfoil area, dependent on chord length [m²]

3.2 Aerodynamic properties of the NACA 4410 Airfoil

It now has to be decided how to obtain the aerodynamic coefficients, c_l, c_d, and c_m. After learning about and studying the program XFOIL, available online for download and use under the GNU General Public License, this is found to be a fit solution for this task [18]. XFOIL is an "interactive program for the design and analysis of subsonic isolated airfoils" [19]. It makes it possible to, among other things, execute a viscous or inviscid aerodynamic calculation on existing airfoils, delivering lift- and drag predictions just beyond c_{lmax}. By combining high-order panel methods with advanced boundary layer and wake computations and, among other parameters, allowing variable Reynolds numbers, XFOIL has achieved recognition and a good reputation over the years.

XFOIL is now being executed for different values for AoA and utilizing the NACA 4410 airfoil, which already is stored in the program's library. In this connection, fixed, predetermined settings for Mach-, Reynolds- and N_{crit} numbers are being used. N_{crit} refers to the "log of the amplification factor of the most-amplified frequency which triggers transition" [19]. In other words is this a parameter, which specifies the disturbance level in the stream and how the transition of the stream consequently is affected. For this work, the default setting "9" for N_{crit} was chosen. The value 9 is a typical value for an average wind tunnel, while a higher value, e.g. 12 -14 would be appropriate for a sailplane. A lower value would indicate e.g. a "dirty" wind tunnel [19]. Even though the blades of a wind turbine are fairly sleek and aerodynamically clean, it also has to be considered that they operate almost continuous in all sort of weather and therefore typically bear marks of this through scaring of the surfaces from dust, ice, etc. The aerodynamically cleanness of the wind turbine blades are therefor classified worse than a sailplane and the default value 9 is found to be appropriate.

For the Mach number, "0,1" was chosen, as this would be a good approximation for most of the wind speeds addressed in this work. As will be explained in more detail in the chapter covering the calculation program, is a correction factor for the Mach number utilized, if the Mach number exceeds the value "0,3" and the compressibility effect has to be taken into account. Regarding the Reynolds number was the value 10^7 chosen. This would represent the approximate average Reynolds number generated over the blades of a wind turbine similar to the reference wind turbine used in this work, which will be presented later.

The operating window and results from XFOIL can be seen in Figure 3.2 and Figure 3.3:

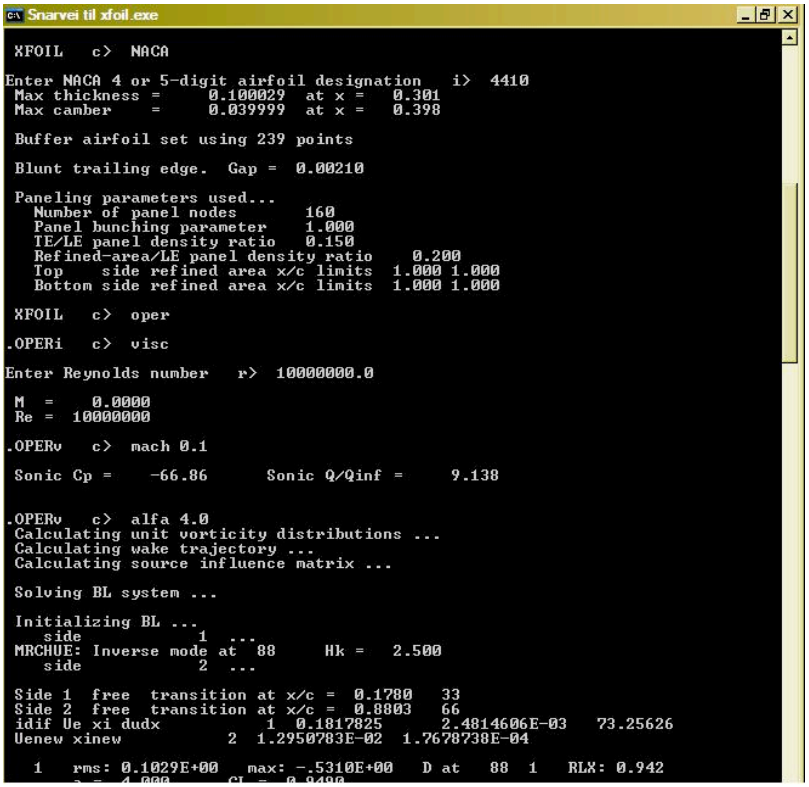

Figure 3.2: XFOIL user window

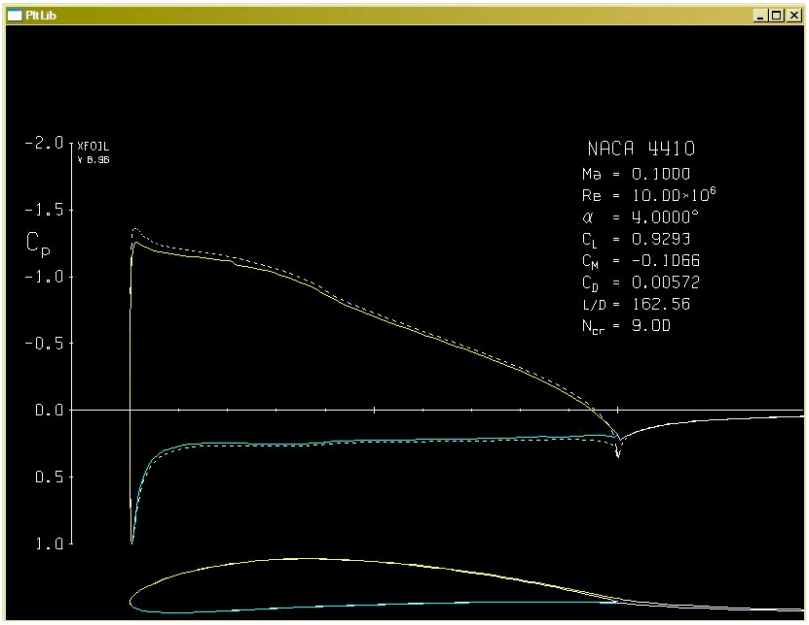

Figure 3.3: XFOIL results

The results for the coefficients c_l, c_d, and c_m from XFOIL are now being stored in the spreadsheet along with the respective AoA, so that graphs over the coefficients may be produced:

Re = 1.0*10^7	**N_{crit} = 9**		
Mach = 0.1			
Alpha	c_l	c_d	c_m
-5	-0,09400	0,00560	-0,10370
-3	0,13640	0,00532	-0,10450
-1	0,36700	0,00519	-0,10540
1	0,59790	0,00508	-0,10670
3	0,82290	0,00534	-0,10720
5	1,03150	0,00658	-0,10490
7	1,24250	0,00848	-0,10290
9	1,44860	0,01030	-0,10020
10	1,54710	0,01135	-0,09820
11	1,64160	0,01250	-0,09560
12	1,72930	0,01384	-0,09180
14	1,85840	0,01754	-0,07700
16	1,95390	0,02393	-0,06190
18	1,99350	0,03721	-0,04950
20	1,98510	0,05977	-0,04580
22	1,91030	0,09431	-0,05130
24	1,78710	0,13934	-0,06880
26	1,64640	0,19394	-0,10420
28	1,42570	0,28744	-0,17880

Table 3.2: Results from XFOIL for the NACA 4410 airfoil

It proved difficult to obtain data from XFOIL at AoA's above 28°, as the program did not manage to conclude the calculations. This can be traced back to the detachment of the airflow experienced at such high AoA's, which in turn not meet the requirements for this sort of calculation method to successfully be completed. As the calculation program is not intended to be used for extreme

settings of the variable pitch system, as e.g. for an aerodynamic brake motion of the rotor, it is decided that the interval of [-5°; 28°] for AoA is sufficient.

As explained above, these results will now be used to produce graphs for the coefficients with respect to AoA, and let Excel generate approximate functions for the graphs. To make the functions as accurate as possible, they are divided into two intervals, and each interval are assigned its own function. The intervals are adjusted individually for each coefficient through testing, to make the transition between the intervals as seamless as possible:

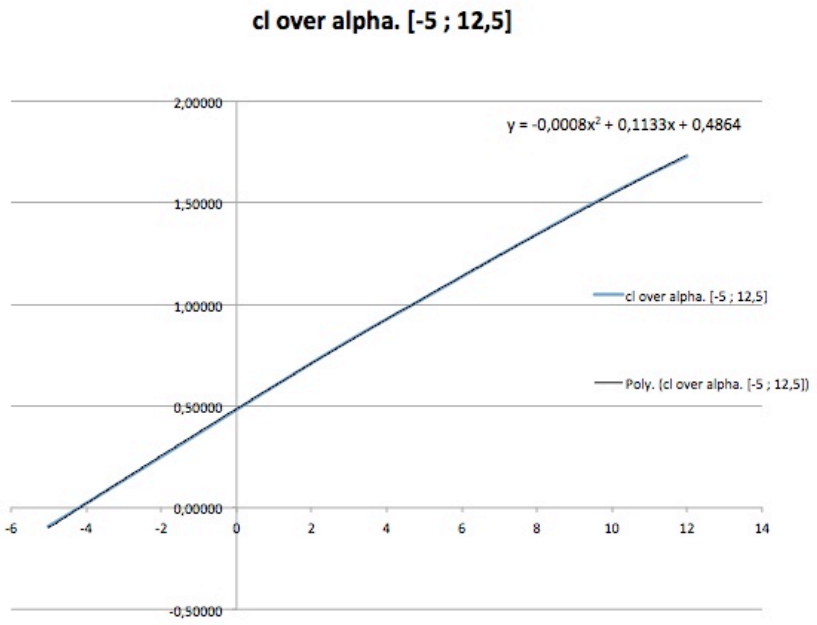

Figure 3.4: c_l over AoA from XFOIL [-5°; 12,5°]

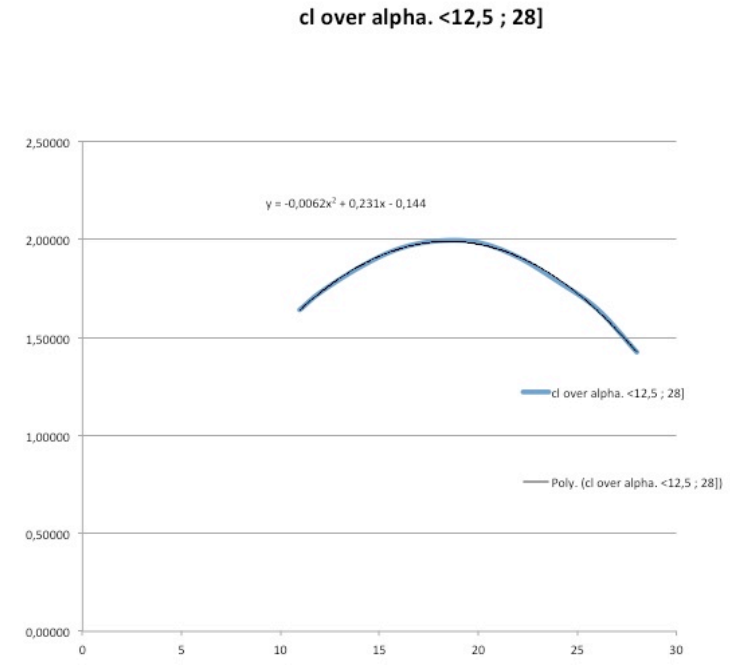

Figure 3.5: c_l over AoA from XFOIL <12,5°; 28°]

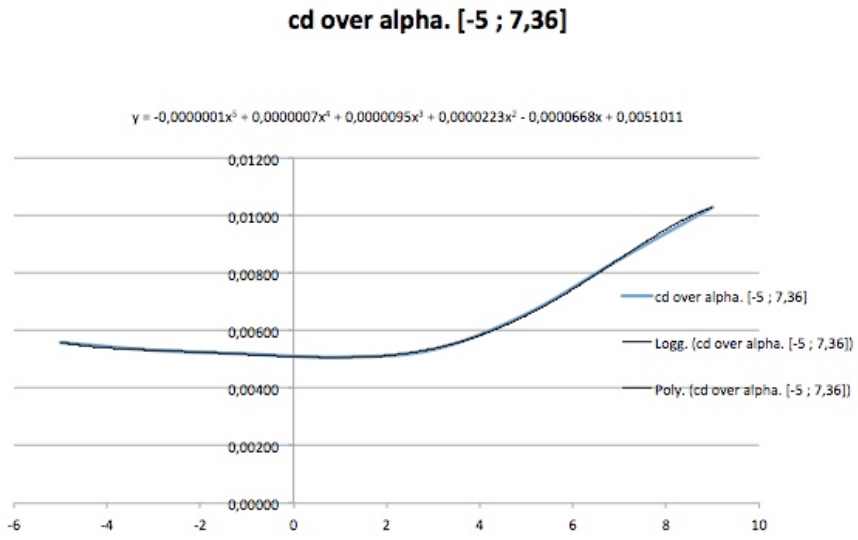

Figure 3.6: c_d over AoA from XFOIL [-5°; 7,36°]

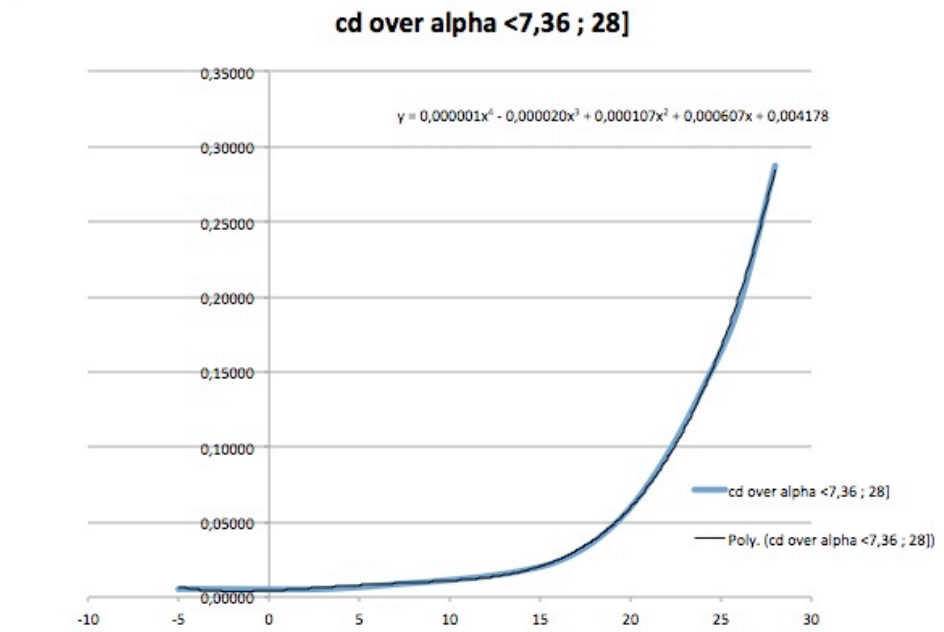

Figure 3.7: c_d over AoA from XFOIL <7,36°; 28°]

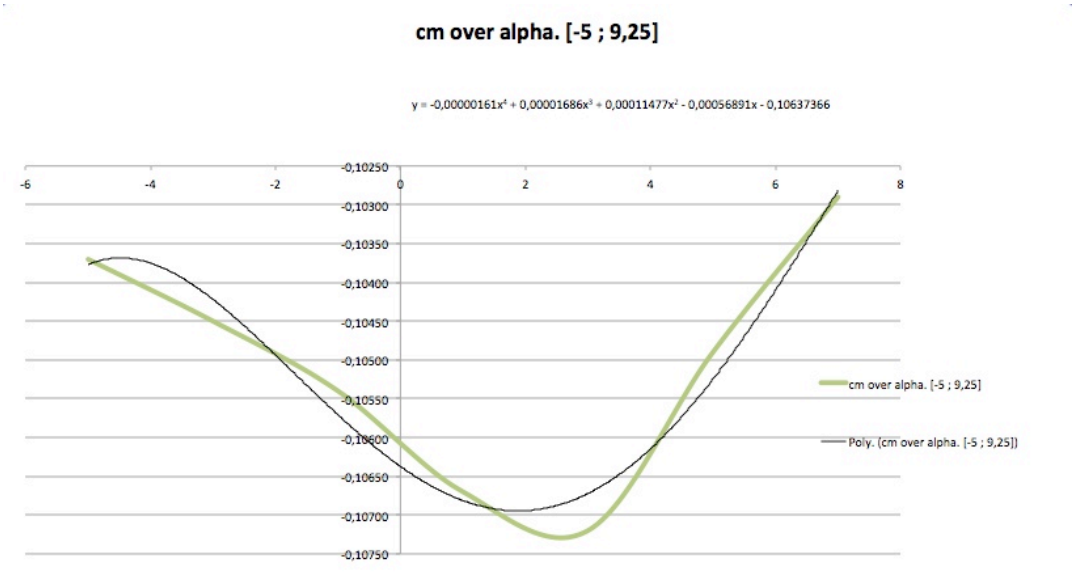

Figure 3.8: c_m over AoA from XFOIL [-5°; 9,25°]

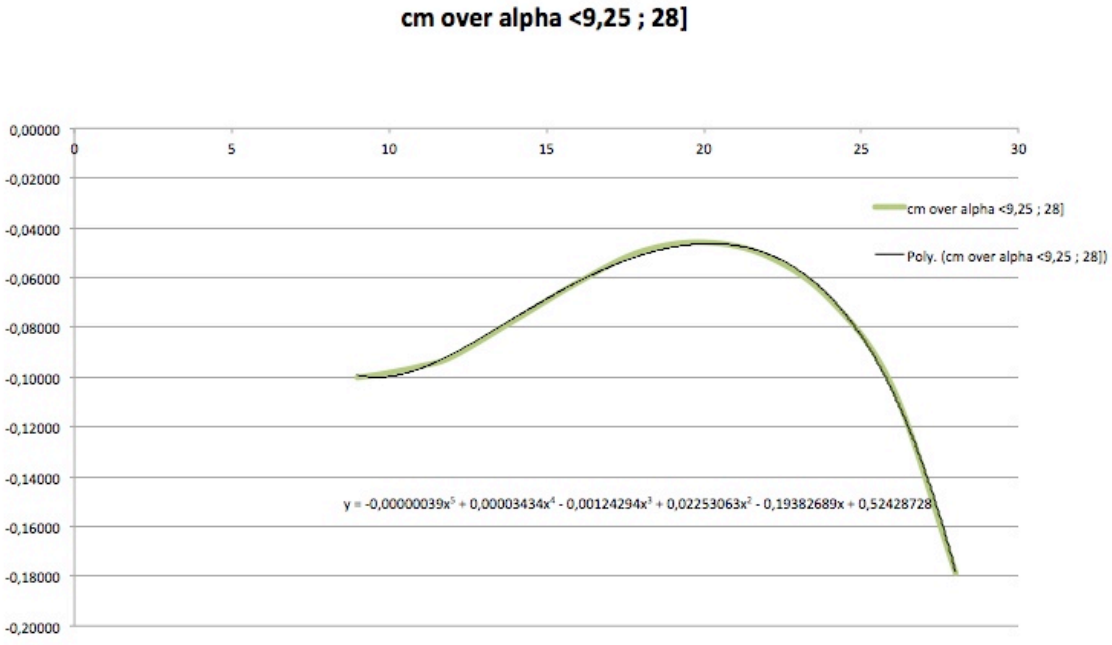

Figure 3.9: c_m over AoA from XFOIL <9,25°; 28°]

The results for the approximated functions for $\mathbf{c_l}$, $\mathbf{c_d}$, and $\mathbf{c_m}$ and their associated intervals are listed below:

c_l:

$\left[-5° \le \alpha \le 12,5°\right]$:

$$c_l(\alpha) = -0,0008\alpha^2 + 0,1133\alpha + 0,4864 \quad \textbf{(3.4)}$$

$\left(12,5° < \alpha \le 28°\right]$:

$$c_l(\alpha) = -0,0062\alpha^2 + 0,231\alpha - 0,144 \quad \textbf{(3.5)}$$

c_d:

$\left[-5° \le \alpha \le 7,36°\right]$:

$$c_d(\alpha) = -0,0000001\alpha^5 + 0,0000007\alpha^4 + 0,0000095\alpha^3 + 0,0000223\alpha^2 - 0,0000668\alpha + 0,0051011 \quad \textbf{(3.6)}$$

$\left(7,36° < \alpha \le 28°\right]$:

$$c_d(\alpha) = 0,000001\alpha^4 - 0,00002\alpha^3 + 0,000107\alpha^2 + 0,000607\alpha + 0,004178 \quad \textbf{(3.7)}$$

c_m:

$\left[-5° \le \alpha \le 9,25°\right]$:

$$c_m(\alpha) = -0,00000161\alpha^4 + 0,00001686\alpha^3 + 0,00011477\alpha^2 - 0,00056891\alpha - 0,10637366 \quad \textbf{(3.8)}$$

$\left(9,25° < \alpha \le 28°\right]$:

$$c_m(\alpha) = -0,00000039\alpha^5 + 0,00003434\alpha^4 - 0,00124294\alpha^3 + 0,02253063\alpha^2 - 0,19382689\alpha + 0,52428728 \quad \textbf{(3.9)}$$

Using these functions for the coefficients, it is now possible to compare them to the results from XFOIL for evaluation:

Alpha	***cl***	$c_{l\ XFOIL}$	***cd***	$c_{d\ XFOIL}$	***cm***	$c_{m\ XFOIL}$
-5,00	-0,10010	-0,09400	0,00556	0,00560	-0,10377	-0,10370
-3,00	0,13930	0,13640	0,00533	0,00532	-0,10422	-0,10450
-1,00	0,37230	0,36700	0,00518	0,00519	-0,10571	-0,10540
1,00	0,59890	0,59790	0,00507	0,00508	-0,10681	-0,10670
3,00	0,81910	0,82290	0,00539	0,00534	-0,10672	-0,10720
5,00	1,03290	1,03150	0,00664	0,00658	-0,10525	-0,10490
7,00	1,24030	1,24250	0,00898	0,00848	-0,10281	-0,10290
9,00	1,44130	1,44860	0,01050	0,01030	-0,10047	-0,10020
10,00	1,53940	1,54710	0,01121	0,01135	-0,09946	-0,09820
11,00	1,63590	1,64160	0,01213	0,01250	-0,09599	-0,09560
12,00	1,73080	1,72930	0,01341	0,01384	-0,09000	-0,09180
14,00	1,87480	1,85840	0,01767	0,01754	-0,07446	-0,07700
16,00	1,96480	1,95390	0,02552	0,02393	-0,05862	-0,06190
18,00	2,00520	1,99350	0,03888	0,03721	-0,04555	-0,04950
20,00	1,99600	1,98510	0,06006	0,05977	-0,03712	-0,04580
22,00	1,93720	1,91030	0,09174	0,09431	-0,03547	-0,05130
24,00	1,82880	1,78710	0,13700	0,13934	-0,04455	-0,06880
26,00	1,67080	1,64640	0,19929	0,19394	-0,07160	-0,10420
28,00	1,46320	1,42570	0,28245	0,28744	-0,12863	-0,17880

Table 3.3: Comparison of functions and XFOIL

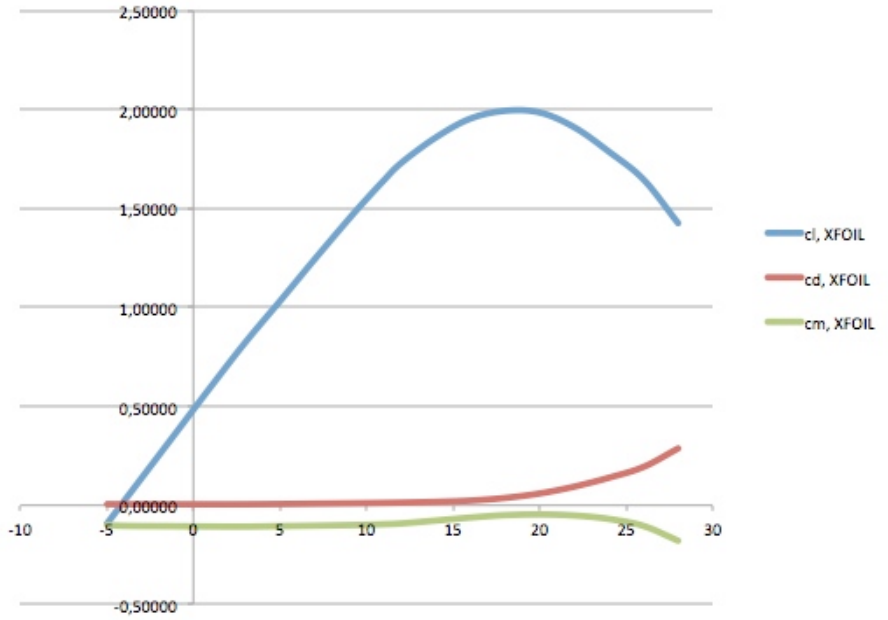

Figure 3.10: Coefficients from XFOIL

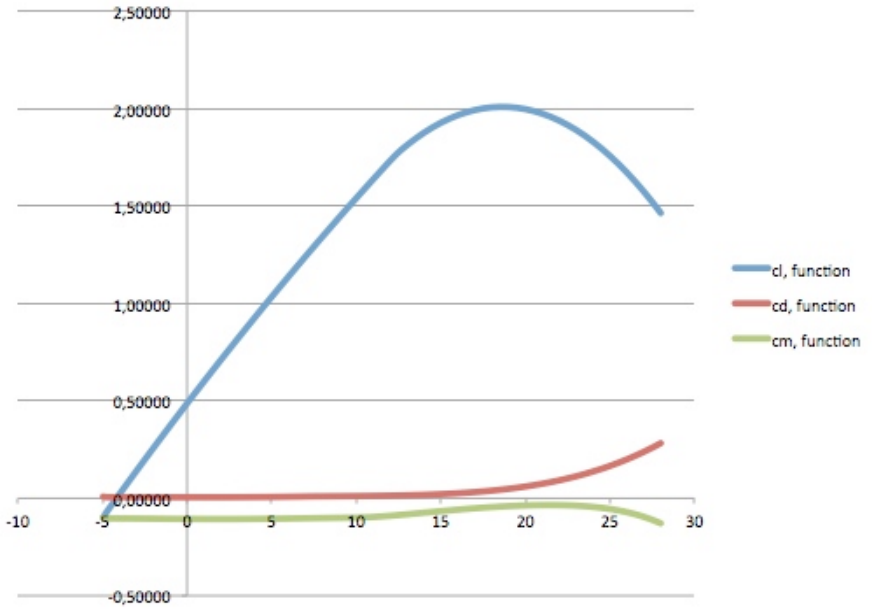

Figure 3.11: Coefficients from functions

The results from the approximate functions for the coefficients c_l, c_d, and c_m are found to be satisfactory, and (3.4) to (3.9) will be incorporated in the calculation program to generate these values when needed in the BEM iterations.

4 Calculation Program

With the theoretical foundation and the prerequisites derived and shown, the computational tool, which executes and automates the methods and equations, can now be presented. It is decided to write the program in the C++ language, and the source to the codes and theory hereby are taken from [20].

4.1 Structure of the Calculation Program

The program is first and foremost intended for testing and experimenting on existing wind turbines for different operational scenarios of wind speeds and efficiency-settings, or wind turbine designs in the preliminary-sizing phase, obtaining results for performance and loads. The user has to submit most of the geometric properties of the applicable wind turbine, and the only geometric value being calculated by the program itself is the twist of the rotor blades. The interface with the program regarding the geometry of the blades has of course its limitations, as the rotor blades usually are of a quite complex shape. In this connection the program has to work on the basis of a few assumptions, which may lead to the program calculating on a geometry that is slightly diverged compared to that of the actual geometry. This also includes the lack of opportunity to use another airfoil than the NACA 4410.

The program is divided into three main parts: In the first or initial part are the geometry and operational design conditions submitted, the blade twist determined and the performance and loads under these conditions calculated. The design point is hereby defined as the transition between the exponential- and flat-rate areas when referring to Figure 2.9. In the second part has the user the possibility to execute the program for other wind speeds, and get the results for performance and loads under these conditions, with the rotor working under maximum efficiency. This part is mainly intended for the exponential area of the power curve; at wind speeds lower than the design wind speed. In the third and final part of the program, it is possible to submit the wind speed and the power output. It is here in other words possible to reduce the efficiency of the rotor by dictating the power it should deliver, which is especially interesting at wind speeds higher then the design wind speed – in the flat-rated area of Figure 2.9.

Further, as a result of the program being intended for the use on existing or preliminary designs, there are no calculations with regards to materials and their allowable/unallowable stress values. The results are not intended for actual strength calculations, displacements and sizing, but rather that the results of the initial run of the program, which are those of the design point of the wind turbine, are defined as the maximum allowable. With the execution of part 2 or 3 of the program, these results can then be compared to those of part 1 and evaluated accordingly. As shown under 2.5, are the load calculations based on the presumption that the material of the rotor blades are of an isotropic type, as e.g. most metals, and not composite materials, which have anisotropic properties. Calculations on composite materials are much more complex and

time-consuming and would exceed the time frame and amount of work that can be dedicated to this work. Also, the knowledge regarding the materials used, the manufacturing methods and the composition of the structure would have had to be comprehensive and exact, for the effort of implementing composite calculations to actually pay off. One would also conclude, that information regarding type of airfoil, materials and composition is hard to come by, as this is frequently subject to secrecy in the industry. Even though almost all of the large, modern wind turbines today have rotor blades consisting of composite materials, mostly GRP (Glass-reinforced plastic), it is the idea that the main purpose of this calculation tool still would apply – to compare performance and rotor-strength of a given rotor under different operational scenarios.

4.1.1 Data types

As this program has to store a lot of data and often many values of the same variable, as e.g. the radius to each of the blade elements, the data type “arrow” is used to initialize these types of variables. In practice, this is done by defining the length, or number of values in this arrow in the heading of the program, which allows an establishment of values of the type “double” of this number, allocated to each variable defined with this arrow. When initializing, the applicable variable is established with a name of the following structure [20]:

dname[Arrowlength]

The arrows can be explained as dimensions in the program and, as mentioned above, is the blade radius one of these dimensions, including all of the different data stored for each blade element. Another such dimension is the number of rotation angles, which will be calculated by the program. As explained under 2.5.2.1 vary the loads on the blades dependent on rotor angle due to gravity. This means that for some of the variables describing loads, there is not just the need to store data for each blade element at a given radius, but also at a given rotation angle, and hence a second dimension/arrow. For the normal- and shear flows/stresses are the calculations further carried out in predetermined positions in the torque box, which results in a third dimension needed for data storage. The predetermined number is the definition of this arrow-length in the heading. This means that there are some variables initialized in the following ways:

dname2[Arrowlength][Arrowlength2], and:

dname3[Arrowlength][Arrowlength2][Arrowlength3]

In addition to these arrow variables, there are variables defined as “double” and “integer” in the program.

In other words, the definitions of Arrowlength, Arrowlength2 and Arrowlength3 in the heading determine directly the number of blade elements, number of rotor angles and number of control positions in the torque box respectively. A simplified and structural overview of the program source file is attached in the Appendix C. The whole source file is found to be too lengthy to attach as an Appendix.

4.2 Input values and initiation

Now the initiation of the program and the values that are submitted by the user will be presented. The input values can either be known, guessed or experimental values in connection with the preliminary-sizing phase. Referring to Figure 4.1 the input values are:

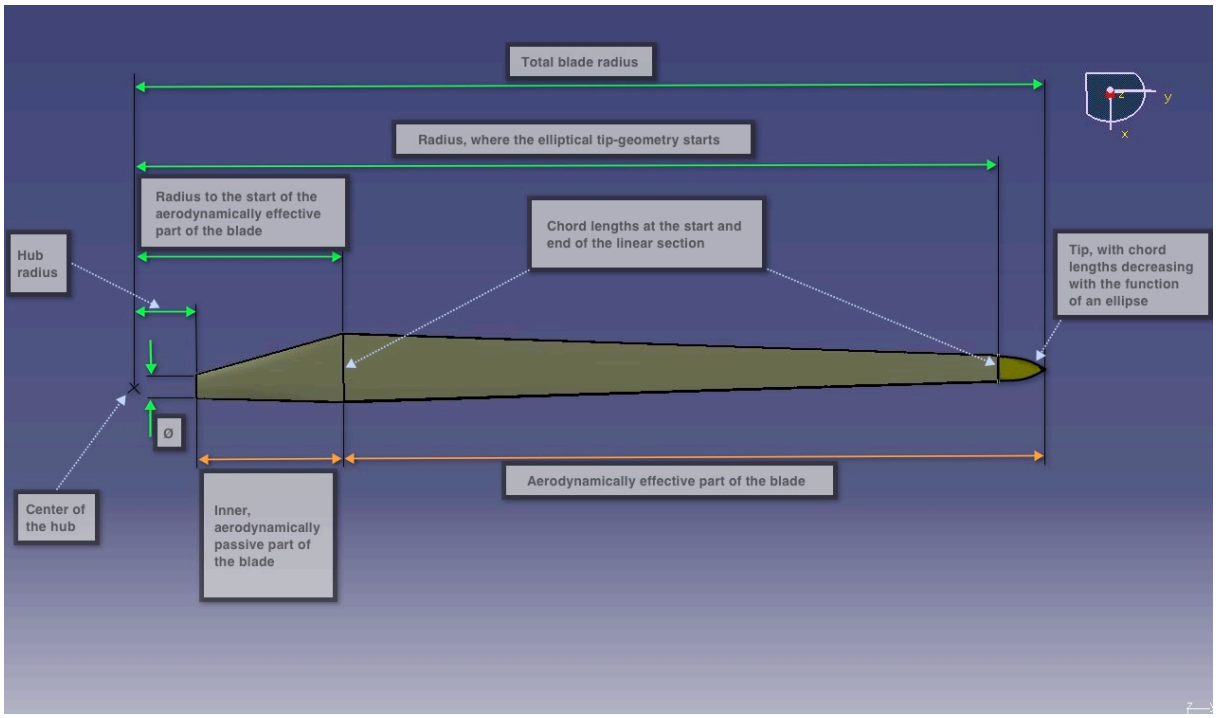

Figure 4.1: Rotor geometry read by the calculation program

1. Air temperature, T [K]
2. Air pressure, p_a [PA]
3. Number of blades, B [-]
4. Wind speed, v_1 [m/s]
5. Rotor-revolutions per minute, rev_{min} [min^{-1}]
6. Blade radius, r_{blade} [m]
7. Relative radius at the start of the aerodynamically effective blade, $r_{r,S}$ [-]
8. Relative radius at the end of the hub, $r_{r,H}$ [-]
9. Relative radius near the tip, where the chord starts to decrease in the form of an ellipse, $r_{r,E}$ [-]
10. Chord-length at the beginning of the effective blade, c_s [m]
11. Chord-length near the end, before the elliptical drop, c_e [m]
12. Position of the front spar relative to chord-length, s_{fs} [-]
13. Position of the rear spar relative to chord-length, s_{rs} [-]
14. Maximum thickness of the upper flange, $t_{uf,max}$ [mm]
15. Maximum thickness of the front spar, $t_{fs,max}$ [mm]
16. Maximum thickness of the lower flange, $t_{lf,max}$ [mm]

17. Maximum thickness of the rear spar, $t_{rs,max}$ [mm]
18. Minimum thickness of the upper flange, $t_{uf,min}$ [mm]
19. Minimum thickness of the front spar, $t_{fs,min}$ [mm]
20. Minimum thickness of the lower flange, $t_{lf,min}$ [mm]
21. Minimum thickness of the rear spar, $t_{rs,min}$ [mm]
22. Total mass of the blade, m_{blade} [kg]
23. Mass of the effective part of the blade relative to total mass, $m_{r,AE}$ [-]
24. Radius of the circular part of the blade attached to the hub, $r_{cross,s}$ [m]

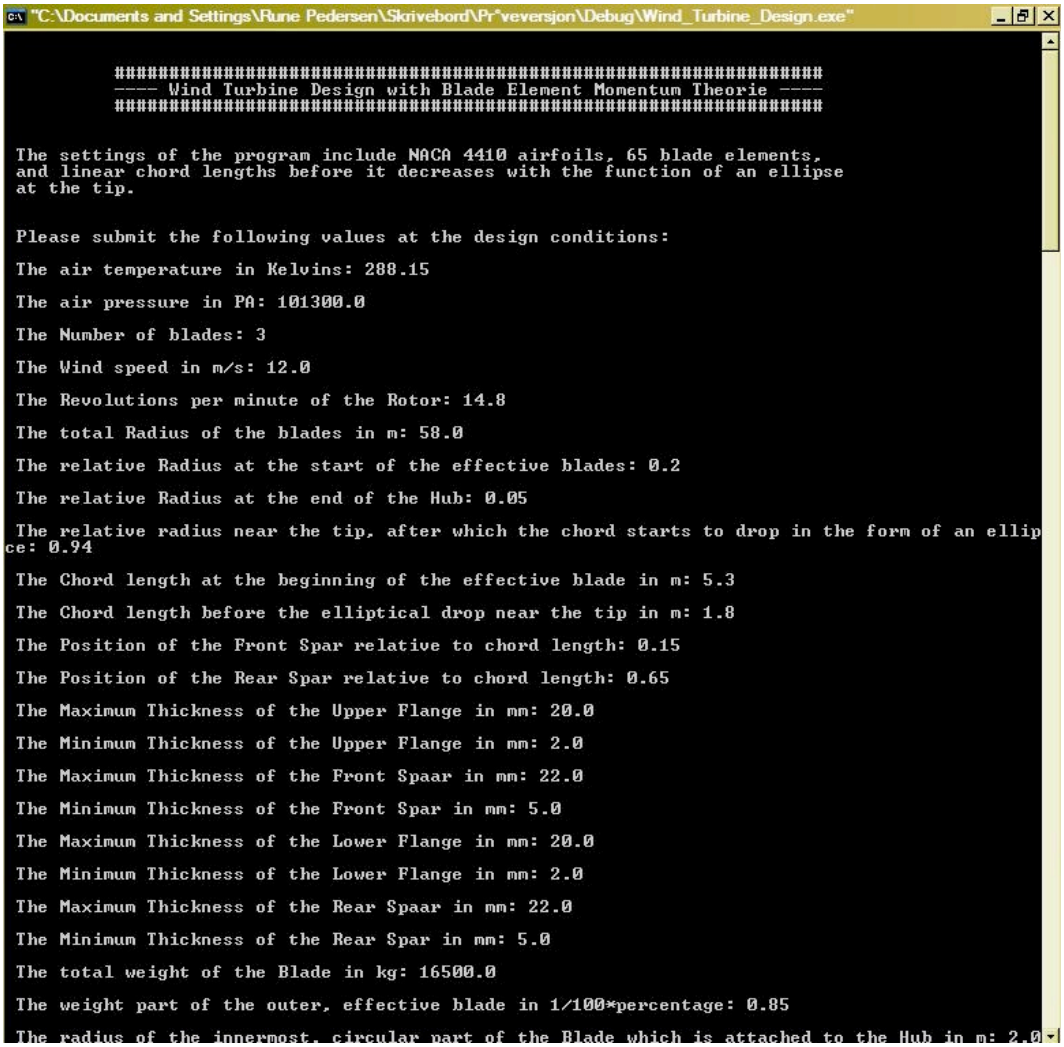

Figure 4.2: User window and input values

Out of these input values, the program immediately calculates some further, necessary values before it enters the BEM-iterations. Out of the submitted start values other details regarding the geometry can be determined:

Atmospheric conditions [21]:

$$a = \sqrt{(T \cdot R \cdot \kappa)} \quad \textbf{(4.1)}$$

a Speed of sound [m/s]

R Specific gas constant for air, 287 [J/(kg*K)]

κ Heat capacity ratio, 1,4 [-]

$$\rho = \frac{p_a}{(R \cdot T)} \quad \textbf{(4.2)}$$

ρ Density of the air [kg/m^3]

$$P_T = 0.5 \cdot \rho \cdot \pi \cdot r_{blade}^2 \cdot v_1^3 \quad \textbf{(4.3)}$$

Blade element width:

$$dr_{be} = \frac{\left(r_{blade} \cdot (1 - r_{RS})\right)}{n_{BE}} \quad \textbf{(4.4)}$$

dr_{be} Width of each blade element [m]

n_{BE} Number of blade elements [-]

The number of blade elements, n_{BE}, is determined in the heading of the calculation program as described under 4.1.1, and cannot be altered by the user. When the program is executed, there is given a message of how many blade elements the program is working with at that time, along with the other start-up messages, containing information about number of rotor angles to be considered and number of positions in the torque box where the shear- and normal flow/stress will be calculated. For this work the program is set up with 65 blade elements. This is a sufficient number to reach accurate results, and at the same time a number low enough to keep the calculation time per run at a conveniently short.

Blade rotational speed, Ω:

$$\Omega = \frac{rev_{\min} \cdot 2 \cdot \pi}{60s \cdot \min^{-1}} \quad \textbf{(4.5)}$$

Radiuses:

$$r_H = r_{blade} \cdot r_{r,H} \quad \textbf{(4.6)}$$

r_H Hub radius [m]

$$r_{S,AE} = r_{r,S} \cdot r_{blade} \quad \textbf{(4.7)}$$

$r_{S,AE}$ Radius at the start of the aerodynamically effective part of the blade [m]

$$r_E = r_{r,E} \cdot r_{blade} \quad \textbf{(4.8)}$$

r_E Radius to the start of the tip geometry [m]

Mass of the two different parts of the blade:

$$m_{AE} = m_{r,AE} \cdot m_{blade} \quad \textbf{(4.9)}$$

m_{AE} Mass of the aerodynamically effective part of the blade [kg]

$$m_{AP} = m_{blade} - m_{AE} \quad \textbf{(4.10)}$$

m_{AP} Mass of the aerodynamically passive part of the blade [kg]

Area of blade sections:

$$A_{blade,HA} = \pi \cdot r_{cross,s}^2 \quad \textbf{(4.11)}$$

$A_{blade,HA}$ Area of the blade hub-attachment cross section [m^2]

$$A_{blade,AE} = 0.068801 \cdot c_s^2 \quad \textbf{(4.12)}$$

$A_{blade,AE}$ Area of the end of the aerodynamically passive part of the blade [m^2] The factor 0.068801 is derived under 3.1.

4.3 Program, Part 1

With the initial values determined, the program now enters the first part of the program, which calculates the performance and loads for the design conditions. The first sequence here contains a “for” loop, and two “do-while” loops. These loops hold the entire codes and equations necessary to calculate the twist of the rotor, the maximum power output and power coefficient of the rotor, as well as the foundation for the load calculations at the submitted design conditions. The nature and functions of these loops will now be explained, and a simplified overview of the whole sequence can be seen in Figure 4.3. This figure will serve as support for the forthcoming text:

```
#include <math.h>
#include <stdio.h>
#define Arrowlength 65 /* Number of blade elements */

void main(void)
{
    for(iNumber_of_Elements == 0 ; iNumber_of_Elements < Arrowlength ; iNumber_of_Elements ++)
    {
        /*Here are the initial geometric values for the blades determined.*/
        iOuterCouter = 0;
        iTest = 1;
        do
        {
            dTorque_aerodynamic[iNumber_of_Elements] = dTorque_old;
            /*In this loop is the optimum pitch found, and thereby also defining the twist of the blades.
            The pitch alterations are here executed based on the results from the evaluation
            from the last run, and the variables "iOuterCounter, "iFortegn" and "iTest".

            Before entering the inner do-while loop are the initial aerodynamic parameters calculated.*/
            iCounter = 0;
            do
            {
                dAxial_Induced[iNumber_of_Elements] = dAxial_Induced_old;
                dTangential_Induced[iNumber_of_Elements] = dTangential_Induced_old;

                /* In this loop is the pitch angle considered fixed, and the flow parameters
                accrordingly iterativ calculated, based on the BEM Tehory.*/

                ddiff1 = dAxial_Induced[iNumber_of_Elements] - dAxial_Induced_old;
                ddiff2 = dTangential_Induced[iNumber_of_Elements] - dTangential_Induced_old;
                iCounter =+ 1;
            }while(ddiff1 > dAccuracy || ddiff2 > dAccuracy);
            /*Following the BEM calculations are the torque for this pitch angle evaluated.*/

            ddiff = dTorque_aerodynamic[iNumber_of_Elements] - dTorque_old;

            /*Based on the result from "ddiff", number of iOuterCounter, and value of
            "iFortegn" are the correct pitch command assigned*/

            if(iTest != 0)
            {
                /*Pitch mode 1, 2, 3 or 4 is chosen*/
            }
            iOuterCounter =+ 1;
        }while(iTest != 0);
    }
```

Figure 4.3: Simplified overview of program sequence

The “for” loop runs through the number of blade elements, using the – in programming typical – interval: [0 – (maximum number -1)]. The variable for the number of blade elements is “iNumber_of_Elements”.

For the first blade element the radius to the control-point in the middle of it is calculated as follows:

$$r_{be,1} = r_{S,AE} + \frac{dr_{be}}{2} \quad \textbf{(4.13)}$$

$r_{be,1}$ Radius to the middle of the first blade element [m]

For any other given blade element, the radius is:

$$r_{be,i} = r_{be-1} + dr_{be} \quad \textbf{(4.14)}$$

$r_{be,i}$ Radius to the middle of a random blade element [m]
r_{be-1} Radius to the middle of the previous blade element [m]

The chord-length with respect to radius are determined through the following equations, dependent on weather the applicable blade element is located in the area of linear changing chord-lengths, or in the tip where the chord-lengths decrease with the function of an ellipse:

$$f_{c1}\left(r_{be,i}\right) = \frac{\left(c_e - c_s\right)}{r_{blade} \cdot \left(r_{r,E} - r_{r,S}\right)} \cdot \left(r_{be,i} - r_{S,AE}\right) + c_s \quad \textbf{(4.15)}$$

$f_{c1}(r)$ Chord-length at a given spot along the radius, before the tip geometry starts [m]

The term $\frac{\left(c_e - c_s\right)}{r_{blade} \cdot \left(r_{r,E} - r_{r,S}\right)}$ is hereby dedicated its own variable in the program, and then used with its applicable radius, as in the BEM-iteration to achieve the results.

$$f_{c2}\left(r_{be,i}\right) = \frac{c_e}{\left(r_{blade} \cdot \left(1 - r_{r,E}\right)\right)} \cdot \sqrt{\left(\left(r_{blade} \cdot \left(1 - r_{r,E}\right)\right)^2 - \left(r_{be,i} - \left(r_{r,E} \cdot r_{blade}\right)\right)^2\right)} \quad \textbf{(4.16)}$$

$f_{c2}(r)$ Chord-length at a given spot along the radius, in the tip geometry [m]

As mentioned earlier, is the program set up to decrease the chord-length after the radius $r_{RE} \cdot r$ with the function of an ellipse. The basis for (4.16) is the standard equation for a generally located ellipse [10]:

$$\frac{(x-x_0)^2}{a^2}+\frac{(y-y_0)^2}{b^2}=1 \qquad \textbf{(4.17)}$$

In this connection are: y_0 = 0, x_0 = $r_{RE}\cdot r_{blade}$, a = $r_{blade}\cdot(1-r_{RE})$, b = c_s, and the equation is solved with respect to *y* to result in (4.16).

The area of a given blade element is determined as follows:

$$A_{be,i}=0.068801\cdot\left(f_{c,i}\left(r_{be,i}\right)\right)^2 \qquad \textbf{(4.18)}$$

$A_{be,i}$ Area of a given blade element [m^2]

$f_{c,i}\left(r_{be,i}\right)$ Chord-length of the applicable blade element [m]

During the run of the "if"-loop, it is prepared to calculate the volume and CoG of the aerodynamically effective blade upon completion of the loop, through numeric integration in the same manner as shown under 2.3.1 and in (2.40). In this connection is a variable established, which sums each of the blade elements' volume contribution, and thereby multiplying the first and the last value by 0.5, conform to the Trapezoid Method.

With these geometric values now available, the sizes "local solidity" and "tip-speed ratio" are calculated as described in (2.29) and (2.32). The compiler enters now two interlaced iteration loops – both of the "do-while" type – which determine the best pitch angle for this blade element with respect to torque (outer iteration), and the BEM-iteration at this pitch-angle (inner iteration). The pitch angle determination of the outer loop ultimately also determines the twist of the blade, as it identifies the relation of the pitch angles between each blade element.

4.3.1 Pitch/twist calculations

It is here still referred to Figure 4.3. In the outer iteration loop is the pitch angle altered for each run and then evaluated at the end of the loop by comparing the torque of the blade element at this pitch angle with that of the previous pitch angle. In this connection is the stop-criterion the value of a dedicated integer variable, "itest", which continues the run of the loop as long as its value is different from zero. Another integer variable, "iOuterCounter", is used to count and control the number of runs, which is especially important during the first few runs, to secure that enough alterations have been carried out, to affirm that indeed a peak has been found. The comparison of the torques from the current and previous run is executed through a variable, "ddiff" that subtract the previous torque from the new. For the first run is simply this comparison bypassed, as there is not enough data to possibly perform this yet. This is executed through an if-query that picks up the counting variable on its first run. Yet another integer variable, "iFortegn", is used to recognize if the alteration in

pitch is positive or negative. The value 1 represents hereby a positive alteration, while 0 indicates a negative. Prior to the first run is the value set at 1.

The alteration of the pitch angle is controlled through 4 different alteration-modes on the basis of the mentioned variables:

Mode #1 alters the pitch angle with +0.05deg, sets “iFortegn” and “itest” to 1 and is carried out if the either of the following statements are true:

- iOuterCounter = 0
- ddiff > 0 AND iFortegn = 1

Mode #2 alters the pitch angle with -0.05deg, sets “itest” to 1 and “iFortegn” to 0 and is carried out if:

- ddiff < 0 AND iOuterCounter = 1
- ddiff > 0 AND iFortegn = 0

Mode #3 alters the pitch angle with -0.05deg, sets “itest” and “iFortegn” to 0. When this mode occurs has a peak been found after a series of positive alternations, and the loop can be terminated. The following circumstances applies:

- ddiff < 0 AND iFortegn = 1 AND iOuterCounter $\neq 1$

Mode #4 alters the pitch angle with +0.05deg, sets “itest” to 0 and “iFortegn” to 1. When this mode occurs has a peak been found after a series of negative alterations, and the loop can be terminated. The following circumstances applies:

- ddiff < 0 AND iFortegn = 0

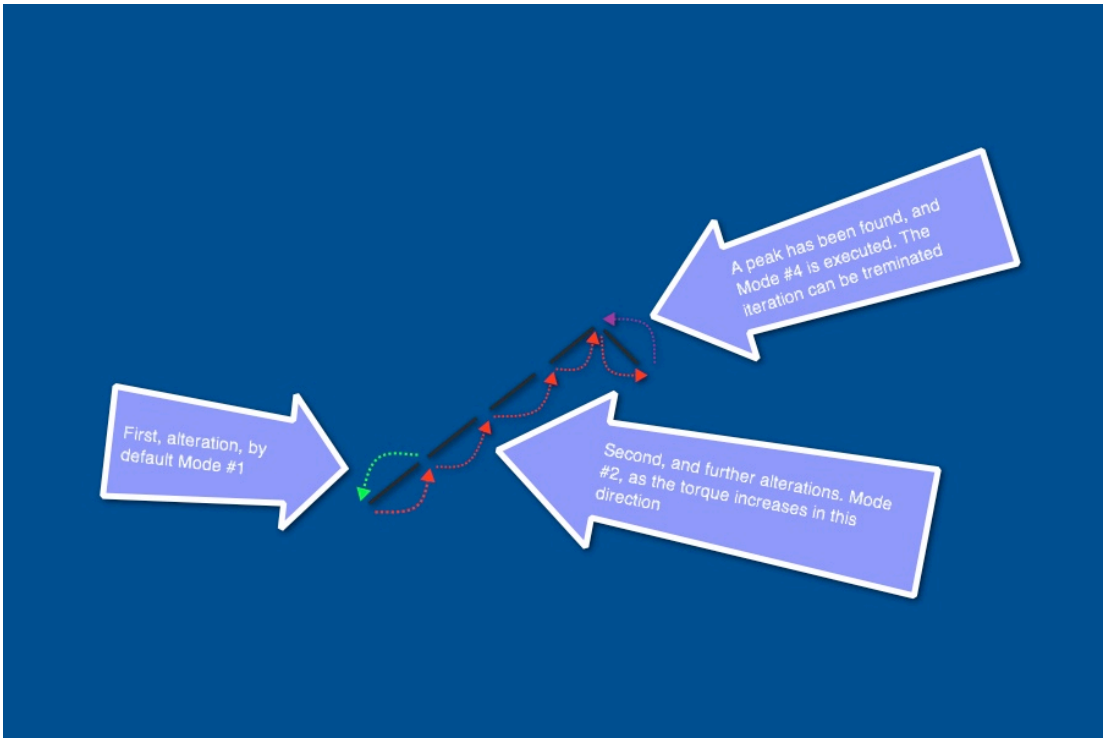

Figure 4.4: Example of pitch alterations

Before the torque-test and subsequently pitch alteration take place, preparations are made for the BEM-calculations that are carried out first in the inner do-while loop. Based on the variables iNumber_of_Elements - which identifies which blade element that currently is being calculated – and the iOuterCounter for the outer- and iCounter for the inner iteration, are the preparations made accordingly:

- If iNumber_of_Elements = 0 AND iOuterCounter = 0 AND iCounter = 0:

$$\alpha_i = \left(-0.018 \cdot iNumber\_of\_Elements + 14.0\right) \cdot \frac{\pi}{180} \quad \textbf{(4.19)}$$

α_i Initial AoA [rad]

$$\beta_i = \frac{\pi}{2} - \frac{2}{3} \cdot \arctan\left(\frac{1}{\lambda_r}\right) \quad \textbf{(4.20)}$$

β_i Initial relative flow angle [rad]

$$\gamma_i = \alpha_i + \beta_i \quad \textbf{(4.21)}$$

γ_i Initial pitch angle [rad]

The details to (4.19) are derived through testing and debugging, with the goal to obtain the values for AoA, relative flow angle and pitch angle as close to the end values as possible, and thereby keeping the calculation time as short as possible. The equations (4.20) and (4.21) are from [7]. In this run, the program next calculates the aerodynamic coefficients as derived under 3.2, and the axial

and angular induction factors a and a' are determined through (2.30) and (2.31) – solved for a and a' respectively – before the compiler continues to the inner iteration [7] and [9]:

$$a = \left(1 + \frac{4 \cdot \left(\cos\left(\beta_i\right) \right)^2}{\sigma' \cdot \left(c_l \cdot \sin\left(\beta_i\right) + c_d \cdot \cos\left(\beta_i\right) \right)} \right)^{-1} \quad \textbf{(4.22)}$$

$$a' = \left(1 - a\right) \cdot \left(\frac{\left(\sigma' \cdot \left(c_l \cdot \cos\left(\beta_i\right) - c_d \cdot \sin\left(\beta_i\right) \right) \right)}{4 \cdot \lambda_r \cdot \left(\cos\left(\beta_i\right) \right)^2} \right) \quad \textbf{(4.23)}$$

In some existing applications that also use the BEM-method, are frequently dedicated equations used to calculate entry values for a and a' when initiating the BEM calculations. That was tested in this program, but found not to be necessary and the actual BEM-equations used inside the iteration for a and a' were also used upon entry.

- Else if iNumber_of_Elements $\neq 0$ AND iOuterCounter = 0 AND iCounter = 0:

$$\gamma_i = \gamma_{be-1} - 0.2 \cdot \frac{\pi}{180} \quad \textbf{(4.24)}$$

γ_{be-1} Pitch angle reached for the previous blade element [rad]

The initial relative flow angle βi is calculated by (4.20)

$$\alpha_i = \gamma_i - \beta_i \quad \textbf{(4.25)}$$

The details to (4.24) are also derived through testing and debugging to achieve an initial value as close to the end-result as possible. Following these equations, the compiler continues to the inner iteration after the aerodynamic coefficients have been calculated as under 3.2, and the induction factors by (4.22) and (4.23).

- Else if iOuterCounter $\neq 0$

If iOuterCounter is higher than zero, it means the compiler has been at the end of the outer do-while loop and been assigned a pitch alternation mode. This is executed through an if-query, and further “ifs” make sure that the correct actions are performed based on the current pitch mode. Next, the initial relative flow angle and initial AoA are calculated according to (4.20) and (4.25), before proceeding to the inner iteration loop, are the aerodynamic coefficients and induction factors calculated in the same manner as above.

4.3.2 BEM calculations

This text still refers to Figure 4.3. In this loop is the pitch angle considered fixed, and the according flow parameters are iteratively calculated based on the geometry, atmospheric conditions and constraints within the BEM-calculations. The calculations follow the philosophy from 2.3, and use the equations (2.22) to (2.36).

As mentioned earlier, uses also this loop an integer variable, “iCounter”, to count and control the number of runs. The stop-criterions for this loop are the axial- and angular induction factors *a* and *a´* and when the values of these have stagnated. This is done by defining the wanted accuracy of these values through a variable, “dAccuracy”, and then by checking the changes of *a* and *a´* after each run. The values of the current run are stored as the old values before a new run is started and then compared to the new results at the end.

If entering the loop and the value of “iCounter” is zero, is the storing of the old values for *a* and *a´* bypassed, as no data for this exists. In the same manner as with the outer do-while loop is the compiler after the first run simply being directed to the top for a second run. First after the second run is enough data being gathered to perform the tests regarding the stop criterions. Beside *a* and *a´* are the values that constantly are being updated the wind speeds v_2 and v_3, α, β, the aerodynamic coefficients – which also here are calculated with the aid of the equations obtained by the use of XFOIL and Excel – and the hub- and tip losses. This in turn leads to the results for the forces and moments being updated.

As the calculations for the aerodynamic coefficients are final in this loop, this section also includes the already mentioned control of the Mach number, and applies a correction for the compressibility effect in the case the current Mach number is equal to, or exceeds the number 0.3. The correction factor is called “The Prandl-Glauert-Rule”, and is calculated as follows [12]:

$$\beta_{PG} = \frac{1}{\sqrt{\left(1 - M^2\right)}} \tag{4.26}$$

β_{PG} Correction factor according to the Prandl-Glauert-Rule [-]

M Local Mach number [-]

This rule is valid for Mach numbers in the interval [0.3 – 0.7], and for small AoA’s [12]. This is found to be unproblematic in this work however, as even the highest Mach numbers reached here are far from 0.7. Further, as the highest Mach numbers – and where the correction factor might apply – occur towards the tip of the blades due to the increasing speed from the rotation, does this mean that the applicable AoA’s are small, as this value is inversely proportional to the radius. This will be shown and proved in the chapter that addresses the results.

The local Mach number is calculated as follows:

$$M = \frac{v_r}{a} \tag{4.27}$$

The values v_r and a are calculated by (2.56) and (4.1)

The corrected aerodynamic coefficients then become:

$$c_{l,c} = c_l \cdot \beta_{PG} \tag{4.28}$$

$c_{l,c}$ = Corrected lift coefficient [-]

$$c_{d,c} = c_d \cdot \beta_{PG} \tag{4.29}$$

$c_{d,c}$= Corrected drag coefficient [-]

$$c_{m,c} = c_m \cdot \beta_{PG} \tag{4.30}$$

$c_{m,c}$= Corrected moment coefficient [-]

One problem regarding this compressibility correction within the BEM-iteration has to be handled, however: It is namely frequently experienced that the BEM-iteration never reaches a conclusion when the Mach numbers are close to 0.3, and that the program subsequently crashes. This is due to the relatively large changes to the aerodynamically coefficients when the correction is applied, which in turn affect all of the other parameters, including the induction factors that have to stagnate to a nearly fixed value for the loop to be terminated. Instead the values just changes back and forth as the Mach number fluctuate around 0.3, and the loop never comes to an end. To counteract this, the section that calculates the new Mach number is added a code, which prevents the new Mach number from dropping back below 0.3, once it has exceeded this number. This section is shown in Figure 4.4:

```
if(iCounter == 0)
{
    dMach[iNumber_of_Elements] = dLocal_relative_speed[iNumber_of_Elements]/dsonic_speed;
}

else
{
    if(dMach[iNumber_of_Elements] > 0.3 || dMach[iNumber_of_Elements] == 0.3)
    {
        dMach[iNumber_of_Elements] = dLocal_relative_speed[iNumber_of_Elements]/dsonic_speed;

        if(dMach[iNumber_of_Elements] < 0.3)
        {
            dMach[iNumber_of_Elements] = 0.3;
        }
    }

    else
    {
        dMach[iNumber_of_Elements] = dLocal_relative_speed[iNumber_of_Elements]/dsonic_speed;
    }
}
```

Figure 4.5: Control of the Mach correction in the program

This solution may reduce the accuracy of the results, but as the correction factor is applied suddenly as the Mach number exceeds 0.3 and changes the coefficients quite dramatically, this in turn also affects the other results as a big leap of their values. As the whole concept of the iteration loop is to consistently narrow the equations down to fixed values, a way had to be found to keep the values from fluctuating eternally and thereby not reaching a conclusion.

The changes for a and a' are stored through two variables, “dDiff” and “dDiff2”, which subtract the old values from the new and then are compared to “dAccuracy” in the end-test of the loop. If both of these variables have values less than “dAccuracy”, the loop is terminated and the compiler continues to the pitch control section explained under 4.3.1. The value of dAccuracy is set to 10^{-7}. In the case that a pitch angle peak was found during the last run, and the pitch has been changed to this value in the current run, is also the variable “itest” now changed to zero from either pitch mode #3 or #4. Following the completion of the inner loop is subsequently also the outer iteration loop immediately terminated, as the end criterion “itest” = 0 is met.

Following the completion of the two do-while loops have all the relevant data for the current blade element been calculated and this is now stored in the text file “Results_WTD_1” before the program moves to the next blade element and starts at the top of the for-loop again. The torque contribution for the applicable blade element is additionally being summed to a variable, in a numeric integration process equal to the one for the volume calculation explained under 4.3. This allows the overall Power of the rotor to be calculated upon completion of the for-loop.

4.3.3 BEM-Results of Part 1

With the for-loop now completed, the results for the numeric integrations for volume, CoG and torque can be determined:

$$V_{AE} = \int_{r_{S,AE}}^{r_{blade}} A_{be,i}\left(r_{be,i}\right) dr = dSum\_Volume \cdot dr_{be} \tag{4.31}$$

V_{AE}	Total volume of the aerodynamically effective part of the blade [m^3]
dSum_Volume	Numeric integration value obtained in the for-loop [m^2]

$$\bar{r}_{blade,AE} = \frac{\int_{r_{S,AE}}^{r_{blade}} A_{be,i}\left(r_{be,i}\right)\cdot r_{be,i}\,dr}{\int_{r_{S,AE}}^{r_{blade}} A_{be,i}\left(r_{be,i}\right)dr} = \frac{\left(dSum\_Volume\_radius\cdot dr_{be,i}\cdot r_{blade}\right)}{V_{AE}} \quad \textbf{(4.32)}$$

$\bar{r}_{blade,AE}$ CoG of the aerodynamically effective blade [m]

$dSum\_Volume\_radius$ Numeric integration value obtained in the for-loop [m^2]

While the value *sSum_Volume* simply is a summation of each of the blade elements' area, conform to the Trapezoid Method, the value *dSum_Volume_radius* also includes information of the radius of the blade elements. This is done in the following manner in the for-loop:

$$dSum\_Volume\_radius = dSum\_Volume\cdot\frac{r_{be,i}}{r_{blade}} \quad \textbf{(4.33)}$$

$$T_{total} = \int_{r_{S,AE}}^{r_{blade}} dT\,dr = dSum\cdot dr_{be,i} \quad \textbf{(4.34)}$$

T_{Total} Total torque of the rotor [Nm]

dSum Numeric integration value obtained in the for-loop [N]

Based on these results, further values can be calculated:

$$\rho_{blade,AE} = \frac{m_{AE}}{V_{AE}} \quad \textbf{(4.35)}$$

$\rho_{blade,AE}$ Density of the aerodynamically effective blade [kg/m^3]

$$P_0 = T_{total}\cdot\Omega \quad \textbf{(4.36)}$$

$$C_P = \frac{P_0}{P_T} \quad \textbf{(4.37)}$$

C_P Power coefficient of the rotor [-]

With the total torque of the rotor at design conditions now available, it is also possible to calculate the torque function for the gears and generator. The load torque function has the following form [22]:

$$T_{load} = c_{gen} \cdot rev_{\min}^2 \quad \textbf{(4.38)}$$

T_{load} Torque from gears and generator [Nm]

c_{gen} Constant for the load torque function [(kg∗m^2∗min^2)/s^2]

rev_{min} Rotor revolutions [min^{-1}]

As the rotor revolutions are the variable in (4.38), c_{gen} the only value that needs to be calculated for the load torque function to be determined. This constant is chosen during the design phase of the wind turbine, to ensure that the desired rotational speed of the rotor is delivered at the desired torque. This is configured for the design conditions, in the same manner as here [22]. For the rotations of the rotor to remain constant at the design wind speed, the load torque has to be equal to that of the rotor, and the solution of the constant thereby become:

$$c_{gen} = \frac{T_{total}}{rev_{\min}^2} \quad \textbf{(4.39)}$$

Now, a new for-loop is entered, which also runs through all of the blade elements, and here is the twist of the rotor calculated and stored in the text file “Twist”. Additionally is the radius to each of the blade elements’ middle point stored in the text file “Radius_Elementer”. These values are later used in Excel during the evaluation of the results. During the first for-loop was the torque contribution from each blade element monitored, and the blade element with the largest contribution stored as the variable “iMax_Position”, and the twist of the rotor is now being calculated with respect to the pitch angle of this blade element. In this way is not only the twist of the blade conveyed, but also which element that has the highest torque contribution. The equation for a given blade elements’ twist with respect to “iMax_Position” is as follows:

$$\psi_{be,i\max} = \gamma_{be,i\max} - \gamma_{be,i} \quad \textbf{(4.40)}$$

$\psi_{be,imax}$ Twist with respect to “iMax_Position” [rad]

$\gamma_{be,imax}$ Pitch angle for “iMax_Position” [rad]

With the completion of this for-loop is now a message given, that the blade design now is finished, and that the performance of the rotor has been calculated.

Before the calculation on the structure can start however, the information about the inner, aerodynamically passive parte of the blade has to be identified. Further, all of the loads from the BEM calculations have to be determined for each blade element in the way explained under 2.5.2. To be able to fully utilize the BEM results, all of the blade elements have to be considered a fixed bearing in the same manner as the blade/hub attachment, and that they support all of the loads from the blade section located outside itself.

The investigations on the aerodynamically passive part of the blade are not as comprehensive as on the outer part, in that this is not parted into several

sections where the calculations can be executed. It is also considered that this part has a different structure then the outer part, so calculations similar to those on the torque box of the aerodynamically effective blade are not carried out. Only the total forces and moments on the hub attachment are included, but these also include the loads induced by the mass of the inner part of the blade. In any case is it the approach of this work not to exceed the loads generated under the design conditions, and by monitoring the loads of the outer blade part and the forces and moments acting at the hub attachment, it is assumed that also the integrity of the inner part of the blade is maintained.

The program works with the constraints that the hub attachment has a cross section of a pure circle while the other end, the transition to the aerodynamically effective blade, has a cross section of the NACA 4410 airfoil. Between this is there a geometric linear transition from the one cross section to the other, based on the area:

The function for the linearization then becomes:

$$f_A(r) = da \cdot r + A_0 = \frac{\left(A_{blade,AE} - A_{blade,HA}\right)}{\left(r_{S,AE} - r_H\right)} \cdot \left(r - r_H\right) + A_{blade,HA} \tag{4.41}$$

$f_A(r)$ Area of a section in the aerodynamically passive part of the blade [m^2]

da Area linearization factor [m]

A_0 Area value for the linear function [m^2]

The volume of this part of the blade is hence defined as:

$$V_{AP} = \int_{r_H}^{r_{S,AE}} f_A(r)\,dr = \int_{r_H}^{r_{S,AE}} da \cdot r\,dr + A_0 \int_{r_H}^{r_{S,AE}} dr \tag{4.42}$$

V_{AP} Volume of the aerodynamically passive part of the blade [m^3]

This finally become the following equation:

$$V_{AP} = \left[0.5 \cdot da \cdot r^2 + A_0 \cdot r\right]_{r_H}^{r_{S,AE}} \tag{4.43}$$

Next is the CoG for the inner blade part calculated. This is done in the same way as described in (2.40):

$$\bar{r}_{AP} = \frac{\int_{r_H}^{r_{S,AE}} a(r) \cdot r \, dr}{\int_{r_H}^{r_{S,AE}} a(r) \, dr} = \frac{\left[\frac{1}{3} \cdot da \cdot r^3 + \frac{1}{2} \cdot A_0 \cdot r^2\right]_{r_H}^{r_{S,AE}}}{V_{AP}} \quad \textbf{(4.44)}$$

$\bar{r}_{AP}$ CoG of the aerodynamically passive part of the blade [m]

Now, from these results can the inertia force generated by the inner blade part be determined. This is done based on the theory from 2.5.2.2:

$$F_{c,AP} = m_{AP} \cdot \bar{r}_{AP} \cdot \Omega^2 \quad \textbf{(4.45)}$$

$F_{c,AP}$ Centripetal force, generated by the aerodynamic passive part of the blade [N]

Next enters the program three interlaced for-loops with the main purpose of calculating all of the resulting forces and moments on each blade element section in addition to the hub attachment. In these loops are also many text files being printed, which will be needed during the evaluation of the results. The structure of this sequence is presented in Figure 4.6:

```
#include <math.h>
#include <stdio.h>

#define Arrowlength 65 /* Number of blade elements */
#define Arrowlength2 6 /* Number of rotor angles to be considered*/
#define Arrowlength3 4 /* Number of positions in each of the walls in the torque box to be calculated*/

void main(void)
{
    for(iNumber_of_Elements == 0 ; iNumber_of_Elements < Arrowlength ; iNumber_of_Elements ++)
    {

        iVariable2 = iNumber_of_Elements;

        for(iVariable2 == iNumber_of_Elements; iVariable2 < Arrowlength ; iVariable2)
        {
            /* Here are the numeric integration that are the foundation for the load calculations
               executed, for the current blade element.
               Also the CoG for each blade segment is determined here through numeric integration.

               The calculations are carried out as described under 2.5.2, for the applicable
               blade segment*/
        }

        /*Here are the completed numeric integrations utilized, and the load cases that are independent
          from rotor angle carried out. These include torque, torque force, thrust, thrust moment,
          inertia, and torsion.The results are thereafter printed to the file "Loads_and_Zentroids1.txt"*/

        for(iRotor_Angle_Position == 0; iRotor_Angle_Position < Arrowlength2; iRotor_Angle_Position++)
        {
            /* In this loop are the loads generated by gravity included, dependent on the current
            rotor angle. These loads are shear force from gravity, normal force from gravity, and
            the bending moment generated by the shear force and the current blade segments' CoG.

            The normal force from gravity is therafter added to the inertia, to describe the total
            normal force. The shear force from gravity is added to that of the torque force, to
            describe the total shear force in the rotor plane. Finally are the bending moments from
            gravity and torque added, to identify the total bending moment in the rotor plane.

            These results are now added to "Loads_and_Zentroids1.txt"*/
        }
    }
}
```

Figure 4.6: Details to program sequence

The first for loop is build up as the previous ones, with the number of elements as the control variable, running from the first to the last. The next for-loop, however, is slightly different as it is completed in its entirety for each time the outer for-loop starts on a new blade element. The control variable for the second for-loop, “iVariable2”, is set to be equal to the current number of elements just under the command line for the outer for-loop, and the second for-loop then runs through the interval [iVariable2 ; (iNumber_of_Elements -1)]. By putting the equations for the forces, with their effective arms, and moments for the blade element/blade section in the second for-loop, is it in this way possible to identify the complete loads on them, as derived under 2.5.2. For example, when the first loop has come to blade element number 25, does this mean that the second for-loop executes calculations for the elements [25 ; 65], and thereby determining all of the loads for element number 25 through numeric integration, which are finished by the completion of the second for-loop.

As the results for each blade element are completed after the second for-loop, they are printed to the text files “Loads_and_Zentroids1”. These initial results to “Loads_and_Zentroids1” include volume, mass, CoG relative to both the current blade element and the hub in addition to all of the forces and moments, minus those that are dependent on rotor angle.

Now, the program enters the third for-loop in this section. This loop does not use the blade elements as control variable, but the number of rotor angles specified in the heading of the program as “Arrowlength2”. Up until now have just the loads that are independent from rotor angle been calculated, but in this loop are the loads from gravity identified and in that way also concluding the load calculations for the blade elements. These results are then appended in the “Loads_and_Zentroids1” file to the current blade element, and written to the rest of the three Excel files that contain the load cases dependent on rotor angle.

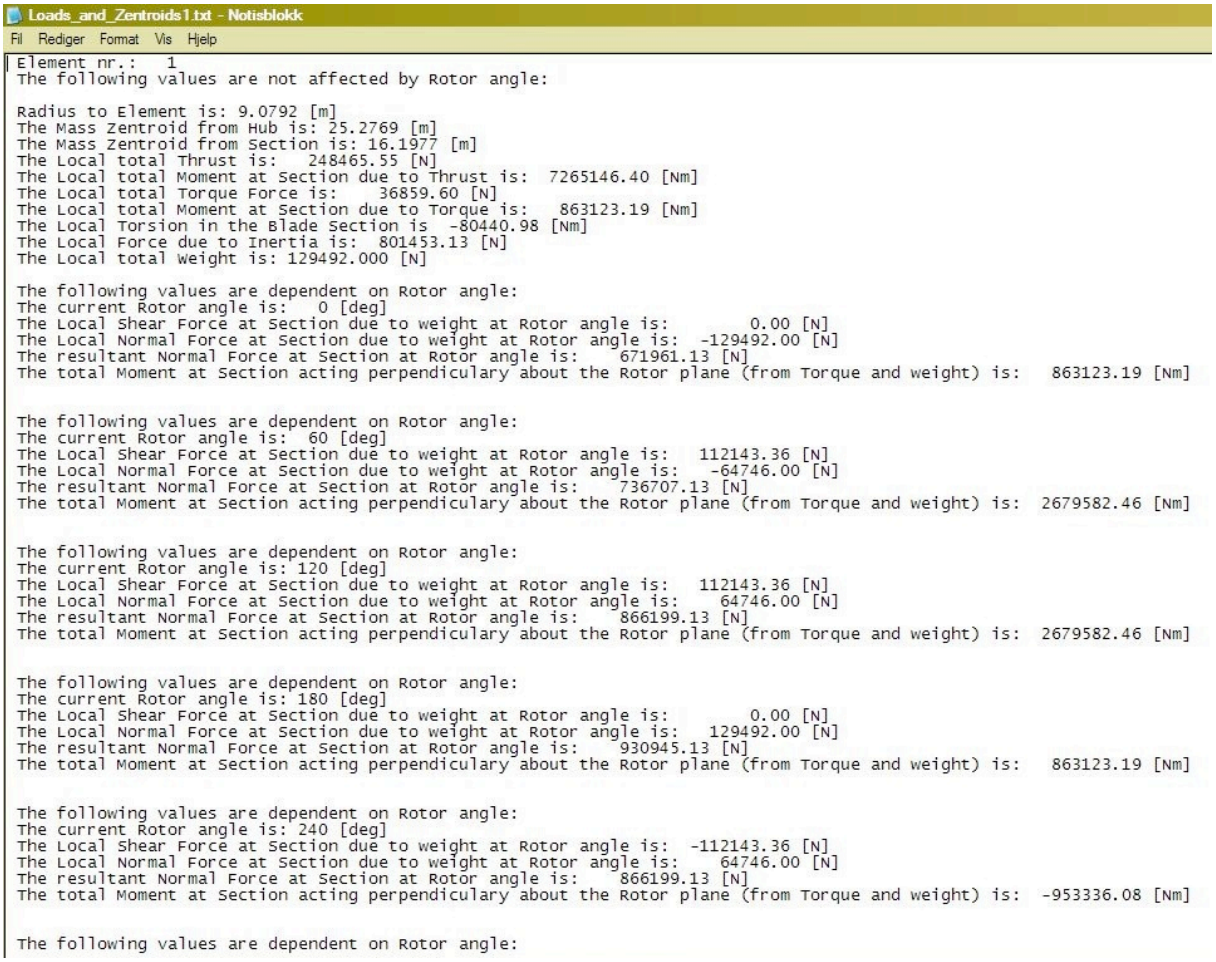

Loads_and_Zentroids1.txt - Notisblokk

Fil Rediger Format Vis Hjelp

```
Element nr.:   1
The following values are not affected by Rotor angle:

Radius to Element is: 9.0792 [m]
The Mass Zentroid from Hub is: 25.2769 [m]
The Mass Zentroid from Section is: 16.1977 [m]
The Local total Thrust is:   248465.55 [N]
The Local total Moment at Section due to Thrust is:  7265146.40 [Nm]
The Local total Torque Force is:    36859.60 [N]
The Local total Moment at Section due to Torque is:   863123.19 [Nm]
The Local Torsion in the Blade Section is  -80440.98 [Nm]
The Local Force due to Inertia is:  801453.13 [N]
The Local total Weight is: 129492.000 [N]

The following values are dependent on Rotor angle:
The current Rotor angle is:   0 [deg]
The Local Shear Force at Section due to weight at Rotor angle is:        0.00 [N]
The Local Normal Force at Section due to weight at Rotor angle is:  -129492.00 [N]
The resultant Normal Force at Section at Rotor angle is:    671961.13 [N]
The total Moment at Section acting perpendiculary about the Rotor plane (from Torque and weight) is:   863123.19 [Nm]


The following values are dependent on Rotor angle:
The current Rotor angle is:  60 [deg]
The Local Shear Force at Section due to weight at Rotor angle is:   112143.36 [N]
The Local Normal Force at Section due to weight at Rotor angle is:   -64746.00 [N]
The resultant Normal Force at Section at Rotor angle is:    736707.13 [N]
The total Moment at Section acting perpendiculary about the Rotor plane (from Torque and weight) is:  2679582.46 [Nm]


The following values are dependent on Rotor angle:
The current Rotor angle is: 120 [deg]
The Local Shear Force at Section due to weight at Rotor angle is:   112143.36 [N]
The Local Normal Force at Section due to weight at Rotor angle is:    64746.00 [N]
The resultant Normal Force at Section at Rotor angle is:    866199.13 [N]
The total Moment at Section acting perpendiculary about the Rotor plane (from Torque and weight) is:  2679582.46 [Nm]


The following values are dependent on Rotor angle:
The current Rotor angle is: 180 [deg]
The Local Shear Force at Section due to weight at Rotor angle is:        0.00 [N]
The Local Normal Force at Section due to weight at Rotor angle is:   129492.00 [N]
The resultant Normal Force at Section at Rotor angle is:    930945.13 [N]
The total Moment at Section acting perpendiculary about the Rotor plane (from Torque and weight) is:   863123.19 [Nm]


The following values are dependent on Rotor angle:
The current Rotor angle is: 240 [deg]
The Local Shear Force at Section due to weight at Rotor angle is:  -112143.36 [N]
The Local Normal Force at Section due to weight at Rotor angle is:    64746.00 [N]
The resultant Normal Force at Section at Rotor angle is:    866199.13 [N]
The total Moment at Section acting perpendiculary about the Rotor plane (from Torque and weight) is:  -953336.08 [Nm]


The following values are dependent on Rotor angle:
```

Figure 4.7: Example of results printed to "Loads_and_Zentroids.txt"

The last section before the compiler moves back to the top of the first for-loop to go to the next blade element, is to calculate dedicated integration values for moment from torque and thrust with respect to the hub attachment. These are set up exactly as for the blade elements, but consider the arms for the thrust- and force moments

Following the conclusion of these three for-loops has the foundation for the structural calculations in the torque box been laid, and the BEM results have now been fully utilized. The last thing that is done before moving on to the structural calculations on the torque box is to calculate the same values for the hub attachment that have been calculated for the blade elements during the previous sequence.

This is done by utilizing the values that were determined in (4.41) - (4.45), and additionally including dedicated numeric integration variables for the hub in the outer for-loop, ref. Figure 4.6. These variables prepare the calculations for the bending moments due to torque and thrust, which have to refer to the hub attachment, and not a blade element. The shear force and bending moment due to gravity is determined by using the total blade weight submitted by the user, and by combining this with the overall blade CoG. The CoG for the aerodynamically effective blade was derived in (4.32), and the CoG for the

inner, passive part of the blade in (4.44). Out of these two values the overall CoG is determined in the following manner:

$$\overline{r}_{blade} = \frac{\left(\left(\overline{r}_{blade,AE} \cdot m_{AE}\right) + \left(\overline{r}_{AP} \cdot m_{AP}\right)\right)}{m_{blade}} \quad \textbf{(4.46)}$$

$\overline{r}_{blade}$ Overall CoG of the blade [m]

Now, after the integration values for the hub has been utilized following the conclusion of the sequence in Figure 4.6, and the bending moments due to torque and thrust accordingly have been determined, a for-loop identical to the third for-loop in that figure is encountered. In this loop is the rotor angle the loop variable, and the following values are calculated for the hub attachment: Shear force and bending moment in the rotor plane due to torque and gravity, and total normal force due to inertia and gravity. The corresponding results are appended in “Loads_and_zentroids1” for each rotor angle in the same way as for the blade elements, as shown in Figure 4.7.

4.3.4 Structural Calculations of Part 1

The following section in the program refers to the theory and equations derived under 2.5.3. Here is the foundation from the completed program sequences utilized, to finally deliver the normal- and shear flows/stress of each of the sides in the torque box for each of the blade elements, for each of the rotor angles. The structural calculations are more straightforward with respect to the programming compared to the previous section, as all of the variables now are known. To achieve the final results the program now works strictly after the theory and corresponding equations, and this is the main problem rather than the programming. The succession of this section is as follows:

Using three interlaced for-loops, each addressing one of the three dimensions/arrows defined for the program, explained under 4.1.1, the loads and stresses for each position in the torque box for each rotor angle at each blade element can be identified. This method or sequence, however, needs to be executed three times in succession for the complete results to be available. The last of these sequences also needs to be executed once for each side in the torque box.

The first sequence addresses the geometry of the torque box, the basic shear flow q_1, and the complete normal flow n_y:

In the first for-loop are the geometric dimensions and properties of the torque box for each blade element are determined, ref. 2.5.3 equations (2.59) - (2.86). Then, moving to the third and inner for-loop is the q_1 basic shear flow for each side in the torque box, for each rotor angle, initially calculated - each starting at zero at its starting point, ref. 2.5.3 equations (2.88) - (2.92). Next are the complete normal flows for each side of the torque box, for each rotor angle calculated, ref. 2.5.3 equations (2.100) - (2.105). The results for the normal flows are then immediately printed to the file “ny_1.txt”s. When the last run of the for-loop controlled by the torque box variable is executed, are the results for

q_1 connected to each other, so that a continuous q_1 exists for the whole torque box at the current rotor angle. This means e.g. that the end result from the upper flange is added to the start result for the front spar, and so on. Following the completion of q_1 is this printed to the file “q1_1.txt”. A simplified overview of this sequence can be seen in Figure 4.8:

```
for(iNumber_of_Elements == 0 ; iNumber_of_Elements < Arrowlength ; iNumber_of_Elements ++)
{
    /*Here are the geometric dimensions and properties for the torque box calculated for the
    current blade element, ref. 2.5.3, equations (2.59) - (2.86)*/

    for(iRotor_Angle_Position == 0; iRotor_Angle_Position < Arrowlength2; iRotor_Angle_Position++)
    {
        for(iTorsionBox_Var == 0; iTorsionBox_Var < Arrowlength3 ; iTorsionBox_Var ++)
        {
            /*In this loop is the shear flow "q1" calculated for each side in the torque box.
            Ref. 2.5.3, equations (2.88) - (2.92).
            They are not connected to each other at this point, and start on zero at the
            beginning of each side.

            Following the calculations for q1, are the complete normal flows determined next,
            and these are hence completed at this point. Ref. 2.5.3, equations (2.100) - (2.105)*/

            /*The results for the normal flow are here printed to the file "ny_1.txt"*/

            if(iTorsionBox_Var == Arrowlength -1)
            {
                for(iTorsionBox_Var == 0; iTorsionBox_Var < Arrowlength3 ; iTorsionBox_Var ++)
                {
                    /*At this point are the results from "q1" for each side added to each
                    other, to deliver a continuous "q1" counter clockwise, starting at
                    the upper flange, on top of the rear spar. This means that the starting
                    value for the rear spar is added to the end value for the upper flange, and
                    so forth.*/

                    /*The now completed values for "q1" are now being stored in the file "q1_1.txt"*/
                }
            }
        }
    }
}
```

Figure 4.8: Details to program sequence for structural calculations

In the next sequence will the constant shear flow, q_0, and the SC be calculated:

The SC, being a geometric value, is calculated for each blade element, while q_0 is calculated for each blade element at each rotor angle. In the program, this is done by letting the compiler run through three for-loops identical to those of the previous sequence, controlled by the number of elements, the rotor angle and the torque box variable respectively. In the inner for-loop is the calculation for q_0 prepared through numeric integration of q_1, ref. 2.5.3 equation (2.93). By the completion of this for-loop, runs the compiler further through the for-loop controlled by the rotor angle, and (2.93) can be executed, and the value for q_0 identified. Through an if-query, which only applies for the first rotor angle for each blade element, is now the distance between the torque box CoG and the SC in x-direction calculated, ref. 2.5.3 equation (2.97). The last action in this sequence is the printing of the result for q_0 to the file “q0_1.txt”. The structure of this sequence can be studied in Figure 4.9:

```
    /*In this sequence are the SC for each blade element, and q0 for each rotor angle
    calculated*/

for(iNumber_of_Elements == 0 ; iNumber_of_Elements < Arrowlength ; iNumber_of_Elements ++)
{
    for(iRotor_Angle_Position == 0; iRotor_Angle_Position < Arrowlength2; iRotor_Angle_Position++)
    {
        for(iTorsionBox_Var == 0; iTorsionBox_Var < Arrowlength3 ; iTorsionBox_Var ++)
        {
            /*In this loop are the calculation of q0 prepared, through numeric integration
            of q1, ref. 2.5.3, equation (2.93)*/
        }

        /* At this point is the completed numeric integration utilized, and equation (2.93)
        executed. q0 for the current rotor angle has now been determined.*/

        if(iRotor_Angle_Position == 0)
        {
            /* For the first rotor angle of each blade element are the distance in x direction
            between the torque box CoG and the SC calculated, ref. 2.5.3, equation (2.97)*/
        }

        /*Here are the value for the current q0 printed to the file "q0_1.txt"*/

    }
}
```

Figure 4.9: Overview of program sequence for calculations on the torque box

In the third and final sequence are the total shear flows calculated, and the complete loading for each position in the torque box, at each rotor angle and for each blade element is hence being identified. This whole sequence is executed once for each side of the torque box, to make the calculations and coding more transparent. Following the calculations of the shear flows are also the normal, shear and comparative stresses calculated.

This sequence is roughly built up in the same manner as the two previous ones, with the same three for-loops. The resulting force flows and stresses are calculated inside the third for-loop, but directly after entering the first for-loop are the deviations for the 0.5c point of the current blade element and the 0.5c points for the effective force arms being calculated, ref. 2.5.3, equation (2.95), and Figure 2.15. These calculations are done for the effective arms of the shear forces from gravity and thrust, and are necessary as they intersect the 0.5c line, (at the height/z-value of the SC) and because the 0.5c line has a sweep along the blade radius. This leads to the occurrence of a distance in the x-direction between the 0.5c point in the blade element and the 0.5c point at the location of the resulting shear forces from gravity and thrust.

With the deviations between the 0.5c points now identified, it is possible to calculate the shear flows due to the torsion from the shear forces that do not have their line of forces through the SC, and thereby the total shear flows. Moving to the third for-loop is now the total shear flow for the current blade element, at the current rotor angle and at the current position in the applicable torque box wall calculated, ref. 2.5.3 equations (2.94) - (2.98). Directly after this are the comparative stresses calculated, ref. 2.5.3 equations (2.107) - (2.109). With the shear- and normal flows/stresses and the comparative stresses identified, starts now a screening process of these values, and the highest values of shear stress, tensional/compressive stress and the three comparative stress types are identified, and linked with the number of element, rotor angle and position in the torque box wall. During the sequence for the rear spar, which is the last of the walls being calculated, are the results for the overall shear flow

at this point printed to the file “qs_1.txt”. With the conclusion of the sequences are then the results from the screening of the stress values printed to “Stress_analysis1.txt”. These sequences are reconstructed in Figure 4.10:

```
/* Now are the final, complete shear flows calculated. This sequence is repeated for
   each of the sides of the torque box*/

for(iNumber_of_Elements == 0 ; iNumber_of_Elements < Arrowlength ; iNumber_of_Elements ++)
{
    /* Here are the deviations between the 0.5c point of the current blade element to the
    0.5c point of the effective arms for the bending moments from gravity and thrust calculated.
    Ref 2.5.3, equation (2.95) and Figures 2.14 and 2.15.*/

    for(iRotor_Angle_Position == 0; iRotor_Angle_Position < Arrowlength2; iRotor_Angle_Position++)
    {
        for(iTorsionBox_Var == 0; iTorsionBox_Var < Arrowlength3 ; iTorsionBox_Var ++)
        {
            /* At this point are the complete shear flows for the given positions in the
            torque box determined. Ref, 2.5.3, equation (2.98).
            These include the allready calculated q1 and q0, and are now being added with
            the shear flow from torsion caused by the aerodynamic torsion of "cm", and the
            resulting torsion from the shear forces.

            For the shear flow from torsion, ref. 2.5.3, equations (2.94)-(2.97)*/

            /* Now, both the complete normal-, and shear flow are known, and out of this are
            the resulting normal, shear and overall stresses calculated.
            The comparative stresses are executed according to 2.5.3.4, equations (2.107)-(2.109)*/

            /*The last part in this sequence is a screening of the resulting normal, shear and
            three types of comparative stresses. Here are the largest contributions from shear
            stress, tensional and compressive normal stress, and the three types of comparative
            stresses screened for each of the walls. The results include in addition to the stress
            value, also wich blade element, at which rotor angle, and at which position of the wall
            they occur.*/

        }
    }
}

/* Here are the results from the screening of the stresses printed to "Stress_analysis1.txt"
```

Figure 4.10: Final calculations for force flows and stresses in the torque box

At this point are all the calculations for the first part of the program completed, and all the results stored in the files mentioned in this subchapter. A message is now conveyed in the user window, that part 1 has been completed, with the applicable result for the power generated at the design conditions. Now, the user has the choice of executing part 2 of the program by pressing “2”, or part 3 by pressing “3”.

4.4 Program, Part 2

Part 2 of the calculation program is built on the same building blocks as Part 1, but has the purpose of calculating the performance and loads for other wind speeds than the design wind speed, with the rotor working at maximum efficiency, or power coefficient, C_P. This makes this part of the program ideal to execute calculations for wind speeds lower than the design wind speed, as higher wind speeds would overload the rotor when working at maximum efficiency. As all the crucial parameters for the wind turbine at this point has been determined, the program now pursues to find the right rotational speed for this wind speed and the right pitch for the blades, so that the torque from the rotor eventually becomes equal to the load torque and a equilibrium hence has been achieved.

4.4.1 Determination of rotational speed and pitch angle

The process of determining the rotational speed, Ω, and the pitch for the blades are mainly controlled by two do-while loops, which also contains the BEM calculations explained under 4.3.2 for part 1. The first do-while loop monitors the total torque delivered by the rotor, and initiates adjustments to the rotational speed accordingly. The next two do-while loops considers only the blade element with the highest torque contribution from program part 1, and uses this to gauge the results when altering the pitch angle. The reason for this is that these calculations can directly be compared to that of the deployment of the variable pitch system for an operational wind turbine. The pitch angles for the rest of the blade elements are hence determined through the rotor twist calculated in part 1. The outer loop here iterative calculates the optimum pitch angle by using the same pitch alteration as explained under 4.3.1, and the inner loop contains the BEM calculations for this blade element. With the conclusion of these two loops are further the BEM calculations executed for the whole rotor, through a for-loop containing a do-while loop. In these two loops are no parameters being screened or gauged, as the current rotational speed and pitch angles at this point are considered constraints. After this is the total torque from the rotor equated against the load torque, and the applicable alteration command for the rotational speed is given, and the compiler moves back to the top of the sequence. With an adjustment to the rotational speed now initiated, the corresponding values assigned for the variables “iFortegn_Energy” and “iTest_Energy”, gives statements about the direction of the alteration and if more alterations have to be carried out respectively. Also the alteration for rotational speed follows the same pattern as explained under 4.3.1.

When entering this part of the program by pressing “2” at the end of part 1, the user is asked to submit the wind speed. The initial value for rotor revolutions are then determined by the following equation:

$$rev_{\min} = 1.22 \cdot v_1 \tag{4.47}$$

The factor 1.22 is derived through testing and debugging with the goal of getting as close to the final result as possible, and thereby reducing the amount of

iterations needed. For the first run is the alteration of rotational speed bypassed, and moving to the next loop, which as explained above only executes the pitch iteration for the blade element with the highest torque contribution from part 1, is the following initial value for the AoA assigned:

$$\alpha_{be,\max} = 5.0° \cdot \frac{\pi}{180°} \quad \textbf{(4.48)}$$

$\alpha_{be,max}$ AoA for the blade element with dT_{max} from part 1 [rad]

The reason for the value of $\alpha_{be,max}$, is that this by experience is a value close to the result for the AoA for this blade element following the conclusion of part 1, and therefor ensures the need for relatively few iteration runs. For the very first run of the sequence are now $\beta_{be,max}$ and $\gamma_{be,max}$ calculated by (4.20) and (4.21) respectively. Following an alteration of the rotational speed, is $\alpha_{be,max}$ calculated as above, the value for $\gamma_{be,max}$ from the last run used, and $\beta_{be,max}$ calculated as follows:

$$\beta_{be,\max} = \gamma_{be,\max} - \alpha_{be,\max} \quad \textbf{(4.49)}$$

$\beta_{be,max}$ Relative flow angle for the blade element with dT_{max} from part 1 [rad]

$\gamma_{be,max}$ Pitch angle for the blade element with dT_{max} from part 1 [rad]

Following the completion of the calculations regarding the blade element with dT_{max} from part 1, the compiler enters the for-loop, which executes the BEM calculations for the whole rotor. As explained above are here the pitch angles determined through the achieved pitch angle in the two previous loops and the blade twist from part 1. The pitch angle for a given blade elements becomes then:

$$\gamma_{be,i} = \gamma_{be,i\max} - \psi_{be,i} \quad \textbf{(4.50)}$$

$\gamma_{be,i}$ Pitch angle for a given blade element [rad]

$\psi_{be,i}$ Twist angle for this blade element [rad]

The evaluation of the rotor torque is carried out as follows: The rotor torque is equated against the load torque from the generator and gears, which is calculated by (4.38), and the criterion for the right rotational speed is when the load torque subtracted from the rotor torque delivers zero. The alteration of the rotational speed follows the exact same pattern as the pitch alteration explained under 4.3.1, and the magnitude of which is ±0,1[min^{-1}]. The criterion is determined by the following equation:

$$T_{total} = T_{load} = c_{gen} \cdot rev_{\min}^2 \qquad \textbf{(4.51)}$$

A simplified overview of this whole sequence is to be seen in Figure 4.11:

```
do
{
    /*Here is the rotational speed adjusted, based on the evaluation of the total torque from
    the rotor, and the values of "iTest_Energy" and "iFortegn_Energy".*/
    do
    {
        /*At this point is the rotational speed from the outer do-while loop assigned to the blade element
        with the largest torque contribution from program part 1 (ref.4.3.3 and equation (4.40) ). The pitch
        alteration follows the same pattern as under Part 1, and screens the values of "iTest" and "iFortegn"
        Further are  preparations made for the BEM calculations.
        In this do-while loop is the pitch angle iterativ improved, based on the pitch command given at the bottom
        of the loop. For the first run is an initial value for the pitch angle given, and the alteration section bypassed.*/
        iCounter = 0;
        do
        {
        /*In this loop are the BEM calculations for the blade element with the highest torque contribution iterativ calculated
        iCounter += 1;
        }
        while(dDiff > dAccuracy || dDiff2 > dAccuracy);
        /*Here are the results for the torque from the blade element with the highest torque
        contribution evaluated, and assigned eiter pitch command 1, 2, 3 or 4*/
        iOuterCounter += 1;
    }
    while(iTest != 0);
    /*When the program has reached this point, does that mean that the optimum pitch has been found
    for the blade element with the highest torque contribution, and the BEM calculations can be executed
    for the whole rotor. The calculated twist is now used to determine the pitch for the other bøade elements.*/
    for(iNumber_of_Elements == 0 ; iNumber_of_Elements < Arrowlength ; iNumber_of_Elements ++)
    {
        /*Here are both the rotational speed and the pitch of the blade known values, and the
        BEM calculations are now carried out for all the blade elements.*/
        iCounter = 0;
        do
        {
            /*In this loop are the BEM calculations for all the blade elements iterativ calculated.*/
            iCounter += 1;
        }
        while(dDiff > dAccuracy || dDiff2 > dAccuracy);
    }
    /*At this point is the total torque from the rotor evaluated agianst the load torque from the
    gear and generator. The decision if the rotational speed has to be altered, is made upon the
    equation of the current rotor torque and the magnitude of the load torque. If these have the
    same value, the correct rotor speed has been found. Also here are either alteration command 1, 2, 3 or 4 made.*/
    iEnergyCounter += 1;
}
while(iTestEnergy != 0);
```

Figure 4.11: Details to the iterations of rotational speed and pitch angle

When the correct rotational speed has been found and the control variable “iTest_Energy” has been assigned the value 0, are the results printed to the file “Results_WTD2.txt” in the for-loop calculating the results for the whole rotor.

When this sequence is completed, is a message printed to the user screen containing the results to the achieved rotational speed, and the corresponding power output and power coefficient.

4.4.2 Structural calculations of Part 2

The codes and workflow of the structural calculations of part 2 are exactly the same as for part 1, explained under 4.3.4. The differences between the two parts lie in the previous sections, containing the BEM iterations, as it is here the current conditions are taken into consideration. When the structural calculations on the torque box are about start, all the needed parameters are known.

The results from the structural calculations are printed to the following files during the course of the sequences:

- Forces and moments: “Loads_and_Zentroids2.txt”
- Normal flow: “ny_2.txt”
- Basic shear flow: “q1_2.txt”
- Constant shear flow: “q0_2.txt”
- Total shear flow: “qs_2.txt”
- Maximum stress values with corresponding blade elements, rotor angle and position in the torque box: “Stress_analysis2.txt”

4.5 Program, Part 3

In the third and final part of the program is the user asked to submit both the wind speed, and the wanted power output from the rotor. In this way is it here possible to manipulate the efficiency of the rotor, which makes this part crucial in the development of the rotor-strength-optimized power curve that are one of the main objectives of this work. As the wind speeds submitted in part 2 of the program are lower than the design wind speed of part 1, it is first in this part that the higher wind speeds will be tested, and therefor the reduction in efficiency will be necessary to maintain the integrity of the rotor strength. In the same manner as part 2 must this part be able to deploy the variable pitch system, and several loops have to be connected with the BEM-iterations to monitor and screen the results, and steadily altering the necessary variables until the correct values have been found.

4.5.1 Program set-up to obtain the unknown values

When the user has submitted the wind speed and wanted power output from the rotor, the unknown parameters now are blade pitch and rotational speed. The way the program now works to obtain these values are as follows: The whole section before the structural calculations can start is divided into two main sequences. In the first sequence is the goal to find at which wind speed the rotor delivers the submitted power output while working at maximum efficiency – here called the equivalent full-rate wind speed. The reason for this is that when this particular wind speed is known, is also the rotational speed known, and the only variable left to determine is the pitch of the blades. This is the same mentality as with the flat rating of wind turbines in general; when the maximum allowable output is reached and the wind speed increases, are the blades turned to lower the efficiency. What actually happens is that the rotational speed and torque from the rotor stay constant, while the torque distribution over the blades changes, which consequently also causes the efficiency to drop.

It is actually possible to obtain the equivalent full-rate wind speed by simply assuming that the C_p value is the same as the one achieved in part 1, and applying (2.6), solved for the wind speed:

$$v_{eq,fr} = \sqrt[3]{\left(\frac{2 \cdot P_{dr}}{C_P \cdot \pi \cdot \rho \cdot r_{blade}^2} \right)} \tag{4.52}$$

$v_{eq,fr}$ Equivalent full-rate wind speed for the submitted power output [m/s]

P_{dr} Submitted de-rated power from user [W]

The corresponding rotational speed, can further be determined by applying (4.38), using the solved constant c_{gen} and finally solving for rev_{min}:

$$P_{dr} = T_{load} \cdot \Omega = c_{gen} \cdot rev_{\min}^2 \cdot \frac{2 \cdot \pi \cdot rev_{\min}}{60} \rightarrow rev_{\min} = \sqrt[3]{\left(\frac{P_{dr} \cdot 60}{2 \cdot \pi \cdot c_{gen}} \right)} \quad \textbf{(4.53)}$$

Even though these two crucial values are available in this relatively simple way, it is in this work nevertheless chosen to calculate them in the same pattern as the previous sections of the program, and determine all the values through the BEM calculations. Thereby is the program work-philosophy in this part of the program also maintained, in that the flow parameters for the rotor are calculated over for each change in the conditions, and in that way putting the rotor to the test when it comes to the power coefficient. The equations (4.52) and (4.53) will, however, be used to compare the results derived from the program, and the validity of these and the quality of the program can hence be evaluated.

In the second sequence are the user-submitted wind speed and the now known rotational speed used, and further the pitch of the blades gradually turned to lower the efficiency of the rotor, until the rotor torque is equal to that of the load torque.

4.5.1.1 Sequence 1

This sequence is identical to the control sequence of part 2, shown in Figure 4.11, except for an additional do-while loop outside, which monitors and alters the equivalent full-rate wind speed. The procedure of this sequence is as follows: First is an initial value for the equivalent full-rate wind speed calculated from this equation:

$$v_{eq,fr} = 0.4 \cdot v_1 \quad \textbf{(4.54)}$$

The value 0.4 in (4.52) is a value, which generally ensures a satisfactory starting point for the iteration, and is derived through testing. Next is the rotational speed determined by using (4.47), and replacing v_1 with $v_{eq,fr}$:

$$rev_{\min} = 1.22 \cdot v_{eq,fr} \quad \textbf{(4.55)}$$

Further are both the alteration of wind speed and rotational speed bypassed as this is the first run, and the compiler moves directly to the third and fourth do-while loops for initial calculations of pitch angle and the BEM equations of the blade element with the highest torque contribution from part 1 – in the same manner as in part 2. Here, however, are slightly different initial values for AoA and relative flow angle used, which have been derived through testing, and to make the program as stable as possible:

$$\alpha_i = 3.0 \cdot \frac{\pi}{180} \tag{4.56}$$

$$\beta_i = \frac{\pi}{2} - \frac{4}{5} \cdot \arctan\left(\frac{1}{\lambda_r}\right) \tag{4.57}$$

Also the next loops follow the same pattern as in part 2 with the execution of the BEM calculations for the whole rotor, and a following evaluation of the total rotor torque against the load torque as in (4.51). The rotational speed is altered until these two reach the same value. When the do-while loop controlling the rotational speed has been completed, is the power output from the rotor calculated by (2.35), and evaluated against the submitted power output from the user. As with the do-while loops altering pitch angle and rotational speed follows also this do-while loop the alteration pattern derived under 4.3.1.

When the outer do-while loop also has been completed, meaning that the equivalent full-rate wind speed that delivers the submitted power output with the rotor working at maximum efficiency has been identified, has sequence 1 come to a conclusion. The result that will be used in sequence 2 is the rotational speed, which was derived along with $v_{eq,fr}$. The set-up of sequence 1 is shown in Figure 4.12:

```
do
{
    /*In this loop is it pursued to find the equivalent full-rate wind speed. In that connection
    is the energy output from the rotor monitored, and the wind speed altered accordingly. The
    control variables are iWindCounter, iFortegnEnergy_2 and iTestEnergy2.*/
    do
    {   /*Here is the rotational speed adjusted, based on the evaluation of the total torque from
        the rotor, and the values of "iEnergyCounter" "iTorque_control" and "iFortegn_Energy".*/
        do
        {
            /*Here is the torque of the blade element with the highest torque contribution from part 1
            screened, and the pitch angle altered accordingly, to find the optimium pitch angle at
            the current wind speed and rotational speed. The control variables are "iOuterCounter",
            "iFortegn" and "test"*/
            do
            {
                /*BEM calculations for the blade element with the highest torque contribution*/
            }
            while(dDiff > dAccuracy || dDiff2 > dAccuracy);
            /*Here is the torque under the current conditions monitored for the blade element with
            the highest torque contribution, and the appropriate command of alteration given,
            until a peak has been found*/
            }
        }
        while(itest != 0);
        /*At this point are the wind speed, rotational speed and pitch constraints, and the
        calculations can be carried out for the whole rotor.*/
        for(iNumber_of_Elements = 0; iNumber_of_Elements < Arrowlength; iNumber_of_Elements++)
        {
            do
            {
                /*In this loop are the BEM calculations for all the blade elements iterativ calculated.*/
            }
            while(dDiff > dAccuracy || dDiff2 > dAccuracy);
            /*Now is the total torque from the rotor evaluated agianst the load torque from the gear and
            generator. The decision if the rotational speed has to be altered, is made upon the equation
            of the current rotor torque and the magnitude of the load torque. If these have the same value,
            the correct rotor speed has been found. Also here are either alteration command 1, 2, 3 or 4 made.*/
    }
    while(iTorque_control !=0);
    /*Here is the total power output from the rotor evaluated, and compared to the submittet power output from the
    user. Based on this comparison is the appropriate command given to alter the wind speed, and thus iterativ
    close in on the equivalent full-rate wind speed.*/
}
while(iTestEnergy2 !=0);
```

Figure 4.12: Details to sequence 1 in part 3

4.5.1.2 Sequence 2

As explained above, is the rotational speed at this point known and the program starts from here using the user-submitted wind speed. The purpose of this sequence is to deploy the variable pitch system to gradually adjust the power output, by evaluating the rotor torque against the load torque and alter the pitch accordingly. While the foundational structure of this sequence is set up exactly as the iterative loops described for part 1 and 2, there is one difference here with regards to the BEM calculations: This is the only sequence in the program where the BEM iteration loop does not work with ideal values for the flow parameters, which further poses a challenge when it comes to calculating the correct initial values for AoA and relative flow angle.

The sequence is set up as follows: A do-while loop monitors and alters the pitch angle based on the rotor torque compared to load torque. The alteration process follows the same pattern as the others in the program, ref. 4.3.1. After the pitch alteration has taken place enters the compiler two interlaced for- and do-while loops, which simply execute the total BEM calculations for all the blade elements. When the rotor torque becomes equal to the load torque has the right pitch been found, and all parameters needed before the structural calculations can start have been identified.

As has been the case for other values in the course of writing the program, it is also here necessary to adjust some of the initial values through testing. Especially this sequence, because the flow parameters are different and may take on extreme values, is vulnerable with regards to the initial values and that these roughly hit the target. The following initial values for α_I, β_I and γ_I have been developed:

Values for the first blade element for the first run:

$$\alpha_{i,be1} = 12.0° \cdot \frac{\pi}{180°} \quad \textbf{(4.58)}$$

$\alpha_{i,be1}$ Initial AoA for the 1st blade element for the 1st run [rad]

$$\beta_{i,be1}: \quad (4.57)$$

$\beta_{i,be1}$ Initial relative flow angle for the 1st blade element for the 1st run [rad]

$$\gamma_{i,be1} = \alpha_{i,be1} + \beta_{i,be1} \quad \textbf{(4.59)}$$

$\gamma_{i,be1}$ Initial pitch angle for the 1st blade element for the 1st run [rad]

For the first blade element after pitch adjustments have been carried out are the following values used:

$$\beta_i : (4.57)$$

$$\alpha_i = \gamma_i - \beta_i \quad \textbf{(4.60)}$$

For all other blade elements:

$$\gamma_i = \gamma_{be-1} + \left(\psi_{i-1} + \psi_i\right) \quad \textbf{(4.61)}$$

ψ_{i-1} Twist angle for the previous blade element [rad]

$$\beta_i : (4.57)$$

$$\alpha_i : (4.59)$$

A schematic overview of this sequence can be seen in Figure 4.13:

```
/*Now has the equivalent full-rate wind speed and the corresponding rotational speed been found, and the only
variable left to calculate is the blade pitch*/

do
{
    /*Here is the pitch of the rotor continous altered to lower the efficiency of the rotor. The submitted
    wind speed is used, and the obtained rotational speed from the previous sequence. The control variables
    are: "iOuterCounter", "iFortegn" and "itest"*/

    for(iNumber_of_Elements = 0; iNumber_of_Elements < Arrowlength; iNumber_of_Elements++)
    {
        do
        {
            /*BEM iteration for all the blade elements*/
        }
        while(dDiff > dAccuracy || dDiff2 > dAccuracy);
    }

    /*Now is the total torque from the rotor evaluated agianst the load torque from the gear and
    generator. The decision if the rotational speed has to be altered, is made upon the equation
    of the current rotor torque and the magnitude of the load torque. If these have the same value,
    the correct rotor speed has been found. Also here are either alteration command 1, 2, 3 or 4 made.*/

}
while(itest != 0);
```

Figure 4.13: Schematic overview of sequence 2

Following the completion of sequence 2 are all variables identified, the complete BEM calculations have been carried out, and the non-structural section of part 3 is thus completed. The results are then printed to the file “Results_WTD3.txt”, and some of these along with the message that the section is completed are also conveyed through the user window.

4.5.2 Structural calculations of Part 3

As also was the case for part 2, are the structural calculations here, and the execution of which, identical to part 1 as explained under 4.3.4. With the completion of the previous section is the foundation for the calculation of all of the forces, moments and consequently force flows and stresses finished.

The results from the structural calculations are printed to the following files during the course of the sequences:

- Forces and moments: “Loads_and_Zentroids3.txt”
- Normal flow: “ny_3.txt”
- Basic shear flow: “q1_3.txt”
- Constant shear flow: “q0_3.txt”
- Total shear flow: “qs_3.txt”
- Maximum stress values with corresponding blade elements, rotor angle and position in the torque box: “Stress_analysis3.txt”

5 Results

At this point has the intention and background for this Diploma Thesis been explained, the theoretical foundation derived and discussed, and the function and development of the computational tool shown. The work, which addresses the use of this tool and the generation of results, can therefor now be initiated. In this connection is it decided to use the program for an appropriate example wind turbine, of which as much data as possible is known and to link the results to an Excel spreadsheet where the results can be evaluated. By executing the program for different wind speeds over the operating range, will it ultimately be developed a power curve for the wind turbine, which at wind speeds higher than the design wind speed is limited by the rotor strength only.

5.1 Test Object

As mentioned in the introduction, are the intention and results from this work currently only applicable for offshore wind turbines, which may be mounted on floating structures when such devices have been made available. It is therefore chosen a wind turbine, which from the very start solely was intended for offshore use, the Areva Wind M5000. This wind turbine is shown in Figure 5.1:

Figure 5.1: The Areva Wind M5000 [23]

This wind turbine is currently in use on standard seabed-fixed towers, but there are already concrete plans to use the wind turbine with the Sway® system floating wind turbine foundation, when this has been cleared for operational use [5]. An overview of some of its technical specifications can be seen in Figure 5.2:

GENERAL

Rated power	5,000 kW
Cut-in wind speed	4 m/s
Rated wind speed	12.5 m/s
Cut-out wind speed	25 m/s
Design life time	20 years
Type class	GL-TK 1 offshore

GEARBOX

Type	step-planetary gear, helical
Rated power	5,590 kW
Rated torque	3,600 kNm
Ratio	1:10

ROTOR

Rotor diameter	116 m
Number of blades	3
Rotor area	10,568 m^2
Speed range	4.5 - 14.8 min^{-1} ± 10%
Rated speed	14.8 min^{-1}
Tilt angle	5°
Cone angle	-2°

GENERATOR AND CONVERTER

Generator type	synchron, permanentmagnet
Rated power generator	5,260 kW
Nominal voltage	3,300 V
Speed range	45.1 - 148.5 min^{-1}
Cooling	Water cooled
Protection class	IP 54
Converter type	4-quadrant-converter
Power factor (grid)	0.9 induktive - 0.9 capacitive

Figure 5.2: Technical specifications for Areva Wind M5000 [23]

Before the results of the calculation program will be presented, the technical specification of Figure 5.2 will be discussed and so making it easier to compare the results of the program with these. As can be seen on top of the specification table is the rated power of the wind turbine 5000kW. This means the power, which is actually delivered to the electrical grid, after the captured power from the rotor has been delivered through the necessary chain of equipment. In other words is 5000kW not the rated power from the rotor. The complete succession of power transmission from stage to stage is as follows [22]:

Power available in the wind through kinetic energy over the disc area (2.6):

$$P_T = \frac{1}{2} \cdot \rho \cdot \pi \cdot r_{blade}^2 \cdot v_1^3 \tag{5.1}$$

Power captured by the rotor and *mechanical input power* to the transmission (2.8):

$$P_0 = C_P \cdot P_T \tag{5.2}$$

Transmission *output* power delivered as input power to the generator [22]:

$$P_{gear} = P_0 \cdot \eta_{gear} = P_T \cdot C_P \cdot \eta_{gear} \tag{5.3}$$

P_{gear} Transmission output power [kW]

η_{gear} Gearbox efficiency [-]

Generator *output* power delivered to the grid connector/transformer [22]:

$$P_e = \eta_e \cdot P_{gear} = P_T \cdot C_P \cdot \eta_{gear} \cdot \eta_e \tag{5.4}$$

P_e Generator output power [kW]

η_e Generator efficiency [-]

Now, interpreting the specifications in Figure 5.2, it has to be beared in mind that the term “rated power” is inconsistently used in the industry, which makes it difficult to know if the power in question is input- or output power. The generator, however, is always rated with regard to *output* power [22]. It can therefor be derived that P_e for the Areva Wind M5000 is 5260kW. As P_0 generally would be referred to as rated *rotor* power, it is further assumed that the 5590kW rated *gearbox* power in fact is the gearbox output power, P_{gear}. With this assumption is it possible to obtain the generator efficiency:

$$\eta_e = \frac{P_e}{P_{gear}} = \frac{5260kW}{5590kW} = 0.94097 \tag{5.5}$$

Because neither the C_P value nor the gearbox efficiency η_{gear} are provided here, the exact power generated by the rotor, P_0 is unknown. With the given data from the specification table is it however possible to derive a guessed, approximate value for η_{gear}. It is stated that the gearbox type is planetary, after studying the info available at the producer's homepage, it is concluded that this is a single stage gear [23]. This type of transmission is in literature stated to have 2% loss per stage at rated power [22]. A chart of gearbox efficiency dependent on power, rated power ratio and number of stages is shown in Figure 5.3:

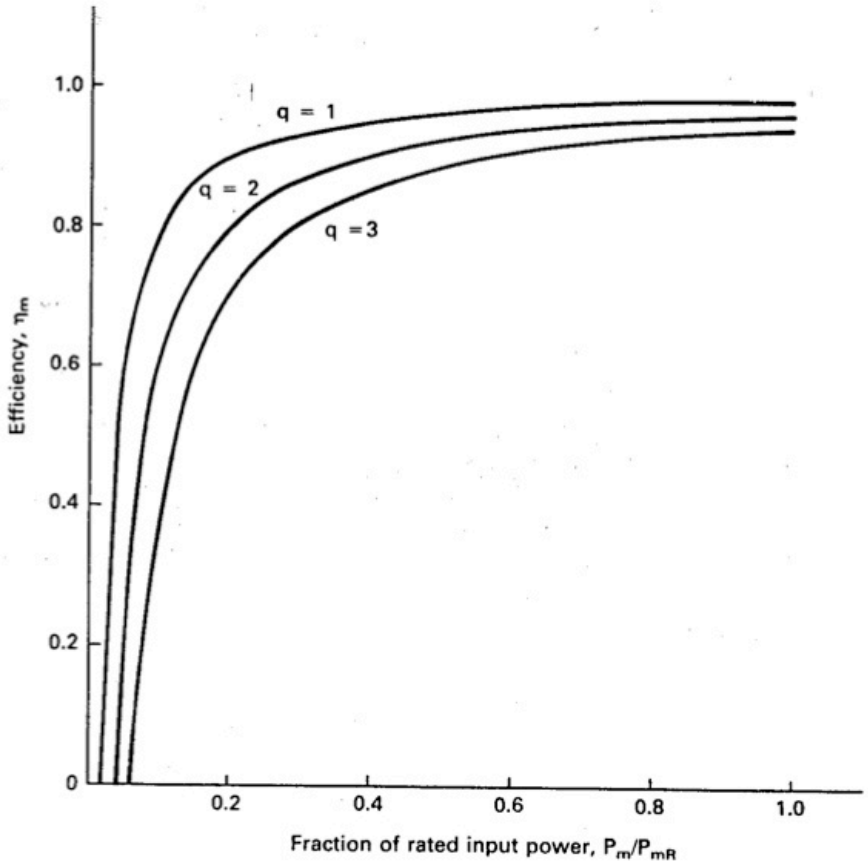

Figure 5.3: Transmission efficiency for planetary gearboxes [22]

Hence, with a transmission efficiency η_{gear} of 0.98 at rated power, the rotor power P_0 can be calculated to:

$$P_0 = \frac{P_{gear}}{\eta_{gear}} = \frac{5590kW}{0.98} = 5704kW \qquad \textbf{(5.6)}$$

Finally can also the C_P for the rotor be determined at standard ISO conditions, using the stated rotor diameter and rated wind speed:

$$C_P = \frac{P_0}{P_T} = \frac{P_0}{\frac{1}{2} \cdot \rho \cdot \pi \cdot r_{blade}^2 \cdot v_1^3}$$
$$= \frac{5704kW}{\frac{1}{2} \cdot 1.225kg/m^3 \cdot \pi \cdot (58m)^2 \cdot (12.5m/s)^3} = 0.4512 \quad \textbf{(5.7)}$$

These results can now be compared to those of part 1 of the calculation program, and thus evaluate this tool. There are naturally several uncertainties to the data of this test object, e.g. the details of the geometry of the rotor, and if the NACA 4410 airfoils applied by the calculation program have somewhat similar aerodynamic properties to those of the airfoil of the Areva Wind M5000.

5.2 Results from the calculation tool

At this point, the results from the calculation program shall be presented. In this connection, the results for C_P and rotor power P_0 from part 1 of the program will be evaluated against the corresponding results for the Areva Wind M5000 derived above. In addition to P_0 and C_P, also the structural results of part 2 and 3 for other wind speeds will further be compared to the results from part 1.

The program generates much data, and not all of these can be analytically compared. It is for instance difficult to compare the results for force flow and stresses in the torque box at every position. The reason for this is that e.g. the normal stress often changes from tensional at one end of the applicable wall, to compressive stress at the other end, and hence passes zero on the way. It is in this connection likely that the results from a run of the program, which generates lower maximum values than another run, at some positions nevertheless have higher values than the higher loaded run. It is therefor decided to use the three types of maximum comparative stresses, ref. 2.5.3.4, and base the evaluation if the results are within or above the limits on these. The maximum values for the comparative stresses are identified during the screening process explained under 4.3.4. This is done by initiating the maximum and minimal values of shear- and normal stress as very high negative- and very high positive values respectively, and thus making sure that the first stress values which are monitored will be set as new maximum/minimum. In this way are all values compared to each other, and by the completion of the loop have the highest values of maximum/minimum been found. These results, for all the runs of the program for different wind speeds, are in Excel connected to the reference values of the rated wind speed in part 1. Through a formula in Excel are either “OK” or “Value above max!” conveyed as the results are pasted into the spreadsheet.

Referring to 4.2, the input values for the calculation tool for the Areva Wind M5000 are stated in Table 5.1. Except for the number of blades, rated wind speed, rotational speed, the blade radius and blade weight are the other values guesses only:

T [K]:	288,15
p_a *[PA]*	101300
B [-]	3
v_1 *[m/s]*	12,5
rev_{min} *[min^{-1}]*	14,8
r_{blade} *[m]*	58
$r_{r,S}$ *[-]*	0,16
$r_{r,H}$ *[-]*	0,05
$r_{r,E}$ *[-]*	0,94
c_s *[m]*	5,3
c_e *[m]*	1,4
s_{fs} *[-]*	0,15
s_{rs} *[-]*	0,65
$t_{uf,max}$ *[mm]*	20
$t_{fs,max}$ *[mm]*	22
$t_{lf,max}$ *[mm]*	20
$t_{rs,max}$ [mm]	22
$t_{uf,min}$ [mm]	2
$t_{fs,min}$ [mm]	5
$t_{lf,min}$ [mm]	2
$t_{rs,min}$ [mm]	5
m_{blade} [kg]	16500
$m_{r,AE}$ [-]	0,8
$r_{cross,s}$ [m]	1,5

Table 5.1: Input values for the Areva Wind M5000

The corresponding results from part 1 of the program are now displayed in Table 5.2:

Part 1			
General Results		Hub loads	
v_1 [m/s]	12,5	$M_{Torsion}$ [Nm]	-66998,4
$rev_{min}[min^{-1}]$	14,8	F_{CF} [N]	821329,92
Max. Mach No. [-]	0,2646	F_{torque} [N]	40978,9
F_{torque} / F_{thrust} [-]	0,1542	F_{thrust} [N]	265826,0
T [Nm]	4023182,51	M_{thrust} [Nm]	10183533,4
P [W]	6235338,97	Resulting arm, Torque [m]	32,7
CP [-]	0,4932	Resulting arm, Thrust [m]	38,3
Maximum Stress values			
Upper Flange		Blade Element [-]	Rotor Angle [deg] / Wall position of occurance [%]
$\tau_{max,UF}$ [N/mm²]	-71,75	55	240 / 100
$\sigma_{max,tens,UF}$ [N/mm2]	21	1	240 / 100
$\sigma_{max,comp,UF}$ [N/mm2]	-627,45	1	300 / 0
$\sigma_{V,N,UF}$ [N/mm2]	627,67	1	300 / 0
$\sigma_{V,S,UF}$ [N/mm2]	629,21	44	60 / 100
$\sigma_{V,F,UF}$ [N/mm2]	627,78	1	300 / 0
Front Spar		Blade Element [-]	Rotor Angle [deg] / Wall position of occurance [%]
$\tau_{max,FS}$ [N/mm2]	-49,6	52	240 / 33,33
$\sigma_{max,tens,FS}$ [N/mm2]	709,05	1	120 / 100
$\sigma_{max,comp,FS}$ [N/mm2]	-620,69	43	60 / 0
$\sigma_{V,N,FS}$ [N/mm2]	709,4	1	120 / 100
$\sigma_{V,S,FS}$ [N/mm2]	709,75	1	120 / 100
$\sigma_{V,F,FS}$ [N/mm2]	709,58	1	120 / 100
Lower Flange		Blade Element [-]	Rotor Angle [deg] / Wall position of occurance [%]
$\tau_{max,LF}$ [N/mm2]	-70,2	55	60 / 0
$\sigma_{max,tens,LF}$ [N/mm2]	709,69	1	120 / 0
$\sigma_{max,comp,LF}$ [N/mm2]	-104,3	1	300 / 100
$\sigma_{V,N,LF}$ [N/mm2]	710,11	1	120 / 0
$\sigma_{V,S,LF}$ [N/mm2]	710,54	1	120 / 0
$\sigma_{V,F,LF}$ [N/mm2]	710,32	1	120 / 0
Rear Spar		Blade Element [-]	Rotor Angle [deg] / Wall position of occurance [%]
$\tau_{max,RS}$ [N/mm2]	16,89	26	60 / 33,33
$\sigma_{max,tens,RS}$ [N/mm2]	521,82	46	120 / 0
$\sigma_{max,comp,RS}$ [N/mm2]	-627,99	1	300 / 100
$\sigma_{V,N,RS}$ [N/mm2]	628,17	1	300 / 100
$\sigma_{V,S,RS}$ [N/mm2]	628,35	1	300 / 100
$\sigma_{V,F,RS}$ [N/mm2]	628,26	1	300 / 100
-			
These are ref. values			

Table 5.2: Calculation Tool results, rated wind speed

As can be seen in the results from the calculation tool, is the power output of 6235.34kW at rated wind speed somewhat higher than the Areva Wind M5000. The C_P is therefore also higher, with a value of 0,4932. Among the uncertainties with regards to the exact dimensions and geometry of the Areva Wind M5000, there is obviously also a leap from the calculations to the obtained operational values. Even so seem these data to be plausible, and confirm that the calculation tool generates data, which corresponds well with an existing wind turbine. It has to be underlined the importance of obtaining as much and accurate data as possible to achieve results of high quality. Naturally, the fixed use of the NACA 4410 airfoil in the program is a constraint, which lower the accuracy of the results. The results of loads and stresses will be discussed after the tables containing the values from other wind speeds have been displayed. With results available from the range 4m/s – 24m/s it is then possible to compare them and to evaluate them with regards to the different conditions. For the results obtained from part 3 of the program, requiring the submission of both wind speed and power output, these were generated through trial, until the values for the maximum comparative stresses were equal to or close below those from part 1. The next tables are listed from lowest to highest wind speed:

Part 2			
General Results		**Hub loads**	
v_1 [m/s]	4	$M_{Torsion}$ [Nm]	-7342,0
$rev_{min}[min^{-1}]$	4,9	F_{CF} [N]	86929,13
Max. Mach No. [-]	0,0874	F_{torque} [N]	4076,0
F_{torque} / F_{thrust} [-]	0,1501	F_{thrust} [N]	27160,2
T [Nm]	400410,79	M_{thrust} [Nm]	1042387,3
P [W]	205042,2	Resulting arm, Torque [m]	32,7
CP [-]	0,495	Resulting arm, Thrust [m]	38,4
Maximum Stress values			
Upper Flange		*Blade Element [-]*	*Rotor Angle [deg] / Wall position of occurance [%]*
$\tau_{max,UF}$ [N/mm²]	-7,62	55	240 / 100
$\sigma_{max,tens,UF}$ [N/mm2]	43,62	1	240 / 100
$\sigma_{max,comp,UF}$ [N/mm2]	-71,26	40	60 / 100
$\sigma_{V,N,UF}$ [N/mm2]	71,62	40	60 / 100
$\sigma_{V,S,UF}$ [N/mm2]	71,99	40	60 / 100
$\sigma_{V,F,UF}$ [N/mm2]	71,81	40	60 / 100
Front Spar		*Blade Element [-]*	*Rotor Angle [deg] / Wall position of occurance [%]*
$\tau_{max,FS}$ [N/mm2]	-5,16	53	240 / 33,33
$\sigma_{max,tens,FS}$ [N/mm2]	77,48	1	120 / 100
$\sigma_{max,comp,FS}$ [N/mm2]	-71,35	40	60 / 0
$\sigma_{V,N,FS}$ [N/mm2]	77,62	1	120 / 100
$\sigma_{V,S,FS}$ [N/mm2]	77,76	1	120 / 100
$\sigma_{V,F,FS}$ [N/mm2]	77,69	1	120 / 100
Lower Flange		*Blade Element [-]*	*Rotor Angle [deg] / Wall position of occurance [%]*
$\tau_{max,LF}$ [N/mm2]	-7,4	55	60 / 0
$\sigma_{max,tens,LF}$ [N/mm2]	77,59	1	120 / 0
$\sigma_{max,comp,LF}$ [N/mm2]	-48,06	1	300 / 100
$\sigma_{V,N,LF}$ [N/mm2]	77,76	1	120 / 0
$\sigma_{V,S,LF}$ [N/mm2]	77,93	1	120 / 0
$\sigma_{V,F,LF}$ [N/mm2]	77,85	1	120 / 0
Rear Spar		*Blade Element [-]*	*Rotor Angle [deg] / Wall position of occurance [%]*
$\tau_{max,RS}$ [N/mm2]	3,18	1	120 / 66,67
$\sigma_{max,tens,RS}$ [N/mm2]	60,67	41	120 / 0
$\sigma_{max,comp,RS}$ [N/mm2]	-70,48	1	300 / 100
$\sigma_{V,N,RS}$ [N/mm2]	70,48	1	300 / 100
$\sigma_{V,S,RS}$ [N/mm2]	70,49	1	300 / 100
$\sigma_{V,F,RS}$ [N/mm2]	70,48	1	300 / 100
Test of Maximum values against ref.			
OK			

Table 5.3: Results for 4m/s and maximum C_P

Part 2			
General Results		**Hub loads**	
v_1 [m/s]	6	$M_{Torsion}$ [Nm]	-16497,0
$rev_{min}[min^{-1}]$	7,3	F_{CF} [N]	195323,97
Max. Mach No. [-]	0,131	F_{torque} [N]	9176,7
F_{torque} / F_{thrust} [-]	0,1502	F_{thrust} [N]	61080,2
T [Nm]	901464,27	M_{thrust} [Nm]	2344059,6
P [W]	691960,19	Resulting arm, Torque [m]	32,7
CP [-]	0,4949	Resulting arm, Thrust [m]	38,4
Maximum Stress values			
Upper Flange		*Blade Element [-]*	*Rotor Angle [deg] / Wall position of occurance [%]*
$\tau_{max,UF}$ [N/mm²]	-16,87	55	240 / 100
$\sigma_{max,tens,UF}$ [N/mm2]	43,81	1	240 / 100
$\sigma_{max,comp,UF}$ [N/mm2]	-152,89	1	300 / 0
$\sigma_{V,N,UF}$ [N/mm2]	152,89	1	300 / 0
$\sigma_{V,S,UF}$ [N/mm2]	152,9	1	300 / 0
$\sigma_{V,F,UF}$ [N/mm2]	152,9	1	300 / 0
Front Spar		*Blade Element [-]*	*Rotor Angle [deg] / Wall position of occurance [%]*
$\tau_{max,FS}$ [N/mm2]	-11,56	52	240 / 33,33
$\sigma_{max,tens,FS}$ [N/mm2]	170,67	1	120 / 100
$\sigma_{max,comp,FS}$ [N/mm2]	-145,56	43	60 / 0
$\sigma_{V,N,FS}$ [N/mm2]	170,83	1	120 / 100
$\sigma_{V,S,FS}$ [N/mm2]	170,98	1	120 / 100
$\sigma_{V,F,FS}$ [N/mm2]	170,9	1	120 / 100
Lower Flange		*Blade Element [-]*	*Rotor Angle [deg] / Wall position of occurance [%]*
$\tau_{max,LF}$ [N/mm2]	-16,46	55	60 / 0
$\sigma_{max,tens,LF}$ [N/mm2]	170,87	1	120 / 0
$\sigma_{max,comp,LF}$ [N/mm2]	-59,45	1	300 / 100
$\sigma_{V,N,LF}$ [N/mm2]	171,05	1	120 / 0
$\sigma_{V,S,LF}$ [N/mm2]	171,24	1	120 / 0
$\sigma_{V,F,LF}$ [N/mm2]	171,14	1	120 / 0
Rear Spar		*Blade Element [-]*	*Rotor Angle [deg] / Wall position of occurance [%]*
$\tau_{max,RS}$ [N/mm2]	4,89	1	60 / 66,67
$\sigma_{max,tens,RS}$ [N/mm2]	122,16	44	120 / 0
$\sigma_{max,comp,RS}$ [N/mm2]	-152,98	1	300 / 100
$\sigma_{V,N,RS}$ [N/mm2]	152,99	1	300 / 100
$\sigma_{V,S,RS}$ [N/mm2]	152,99	1	300 / 100
$\sigma_{V,F,RS}$ [N/mm2]	152,99	1	300 / 100
Test of Maximum values against ref.			
OK			

Table 5.4: Results for 6m/s and maximum C_P

Part 2			
General Results		**Hub loads**	
v_1 [m/s]	8	$M_{Torsion}$ [Nm]	-29308,1
$rev_{min}[min^{-1}]$	9,8	F_{CF} [N]	347005,79
Max. Mach No. [-]	0,1746	F_{torque} [N]	16319,0
F_{torque} / F_{thrust} [-]	0,1503	F_{thrust} [N]	108560,2
T [Nm]	1603082,86	M_{thrust} [Nm]	4166050,5
P [W]	1640133,32	Resulting arm, Torque [m]	32,7
CP [-]	0,4949	Resulting arm, Thrust [m]	38,4
Maximum Stress values			
Upper Flange		*Blade Element [-]*	*Rotor Angle [deg] / Wall position of occurance [%]*
$\tau_{max,UF}$ [N/mm²]	-29,82	55	240 / 100
$\sigma_{max,tens,UF}$ [N/mm2]	44,05	1	240 / 100
$\sigma_{max,comp,UF}$ [N/mm2]	-268,24	1	300 / 0
$\sigma_{V,N,UF}$ [N/mm2]	268,29	1	300 / 0
$\sigma_{V,S,UF}$ [N/mm2]	268,33	1	300 / 0
$\sigma_{V,F,UF}$ [N/mm2]	268,31	1	300 / 0
Front Spar		*Blade Element [-]*	*Rotor Angle [deg] / Wall position of occurance [%]*
$\tau_{max,FS}$ [N/mm2]	-20,52	52	240 / 33,33
$\sigma_{max,tens,FS}$ [N/mm2]	301,11	1	120 / 100
$\sigma_{max,comp,UF}$ [N/mm2]	-250,21	43	60 / 0
$\sigma_{V,N,FS}$ [N/mm2]	301,3	1	120 / 100
$\sigma_{V,S,FS}$ [N/mm2]	301,49	1	120 / 100
$\sigma_{V,F,FS}$ [N/mm2]	301,4	1	120 / 100
Lower Flange		*Blade Element [-]*	*Rotor Angle [deg] / Wall position of occurance [%]*
$\tau_{max,LF}$ [N/mm2]	-29,14	55	60 / 0
$\sigma_{max,tens,LF}$ [N/mm2]	301,42	1	120 / 0
$\sigma_{max,comp,LF}$ [N/mm2]	-75,37	1	300 / 100
$\sigma_{V,N,LF}$ [N/mm2]	301,65	1	120 / 0
$\sigma_{V,S,LF}$ [N/mm2]	301,88	1	120 / 0
$\sigma_{V,F,LF}$ [N/mm2]	301,76	1	120 / 0
Rear Spar		*Blade Element [-]*	*Rotor Angle [deg] / Wall position of occurance [%]*
$\tau_{max,RS}$ [N/mm2]	7,27	1	120 / 66,67
$\sigma_{max,tens,RS}$ [N/mm2]	208,95	44	120 / 0
$\sigma_{max,comp,RS}$ [N/mm2]	-268,45	1	300 / 100
$\sigma_{V,N,RS}$ [N/mm2]	268,49	1	300 / 100
$\sigma_{V,S,RS}$ [N/mm2]	268,52	1	300 / 100
$\sigma_{V,F,RS}$ [N/mm2]	268,51	1	300 / 100
Test of Maximum values against ref.			
OK			

Table 5.5: Results for 8m/s and maximum C_P

Part 2			
General Results		**Hub loads**	
v_1 [m/s]	10	$M_{Torsion}$ [Nm]	-45775,3
$rev_{min}[min^{-1}]$	12,2	F_{CF} [N]	541974,58
Max. Mach No. [-]	0,2182	F_{torque} [N]	25503,1
F_{torque} / F_{thrust} [-]	0,1504	F_{thrust} [N]	169600,1
T [Nm]	2505266,56	M_{thrust} [Nm]	6508359,8
P [W]	3203304,5	Resulting arm, Torque [m]	32,7
CP [-]	0,4949	Resulting arm, Thrust [m]	38,4
Maximum Stress values			
Upper Flange		*Blade Element [-]*	*Rotor Angle [deg] / Wall position of occurance [%]*
$\tau_{max,UF}$ [N/mm²]	-46,47	55	240 / 100
$\sigma_{max,tens,UF}$ [N/mm2]	44,36	1	240 / 100
$\sigma_{max,comp,UF}$ [N/mm2]	-416,53	1	300 / 0
$\sigma_{V,N,UF}$ [N/mm2]	416,64	1	300 / 0
$\sigma_{V,S,UF}$ [N/mm2]	416,74	1	300 / 0
$\sigma_{V,F,UF}$ [N/mm2]	416,69	1	300 / 0
Front Spar		*Blade Element [-]*	*Rotor Angle [deg] / Wall position of occurance [%]*
$\tau_{max,FS}$ [N/mm2]	-32,04	52	240 / 33,33
$\sigma_{max,tens,FS}$ [N/mm2]	468,79	1	120 / 100
$\sigma_{max,comp,FS}$ [N/mm2]	-384,83	44	60 / 0
$\sigma_{V,N,FS}$ [N/mm2]	469,03	1	120 / 100
$\sigma_{V,S,FS}$ [N/mm2]	469,28	1	120 / 100
$\sigma_{V,F,FS}$ [N/mm2]	469,16	1	120 / 100
Lower Flange		*Blade Element [-]*	*Rotor Angle [deg] / Wall position of occurance [%]*
$\tau_{max,LF}$ [N/mm2]	-45,44	55	60 / 0
$\sigma_{max,tens,LF}$ [N/mm2]	469,23	1	120 / 0
$\sigma_{max,comp,LF}$ [N/mm2]	-95,83	1	300 / 100
$\sigma_{V,N,LF}$ [N/mm2]	469,54	1	120 / 0
$\sigma_{V,S,LF}$ [N/mm2]	469,84	1	120 / 0
$\sigma_{V,F,LF}$ [N/mm2]	469,69	1	120 / 0
Rear Spar		*Blade Element [-]*	*Rotor Angle [deg] / Wall position of occurance [%]*
$\tau_{max,RS}$ [N/mm2]	10,84	25	60 / 33,33
$\sigma_{max,tens,RS}$ [N/mm2]	321,12	46	120 / 0
$\sigma_{max,comp,RS}$ [N/mm2]	-416,88	1	300 / 100
$\sigma_{V,N,RS}$ [N/mm2]	416,97	1	300 / 100
$\sigma_{V,S,RS}$ [N/mm2]	417,06	1	300 / 100
$\sigma_{V,F,RS}$ [N/mm2]	417,01	1	300 / 100
Test of Maximum values against ref.			
OK			

Table 5.6: Results for 10 m/s and maximum C_P

Part 2			
General Results		**Hub loads**	
v_1 [m/s]	12	$M_{Torsion}$ [Nm]	-65898,5
$rev_{min}[min^{-1}]$	14,7	F_{cF} [N]	780230,36
Max. Mach No. [-]	0,2618	F_{torque}	36728,9
F_{torque} / F_{thrust} [-]	0,1504	F_{thrust} [N]	244200,0
T [Nm]	3608015,39	M_{thrust} [Nm]	9370987,6
P [W]	5535216,64	Resulting arm, Torque [m]	32,7
CP [-]	0,4949	Resulting arm, Thrust [m]	38,4
Maximum Stress values			
Upper Flange		*Blade Element [-]*	*Rotor Angle [deg] / Wall position of occurance [%]*
$\tau_{max,UF}$ [N/mm²]	-66,81	55	240 / 100
$\sigma_{max,tens,UF}$ [N/mm2]	44,72	1	240 / 100
$\sigma_{max,comp,UF}$ [N/mm2]	-597,75	1	300 / 0
$\sigma_{V,N,UF}$ [N/mm2]	597,93	1	300 / 0
$\sigma_{V,S,UF}$ [N/mm2]	598,11	1	300 / 0
$\sigma_{V,F,UF}$ [N/mm2]	598,02	1	300 / 0
Front Spar		*Blade Element [-]*	*Rotor Angle [deg] / Wall position of occurance [%]*
$\tau_{max,FS}$ [N/mm2]	-46,12	52	240 / 33,33
$\sigma_{max,tens,FS}$ [N/mm2]	673,7	1	120 / 100
$\sigma_{max,comp,FS}$ [N/mm2]	-549,54	44	60 / 0
$\sigma_{V,N,FS}$ [N/mm2]	674,02	1	120 / 100
$\sigma_{V,S,FS}$ [N/mm2]	674,34	1	120 / 100
$\sigma_{V,F,FS}$ [N/mm2]	674,18	1	120 / 100
Lower Flange		*Blade Element [-]*	*Rotor Angle [deg] / Wall position of occurance [%]*
$\tau_{max,LF}$ [N/mm2]	-65,36	55	60 / 0
$\sigma_{max,tens,LF}$ [N/mm2]	674,32	1	120 / 0
$\sigma_{max,comp,LF}$ [N/mm2]	-120,82	1	300 / 100
$\sigma_{V,N,LF}$ [N/mm2]	674,71	1	120 / 0
$\sigma_{V,S,LF}$ [N/mm2]	675,1	1	120 / 0
$\sigma_{V,F,LF}$ [N/mm2]	674,91	1	120 / 0
Rear Spar		*Blade Element [-]*	*Rotor Angle [deg] / Wall position of occurance [%]*
$\tau_{max,RS}$ [N/mm2]	15,48	26	60 / 33,33
$\sigma_{max,tens,RS}$ [N/mm2]	458,23	46	120 / 0
$\sigma_{max,comp,RS}$ [N/mm2]	-598,28	1	300 / 100
$\sigma_{V,N,RS}$ [N/mm2]	598,43	1	300 / 100
$\sigma_{V,S,RS}$ [N/mm2]	598,58	1	300 / 100
$\sigma_{V,F,RS}$ [N/mm2]	598,5	1	300 / 100
Test of Maximum values against ref.			
OK			

Table 5.7: Results 12m/s and maximum C_P

Part 3			
General Results		**Hub loads**	
v_1 [m/s]	14	$M_{Torsion}$ [Nm]	-81961,6
$rev_{min}[min^{-1}]$	16,1	F_{cF} [N]	942322,03
Max. Mach No. [-]	0,2883	F_{torque} [N]	46092,1
F_{torque} / F_{thrust} [-]	0,1963	F_{thrust} [N]	234833,8
T [Nm]	4440240,46	M_{thrust} [Nm]	8814805,4
P [W]	7486192,38	Resulting arm, Torque [m]	32,1
CP [-]	0,4215	Resulting arm, Thrust [m]	37,5
Maximum Stress values			
Upper Flange		*Blade Element [-]*	*Rotor Angle [deg] / Wall position of occurance [%]*
$\tau_{max,UF}$ [N/mm²]	-62,26	55	60 / 100
$\sigma_{max,tens,UF}$ [N/mm2]	118,13	1	240 / 100
$\sigma_{max,comp,UF}$ [N/mm2]	-623,06	1	60 / 0
$\sigma_{V,N,UF}$ [N/mm2]	623,38	1	60 / 0
$\sigma_{V,S,UF}$ [N/mm2]	623,7	1	60 / 0
$\sigma_{V,F,UF}$ [N/mm2]	623,54	1	60 / 0
Front Spar		*Blade Element [-]*	*Rotor Angle [deg] / Wall position of occurance [%]*
$\tau_{max,FS}$ [N/mm2]	-43,28	52	60 / 33,33
$\sigma_{max,tens,FS}$ [N/mm2]	703,28	1	120 / 100
$\sigma_{max,comp,FS}$ [N/mm2]	-401,09	44	60 / 0
$\sigma_{V,N,FS}$ [N/mm2]	703,6	1	120 / 100
$\sigma_{V,S,FS}$ [N/mm2]	703,92	1	120 / 100
$\sigma_{V,F,FS}$ [N/mm2]	703,76	1	120 / 100
Lower Flange		*Blade Element [-]*	*Rotor Angle [deg] / Wall position of occurance [%]*
$\tau_{max,LF}$ [N/mm2]	-61,09	55	60 / 0
$\sigma_{max,tens,LF}$ [N/mm2]	704,03	1	120 / 0
$\sigma_{max,comp,LF}$ [N/mm2]	-186,62	1	300 / 100
$\sigma_{V,N,LF}$ [N/mm2]	704,41	1	120 / 0
$\sigma_{V,S,LF}$ [N/mm2]	704,8	1	120 / 0
$\sigma_{V,F,LF}$ [N/mm2]	704,61	1	120 / 0
Rear Spar		*Blade Element [-]*	*Rotor Angle [deg] / Wall position of occurance [%]*
$\tau_{max,RS}$ [N/mm2]	14,18	21	60 / 33,33
$\sigma_{max,tens,RS}$ [N/mm2]	317,04	46	120 / 0
$\sigma_{max,comp,RS}$ [N/mm2]	-623,71	1	60 / 100
$\sigma_{V,N,RS}$ [N/mm2]	623,97	1	60 / 100
$\sigma_{V,S,RS}$ [N/mm2]	624,24	1	60 / 100
$\sigma_{V,F,RS}$ [N/mm2]	624,1	1	60 / 100
Test of Maximum values against ref.			
OK			

Table 5.8: Results 14m/s and de-rated C_P

Part 3			
General Results		**Hub loads**	
v_1 [m/s]	16	$M_{Torsion}$ [Nm]	-90272,3
$rev_{min}[min^{-1}]$	16,7	F_{CF} [N]	1017511,85
Max. Mach No. [-]	0,3003	F_{torque} [N]	55135,3
F_{torque} / F_{thrust} [-]	0,2383	F_{thrust} [N]	231334,0
T [Nm]	5148798,65	M_{thrust} [Nm]	8459297,4
P [W]	9020497,02	Resulting arm, Torque [m]	31,1
CP [-]	0,3402	Resulting arm, Thrust [m]	36,6
Maximum Stress values			
Upper Flange		*Blade Element [-]*	*Rotor Angle [deg] / Wall position of occurance [%]*
$\tau_{max,UF}$ [N/mm²]	-58,06	55	60 / 100
$\sigma_{max,tens,UF}$ [N/mm2]	141,35	1	240 / 100
$\sigma_{max,comp,UF}$ [N/mm2]	-620,16	1	60 / 0
$\sigma_{V,N,UF}$ [N/mm2]	620,49	1	60 / 0
$\sigma_{V,S,UF}$ [N/mm2]	620,81	1	60 / 0
$\sigma_{V,F,UF}$ [N/mm2]	620,65	1	60 / 0
Front Spar		*Blade Element [-]*	*Rotor Angle [deg] / Wall position of occurance [%]*
$\tau_{max,FS}$ [N/mm2]	-40,51	52	60 / 33,33
$\sigma_{max,tens,FS}$ [N/mm2]	698,63	1	120 / 100
$\sigma_{max,comp,FS}$ [N/mm2]	-325,57	46	60 / 0
$\sigma_{V,N,FS}$ [N/mm2]	698,97	1	120 / 100
$\sigma_{V,S,FS}$ [N/mm2]	699,3	1	120 / 100
$\sigma_{V,F,FS}$ [N/mm2]	699,13	1	120 / 100
Lower Flange		*Blade Element [-]*	*Rotor Angle [deg] / Wall position of occurance [%]*
$\tau_{max,LF}$ [N/mm2]	-56,91	55	60 / 0
$\sigma_{max,tens,LF}$ [N/mm2]	699,43	1	120 / 0
$\sigma_{max,comp,LF}$ [N/mm2]	-204,57	1	300 / 100
$\sigma_{V,N,LF}$ [N/mm2]	699,84	1	120 / 0
$\sigma_{V,S,LF}$ [N/mm2]	700,24	1	120 / 0
$\sigma_{V,F,LF}$ [N/mm2]	700,04	1	120 / 0
Rear Spar		*Blade Element [-]*	*Rotor Angle [deg] / Wall position of occurance [%]*
$\tau_{max,RS}$ [N/mm2]	13,74	1	12 / 33,33
$\sigma_{max,tens,RS}$ [N/mm2]	248,11	46	120 / 0
$\sigma_{max,comp,RS}$ [N/mm2]	-620,87	1	60 / 100
$\sigma_{V,N,RS}$ [N/mm2]	621,13	1	60 / 100
$\sigma_{V,S,RS}$ [N/mm2]	621,4	1	60 / 100
$\sigma_{V,F,RS}$ [N/mm2]	621,26	1	60 / 100
Test of Maximum values against ref.			
OK			

Table 5.9: Results 16m/s and de-rated C_P

Part 3			
General Results		**Hub loads**	
v_1 [m/s]	18	$M_{Torsion}$ [Nm]	-100281,4
$rev_{min}[min^{-1}]$	17,5	F_{CF} [N]	1110786,13
Max. Mach No. [-]	0,3144	F_{torque} [N]	62730,0
F_{torque} / F_{thrust} [-]	0,2754	F_{thrust} [N]	227775,8
T [Nm]	5658053,36	M_{thrust} [Nm]	8103891,1
P [W]	10357074,14	Resulting arm, Torque [m]	30,1
CP [-]	0,2744	Resulting arm, Thrust [m]	35,6
Maximum Stress values			
Upper Flange		*Blade Element [-]*	*Rotor Angle [deg] / Wall position of occurance [%]*
$\tau_{max,UF}$ [N/mm²]	-54,26	55	60 / 100
$\sigma_{max,tens,UF}$ [N/mm2]	160,49	1	240 / 100
$\sigma_{max,comp,UF}$ [N/mm2]	-612,55	1	60 / 0
$\sigma_{V,N,UF}$ [N/mm2]	612,87	1	60 / 0
$\sigma_{V,S,UF}$ [N/mm2]	613,19	1	60 / 0
$\sigma_{V,F,UF}$ [N/mm2]	613,03	1	60 / 0
Front Spar		*Blade Element [-]*	*Rotor Angle [deg] / Wall position of occurance [%]*
$\tau_{max,FS}$ [N/mm2]	-37,96	51	60 / 33,33
$\sigma_{max,tens,FS}$ [N/mm2]	689,56	1	120 / 100
$\sigma_{max,comp,FS}$ [N/mm2]	-260,82	46	60 / 0
$\sigma_{V,N,FS}$ [N/mm2]	689,91	1	120 / 100
$\sigma_{V,S,FS}$ [N/mm2]	690,26	1	120 / 100
$\sigma_{V,F,FS}$ [N/mm2]	690,09	1	120 / 100
Lower Flange		*Blade Element [-]*	*Rotor Angle [deg] / Wall position of occurance [%]*
$\tau_{max,LF}$ [N/mm2]	-53,15	55	60 / 0
$\sigma_{max,tens,LF}$ [N/mm2]	690,43	1	120 / 0
$\sigma_{max,comp,LF}$ [N/mm2]	-218,08	1	300 / 100
$\sigma_{V,N,LF}$ [N/mm2]	690,85	1	120 / 0
$\sigma_{V,S,LF}$ [N/mm2]	691,28	1	120 / 0
$\sigma_{V,F,LF}$ [N/mm2]	691,07	1	120 / 0
Rear Spar		*Blade Element [-]*	*Rotor Angle [deg] / Wall position of occurance [%]*
$\tau_{max,RS}$ [N/mm2]	13,62	1	60 / 33,33
$\sigma_{max,tens,RS}$ [N/mm2]	190,19	48	120 / 0
$\sigma_{max,comp,RS}$ [N/mm2]	-613,33	1	60 / 100
$\sigma_{V,N,RS}$ [N/mm2]	613,59	1	60 / 100
$\sigma_{V,S,RS}$ [N/mm2]	613,85	1	60 / 100
$\sigma_{V,F,RS}$ [N/mm2]	613,72	1	60 / 100
Test of Maximum values against ref.			

Table 5.10: Results 18m/s and de-rated C_P

Part 3			
General Results		**Hub loads**	
v_1 [m/s]	20	$M_{Torsion}$ [Nm]	-112400,7
rev_{min}[min^{-1}]	18,4	F_{CF} [N]	1226777,8
Max. Mach No. [-]	0,331	F_{torque} [N]	71293,4
F_{torque} / F_{thrust} [-]	0,3053	F_{thrust} [N]	233520,7
T [Nm]	6240435,06	M_{thrust} [Nm]	8111304,2
P [W]	12004736,8	Resulting arm, Torque [m]	29,2
CP [-]	0,2318	Resulting arm, Thrust [m]	34,7
Maximum Stress values			
Upper Flange		*Blade Element [-]*	*Rotor Angle [deg] / Wall position of occurance [%]*
$\tau_{max,UF}$ [N/mm^2]	-53,47	55	60 / 100
$\sigma_{max,tens,UF}$ [N/mm2]	174,7	1	240 / 100
$\sigma_{max,comp,UF}$ [N/mm2]	-623,06	1	60 / 0
$\sigma_{V,N,UF}$ [N/mm2]	623,38	1	60 / 0
$\sigma_{V,S,UF}$ [N/mm2]	623,71	1	60 / 0
$\sigma_{V,F,UF}$ [N/mm2]	623,55	1	60 / 0
Front Spar		*Blade Element [-]*	*Rotor Angle [deg] / Wall position of occurance [%]*
$\tau_{max,FS}$ [N/mm2]	-37,31	51	60 / 33,33
$\sigma_{max,tens,FS}$ [N/mm2]	701,5	1	120 / 100
$\sigma_{max,comp,FS}$ [N/mm2]	-224,19	46	60 / 0
$\sigma_{V,N,FS}$ [N/mm2]	701,88	1	120 / 100
$\sigma_{V,S,FS}$ [N/mm2]	702,26	1	120 / 100
$\sigma_{V,F,FS}$ [N/mm2]	702,07	1	120 / 100
Lower Flange		*Blade Element [-]*	*Rotor Angle [deg] / Wall position of occurance [%]*
$\tau_{max,LF}$ [N/mm2]	-52,35	55	60 / 0
$\sigma_{max,tens,LF}$ [N/mm2]	702,45	1	120 / 0
$\sigma_{max,comp,LF}$ [N/mm2]	-230	1	300 / 100
$\sigma_{V,N,LF}$ [N/mm2]	702,92	1	120 / 0
$\sigma_{V,S,LF}$ [N/mm2]	703,38	1	120 / 0
$\sigma_{V,F,LF}$ [N/mm2]	703,15	1	120 / 0
Rear Spar		*Blade Element [-]*	*Rotor Angle [deg] / Wall position of occurance [%]*
$\tau_{max,RS}$ [N/mm2]	13,94	1	60 / 33,33
$\sigma_{max,tens,RS}$ [N/mm2]	157,66	48	120 / 0
$\sigma_{max,comp,RS}$ [N/mm2]	-623,91	1	60 / 100
$\sigma_{V,N,RS}$ [N/mm2]	624,18	1	60 / 100
$\sigma_{V,S,RS}$ [N/mm2]	624,45	1	60 / 100
$\sigma_{V,F,RS}$ [N/mm2]	624,32	1	60 / 100
Test of Maximum values against ref.			
OK			

Table 5.11: Results 20m/s and de-rated C_P

Part 3			
General Results		**Hub loads**	
v_1 [m/s]	22	$M_{Torsion}$ [Nm]	-124107,4
rev_{min}[min^{-1}]	19,2	F_{CF} [N]	1334561,5
Max. Mach No. [-]	0,3458	F_{torque} [N]	80096,1
F_{torque} / F_{thrust} [-]	0,3358	F_{thrust} [N]	238515,5
T [Nm]	6796852,37	M_{thrust} [Nm]	8070932,9
P [W]	13637411,96	Resulting arm, Torque [m]	28,3
CP [-]	0,1979	Resulting arm, Thrust [m]	33,8
Maximum Stress values			
Upper Flange		*Blade Element [-]*	*Rotor Angle [deg] / Wall position of occurance [%]*
$\tau_{max,UF}$ [N/mm^2]	-52,07	54	60 / 100
$\sigma_{max,tens,UF}$ [N/mm2]	183,26	1	240 / 100
$\sigma_{max,comp,UF}$ [N/mm2]	-624,79	1	60 / 0
$\sigma_{V,N,UF}$ [N/mm2]	625,13	1	60 / 0
$\sigma_{V,S,UF}$ [N/mm2]	625,47	1	60 / 0
$\sigma_{V,F,UF}$ [N/mm2]	625,3	1	60 / 0
Front Spar		*Blade Element [-]*	*Rotor Angle [deg] / Wall position of occurance [%]*
$\tau_{max,FS}$ [N/mm2]	-36,3	51	60 / 33,33
$\sigma_{max,tens,FS}$ [N/mm2]	704,39	1	120 / 100
$\sigma_{max,comp,FS}$ [N/mm2]	-190,02	46	60 / 0
$\sigma_{V,N,FS}$ [N/mm2]	704,81	1	120 / 100
$\sigma_{V,S,FS}$ [N/mm2]	705,23	1	120 / 100
$\sigma_{V,F,FS}$ [N/mm2]	705,02	1	120 / 100
Lower Flange		*Blade Element [-]*	*Rotor Angle [deg] / Wall position of occurance [%]*
$\tau_{max,LF}$ [N/mm2]	-50,97	54	60 / 0
$\sigma_{max,tens,LF}$ [N/mm2]	705,43	1	120 / 0
$\sigma_{max,comp,LF}$ [N/mm2]	-235,76	1	300 / 100
$\sigma_{V,N,LF}$ [N/mm2]	705,93	1	120 / 0
$\sigma_{V,S,LF}$ [N/mm2]	706,44	1	120 / 0
$\sigma_{V,F,LF}$ [N/mm2]	706,19	1	120 / 0
Rear Spar		*Blade Element [-]*	*Rotor Angle [deg] / Wall position of occurance [%]*
$\tau_{max,RS}$ [N/mm2]	14,22	1	60 / 33,33
$\sigma_{max,tens,RS}$ [N/mm2]	128,8	49	120 / 0
$\sigma_{max,comp,RS}$ [N/mm2]	-625,73	1	60 / 100
$\sigma_{V,N,RS}$ [N/mm2]	626,01	1	60 / 100
$\sigma_{V,S,RS}$ [N/mm2]	626,28	1	60 / 100
$\sigma_{V,F,RS}$ [N/mm2]	626,14	1	60 / 100
Test of Maximum values against ref.			
OK			

Table 5.12: Results 22m/s and de-rated C_P

Part 3			
General Results		**Hub loads**	
v_1 [m/s]	24	$M_{Torsion}$ [Nm]	-130758,4
$rev_{min}[min^{-1}]$	19,5	F_{CF} [N]	1379512,05
Max. Mach No. [-]	0,3525	F_{torque} [N]	86894,1
F_{torque} / F_{thrust} [-]	0,3804	F_{thrust} [N]	228403,3
T [Nm]	7046540,4	M_{thrust} [Nm]	7417652,9
P [W]	14374525,47	Resulting arm, Torque [m]	27,0
CP [-]	0,1606	Resulting arm, Thrust [m]	32,5
Maximum Stress values			
Upper Flange		*Blade Element [-]*	*Rotor Angle [deg] / Wall position of occurance [%]*
$\tau_{max,UF}$ [N/mm²]	-45,28	54	60 / 100
$\sigma_{max,tens,UF}$ [N/mm2]	178,4	1	240 / 100
$\sigma_{max,comp,UF}$ [N/mm2]	-574,49	1	60 / 0
$\sigma_{V,N,UF}$ [N/mm2]	574,84	1	60 / 0
$\sigma_{V,S,UF}$ [N/mm2]	575,18	1	60 / 0
$\sigma_{V,F,UF}$ [N/mm2]	575,01	1	60 / 0
Front Spar		*Blade Element [-]*	*Rotor Angle [deg] / Wall position of occurance [%]*
$\tau_{max,FS}$ [N/mm2]	-31,8	51	60 / 33,33
$\sigma_{max,tens,FS}$ [N/mm2]	650,69	1	120 / 100
$\sigma_{max,comp,FS}$ [N/mm2]	-136,73	46	60 / 0
$\sigma_{V,N,FS}$ [N/mm2]	651,15	1	120 / 100
$\sigma_{V,S,FS}$ [N/mm2]	651,6	1	120 / 100
$\sigma_{V,F,FS}$ [N/mm2]	651,37	1	120 / 100
Lower Flange		*Blade Element [-]*	*Rotor Angle [deg] / Wall position of occurance [%]*
$\tau_{max,LF}$ [N/mm2]	-44,38	54	60 / 0
$\sigma_{max,tens,LF}$ [N/mm2]	651,76	1	120 / 0
$\sigma_{max,comp,LF}$ [N/mm2]	-222,39	1	300 / 100
$\sigma_{V,N,LF}$ [N/mm2]	652,31	1	120 / 0
$\sigma_{V,S,LF}$ [N/mm2]	652,86	1	120 / 0
$\sigma_{V,F,LF}$ [N/mm2]	652,58	1	120 / 0
Rear Spar		*Blade Element [-]*	*Rotor Angle [deg] / Wall position of occurance [%]*
$\tau_{max,RS}$ [N/mm2]	13,8	1	60 / 33,33
$\sigma_{max,tens,RS}$ [N/mm2]	88,05	49	120 / 0
$\sigma_{max,comp,RS}$ [N/mm2]	-575,46	1	60 / 100
$\sigma_{V,N,RS}$ [N/mm2]	575,75	1	60 / 100
$\sigma_{V,S,RS}$ [N/mm2]	576,03	1	60 / 100
$\sigma_{V,F,RS}$ [N/mm2]	575,89	1	60 / 100
Test of Maximum values against ref.			
OK			

Table 5.13: Results 24m/s and de-rated C_P

5.2.1 Discussion of the Calculation Tool Results

From these results can be seen, that even though the amount of produced power from the rotor rises considerably higher than the limit of the Areva Wind M5000, it is also clear that the C_P value at higher wind speeds drops sharply from the value at and below the rated wind speed. This fact underlines that the blade loading in terms of efficiency indeed has to be lowered quite much for the strain on the blades to be kept within limits. The comparison of the C_P value developed here, with the C_P value of a flat rating above the reference wind speed can be seen in Figure 5.4:

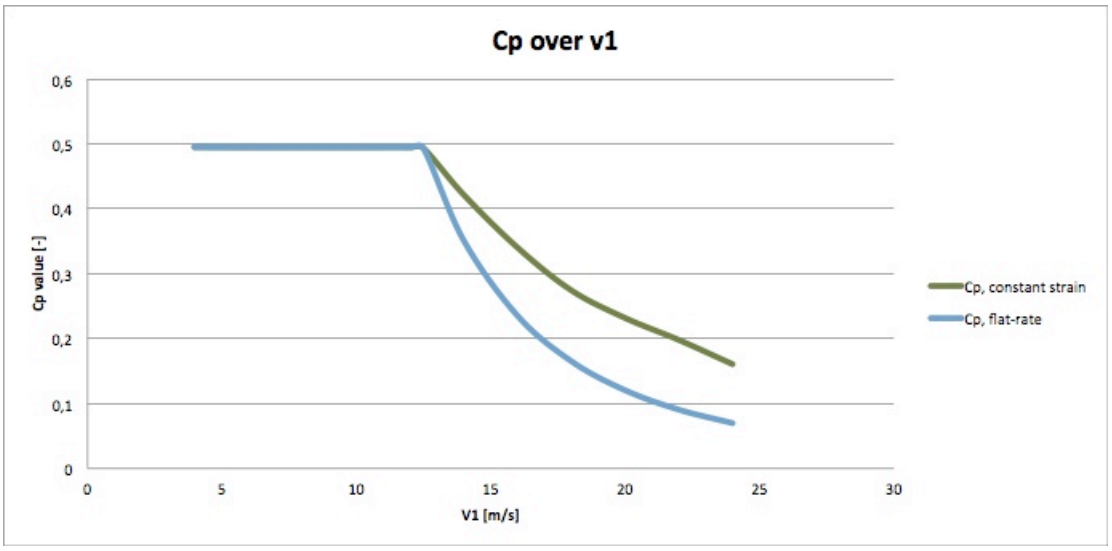

Figure 5.4: Comparison of the developed- and flat-rated C_P

As Figure 5.4 shows, is there a marked difference in C_P value compared to that of the flat rate scenario. Maybe somewhat unexpected, however, seems the difference, after an initial increase, to decrease to a certain degree towards the highest wind speeds. The difference of these two C_P values are displayed in Figure 5.5:

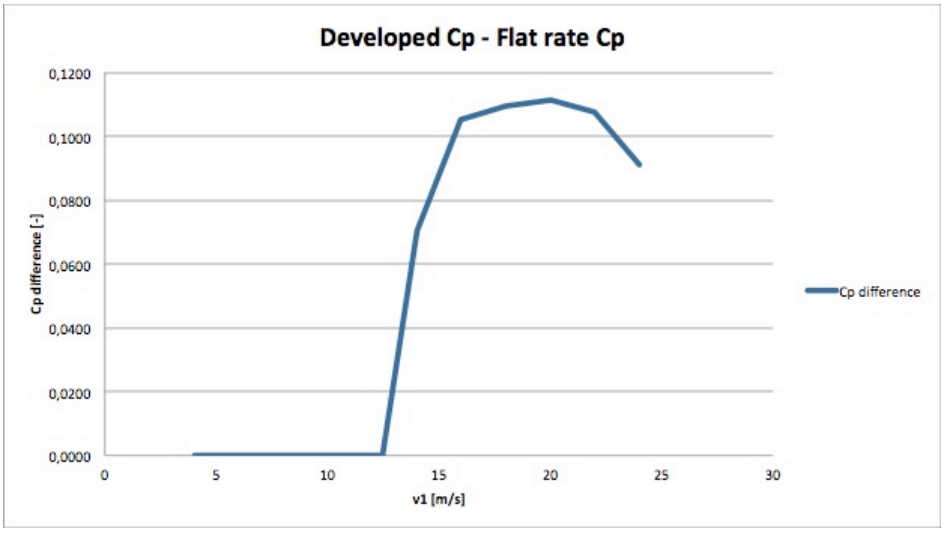

Figure 5.5: Difference in C_P value: Developed - Flat rate

Another interesting relationship to study is that of the available power in the wind over the rotor disc area, the captured power by flat rating and the captured power from these calculations. This is to be seen in Figure 5.6:

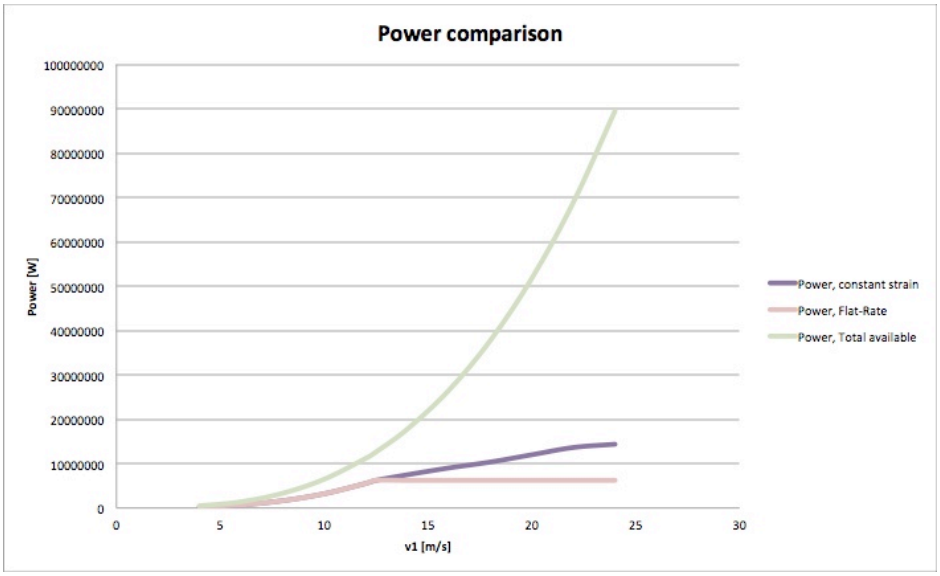

Figure 5.6: Comparison of available and captured power

From Figure 5.6 it is evident that even though the power output from the rotor by 24m/s has risen with a factor of about 2.3 compared to the power output at 12,5m/s, this is still just a small fraction of the available power in the wind. As shown in (5.1), increases the available power with the cube of the wind speed. From this figure, one can also derive, that the relationship between the developed power curve and the wind speed above the rated wind speed seems to be virtually linear.

To understand the relationship between the decreasing C_P value and the nearly constant strain on the blades, the results for the forces and moments will have to be studied in detail. This is also important for the validation of the quality of the results from the calculation tool. The loads due to gravity are omitted in the tables, as these are constant for all conditions, and are only dependent on rotor angle. Here will the maximum value of compressive stress, $\sigma_{max,comp}$ for the upper flange from Table 5.3 to Table 5.13 serve as an example. In Table 5.3, for a wind speed of 4m/s, is $\sigma_{max,comp}$ given at a rotor angle of 60°, and 100% of the side, meaning the position directly above the front spar. When the wind speed increases, however, this location changes to 300° and 0% of the side, before at wind speeds above the rated wind speed the location becomes 60° and 0%.

Trying to understand this, one have to consider the load picture on the torque box, shown in Figure 2.14. One can derive from this picture, that the resulting compression or tension in either torque box wall is the combined picture of the bending moments perpendicular to the chord line, the bending moments parallel to the chord line, and the normal forces. Because of the pitch angle do all of the shear forces, which also generate bending moments, have components in both directions. The results of part 2 of the program are further ideal to study the development and changes in the occurrences of the maximum values, as they all are obtained under maximum C_P value, and therefor also a virtually constant tip speed ratio, which in turn also keep the pitch angles at the corresponding blade elements almost constant. In other words are the angles of the cross sections at the corresponding blade elements as shown in Figure 2.14 the same, and the only sizes that change as the wind speed increases, are the magnitude of the forces and moments. At wind speeds above the rated wind speed one has to consider the alteration of the forces, moments *and* the pitch angles.

As described in the text for Figure 2.14, is this picture applicable for a rotor angle between 181° and 359°, recognizable by the direction of the shear force from gravity. For the case of 4m/s as mentioned above, it is evident that the effect of the bending moments from torque and gravity shear force perpendicular to the chord line at a rotor angle of 60° are greater than that of the bending moments from thrust and gravity shear force parallel to the chord line at 300°. This does not mean that the torque is greater than the thrust, because the pitch angle determines the magnitude of the force components in each direction, and naturally are the values for SMA in each of the directions crucial to the resulting stresses. As indicated above changes this picture as the wind speed increases, and the effect of the bending moments from thrust and gravity shear force become the major components. This can further be quantified and logically explained with the wall positions of occurrences: For 4m/s, where the bending moments perpendicular to the chord line from torque and gravity shear force at 60° are the decisive components, the maximum compressive stress occurs at 100% of the side, which makes sense, as this position has the highest z-value, ref. the equation:

$$\sigma_{yx} = \frac{M_X}{I_X} \cdot z \qquad (5.8)$$

At this position is also the result of the bending moments from torque and gravity shear force *parallel* to the chord line compressive stresses, whereas the effect on the 0% position, which is directly above the rear spar, is a tensional stress.

This is further also the explanation why the position of occurrence at higher wind speeds, when at 300° the bending moments from thrust and gravity parallel to the chord line are the major effect, is at 0% of the wall. This position is hence the position with the highest x-value, and when applying (5.8) for this direction, the position that also delivers the highest compressive stress value. In Figure 5.7 are the changes of the forces inertia, torque force and thrust shown, and this can explain the change in the rotor angle and position of occurrence for the maximum compressive stress explained above:

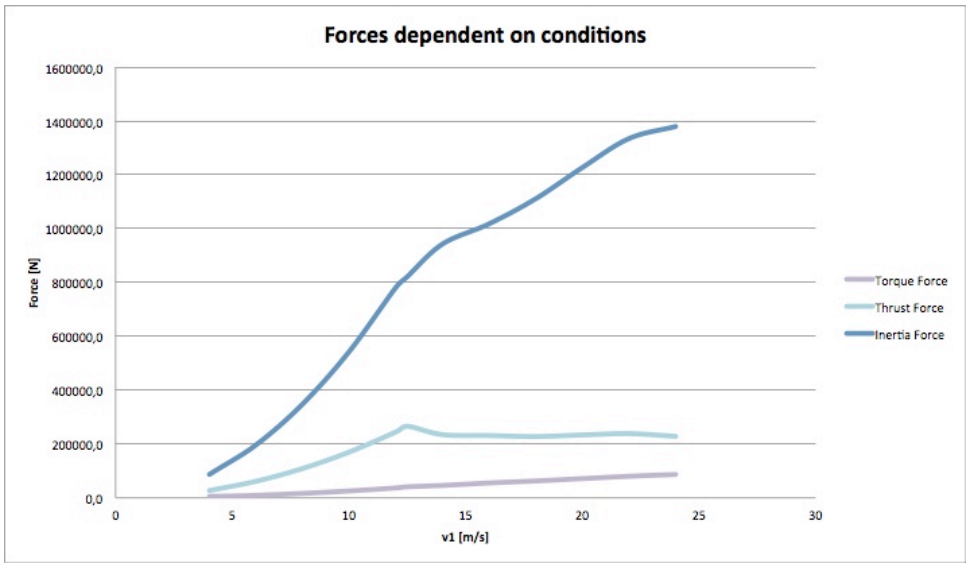

Figure 5.7: Changes in inertia, torque force and thrust over increasing wind speed

One can recognize that the thrust increases far more rapidly than the torque, and the corresponding bending moment is probably the reason for the change from 4m/s to higher wind speeds up to the rated wind speed. The inertia force is clearly the greatest force in value, but this is also a pure normal force, which does not cause a bending moment. Because of the much higher radius/length of the blade compared to the chord, the bending moments have a greater impact on the tensional and compressive stresses in the torque box than the normal forces. This is also recognizable in the tables, in that none of the maximum tensional stress values, $\sigma_{max,tens}$, occur at 180° where the complete mass of the blade strains the torque box as a normal force. The strains are greater at 120° or 240°, where a component of the mass acts like a shear force,

and causes tensional stress at one side and compressional stress at the other side.

At higher wind speeds, however, changes the position of occurrence for the maximum compressive stress to 60° and 0% of the side. One has to bear in mind that with the decreasing C_P value changes also the pitch angles in the torque box sections, which further alter the magnitude of the bending moments perpendicular and parallel to the chord line. What can be said about the scenario at 60°, however, is that all of the three bending moments have a compressive effect perpendicular to the chord line on the upper flange, and this seems to be the decisive factor. The thrust also has a compressive effect parallel to the chord line; whereas torque and gravity shear force have tensional effects. The final result is decided by the combination of the magnitude of the forces and moments and the pitch angle, but in light of the changing loading picture as the C_P value changes, this is also a result that makes sense, because the thrust force decreases and the torque force increases. The bending moment from thrust together with the bending moment from the gravity shear force is at 300° parallel to the chord line in other words not greater than the combined effect of all three bending moments perpendicular to the chord line at 60° any more.

It can further be observed that all of the maximum compressive stress values for all sides of the torque box occur at either 60° or 300°, which make sense due to the compressive stress of the gravity normal force at these angles. Correspondingly, as mentioned above, occur all of the maximum tensional stress values at either 120° or 240°, when the gravity normal force causes tensional stress. Another logical connection which can be derived from the results, are that the maximum tensional stress in the rear spar occur approximately at the same spot along the blade radius as the maximum compressive stress in the front spar, at a rotor angle of 120° and 60° respectively. As the C_P value drops, they actually close in on each other before they meet at the same blade element at the results from16m/s wind speed.

The main explanation to how it is possible to extract so much more power at higher wind speeds with the decreasing C_P value is the change in the bending moments. Because of the geometry of the blade, with a high length to chord ratio, are these loads the decisive factors. It is recognizable from Figure 5.7 that the value of the thrust force is actually initially decreasing at wind speeds above the reference value, and further kept constant throughout the wind speed range. Simultaneously, as can be identified from the Table 5.7 through Table 5.13, are the arms for the resulting forces of thrust and torque decreasing. Based on this, one can already conclude that the bending moment from thrust has to decrease at higher wind speeds, and this is confirmed in Figure 5.8:

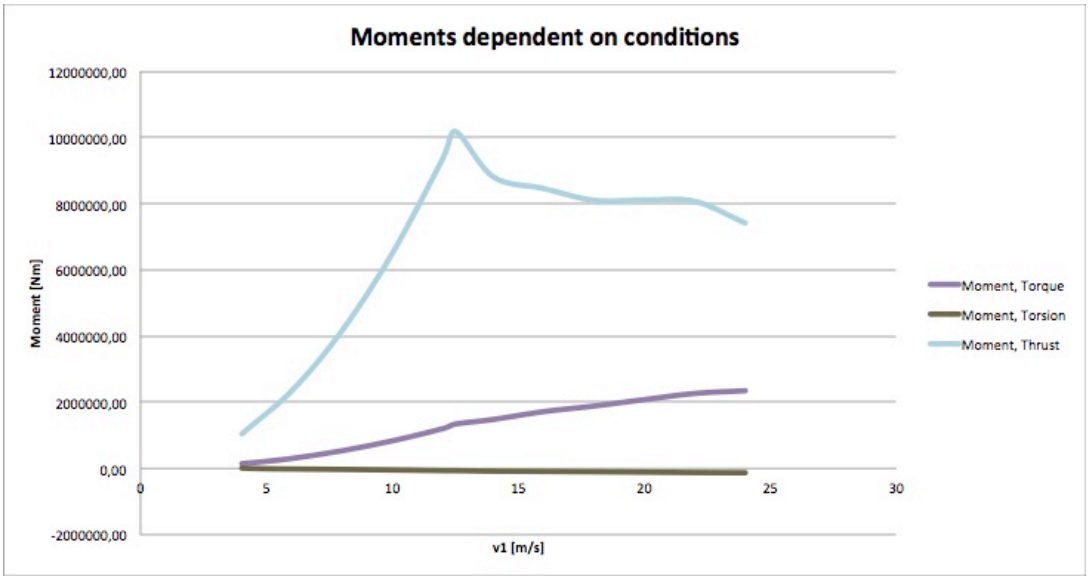

Figure 5.8: Change in bending moments over wind speed

It is here visualized how much greater the moment from thrust is compared to that of the torque, and also that the *decrease* in bending moment from thrust above the rated wind speed is greater than the *increase* in the bending moment from torque.

The torsional moment is relative to thrust and torque relatively small, but has physically a completely different effect on the blade. One can derive from the result tables that the amount of torsion moment is actually almost doubled at 24m/s compared to 12,5m/s, and even though the shear stress is within limit and probably not the sizing factor for the blades, the blade pitch system would most likely have had to be strengthened to be able to cope with this considerable increase in load.

Another interesting relationship above the rated wind speed and in connection with the decreasing C_P value is that between torque and thrust. Roughly speaking one can say that torque is the “wanted” load, and thrust the “unwanted” load. Evident in the result tables, and that can also be derived from Figure 5.7, is that the ratio torque/thrust is increasing alongside the decreasing C_P value. It can therefor be concluded that even though the effectiveness of the rotor is lowered at the higher wind speeds, it is nevertheless loaded relatively to a higher degree with the “wanted” load. This, together with the decreasing arms for the resulting forces of torque and thrust is shown in Figure 5.9:

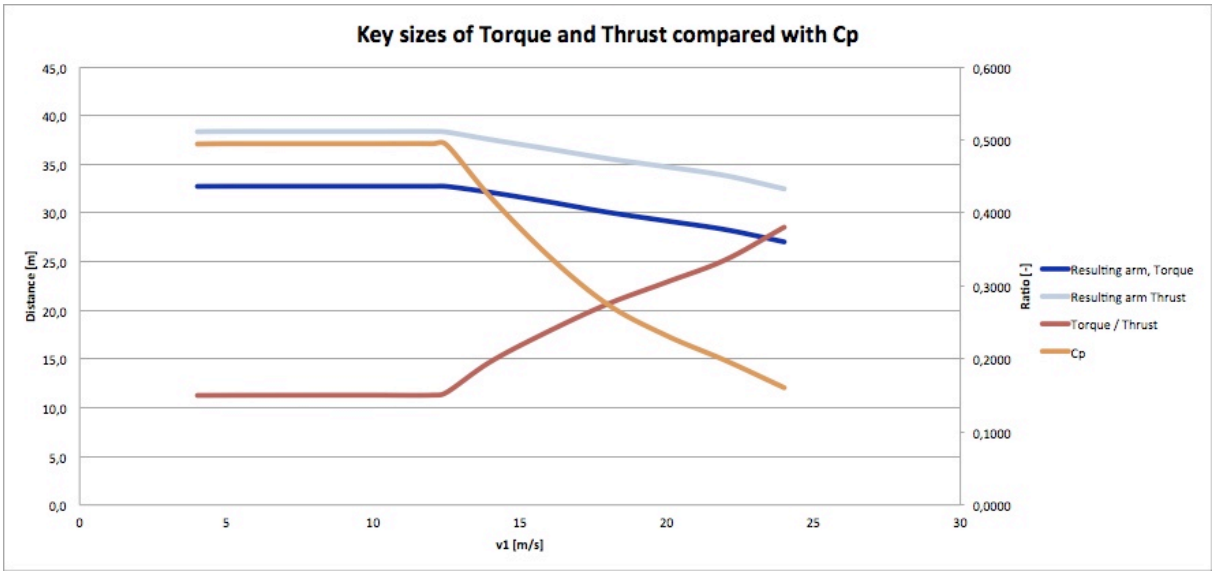

Figure 5.9: Key sizes of Torque and Thrust compared with C_P

5.2.2 Changes in tensional and compressive stress with decreasing C_P

The acceptance criteria for the load cases at higher wind speeds were, as mentioned under 5.2, the three types of comparative stress, $\sigma_{V,N}$, $\sigma_{V,S}$ and $\sigma_{V,F}$. This will now, however be seen in context with the changes in tensional and compressive stress. As mentioned earlier, seem the shear stress not to be the sizing load for any of the torque box walls.

One thing one will affirm when studying the results of the maximum tensional and compressive stress values for the torque box walls, is that the same type of normal stress, which is the greatest at the rated wind speed, is still the greatest at 24m/s. For example, for the front spar at rated wind speed, is the maximum tensional stress greater than the maximum compressive stress, and this is still the case at 24m/s. Further, if one calculates the difference between the maximum tensional and absolute value of maximum compressive stress for each wall, one will make an interesting conclusion: The difference has increased a little for the upper and lower flanges, whereas it has decreased greatly for the front and rear spar. This is probably due to the same effect discussed under 5.2.1, that the changes in pitch angle for the corresponding blade elements, compared with the altered forces and moments have created a different load picture at 24m/s compared with that of the rated wind speed. The maximum tensional and compressive stresses, with the respective difference, for each wall for these two wind speeds are listed below:

Upper flange:

12,5m/s:

$$\sigma_{\max,tens,UF} = 21,00 Mpa \quad \textbf{(5.9)}$$

$$\sigma_{\max,comp,UF} = -627,45 Mpa \quad \textbf{(5.10)}$$

$$abs\Delta\sigma = 648,45 Mpa \quad \textbf{(5.11)}$$

24m/s:

$$\sigma_{\max,tens,UF} = 178,40 Mpa \quad \textbf{(5.12)}$$

$$\sigma_{\max,comp,UF} = -574,49 Mpa \quad \textbf{(5.13)}$$

$$abs\Delta\sigma = 752,89 Mpa \quad \textbf{(5.14)}$$

Front spar:

12,5m/s:

$$\sigma_{\max,tens,FS} = 709,05 Mpa \quad \textbf{(5.15)}$$

$$\sigma_{\max,comp,FS} = -620,69 Mpa \quad \textbf{(5.16)}$$

$$abs\Delta\sigma = 1329,74 Mpa \quad \textbf{(5.17)}$$

24m/s:

$$\sigma_{\max,tens,FS} = 650,69 Mpa \quad \textbf{(5.18)}$$

$$\sigma_{\max,comp,FS} = -136,73 Mpa \quad \textbf{(5.19)}$$

$$abs\Delta\sigma = 787,42 Mpa \quad \textbf{(5.20)}$$

Lower Flange:

12,5m/s:

$$\sigma_{\max,tens,LF} = 709,69 Mpa \quad \textbf{(5.21)}$$

$$\sigma_{\max,comp,LF} = -104,30 Mpa \quad \textbf{(5.22)}$$

$$abs\Delta\sigma = 813,99 Mpa \quad \textbf{(5.23)}$$

24m/s:

$$\sigma_{\max,tens,LF} = 651,76 Mpa \quad \textbf{(5.24)}$$

$$\sigma_{\max,comp,LF} = -222,39 Mpa \quad \textbf{(5.25)}$$

$$abs\Delta\sigma = 874,15 Mpa \quad \textbf{(5.26)}$$

Rear spar:

12,5m/s:

$$\sigma_{\max,tens,RS} = 521,82 Mpa \quad \textbf{(5.27)}$$

$$\sigma_{\max,comp,RS} = -627,99 Mpa \quad \textbf{(5.28)}$$

$$abs\Delta\sigma = 1149,81 Mpa \quad \textbf{(5.29)}$$

24m/s:

$$\sigma_{\max,tens,RS} = 88,05 Mpa \quad \textbf{(5.30)}$$

$$\sigma_{\max,comp,RS} = -575,46 Mpa \quad \textbf{(5.31)}$$

$$abs\Delta\sigma = 663,51 Mpa \quad \textbf{(5.32)}$$

The main changes from the rated wind speed to 24m/s are that the front and rear spars are more uniformly loaded – tensional and compressive respectively. The case is opposite for the upper and lower flanges, which have gotten an increase in tensional and compressive stress respectively, and have thus become a greater difference in normal stress.

From these values, however, is it evident that from the static loading point of view is there not many problems in terms of allowing the rotor to follow this

developed power curve. One of the few things in need of confirmation would be to prove that lower flange would withstand the increase of compressive stress without experiencing stability issues. The dynamic loading, and the strength in terms of fatigue is of course quite a different story, and this will be discussed in the next chapter. The developed power curve, which is one of the main objectives of this diploma thesis, is displayed in Figure 5.10:

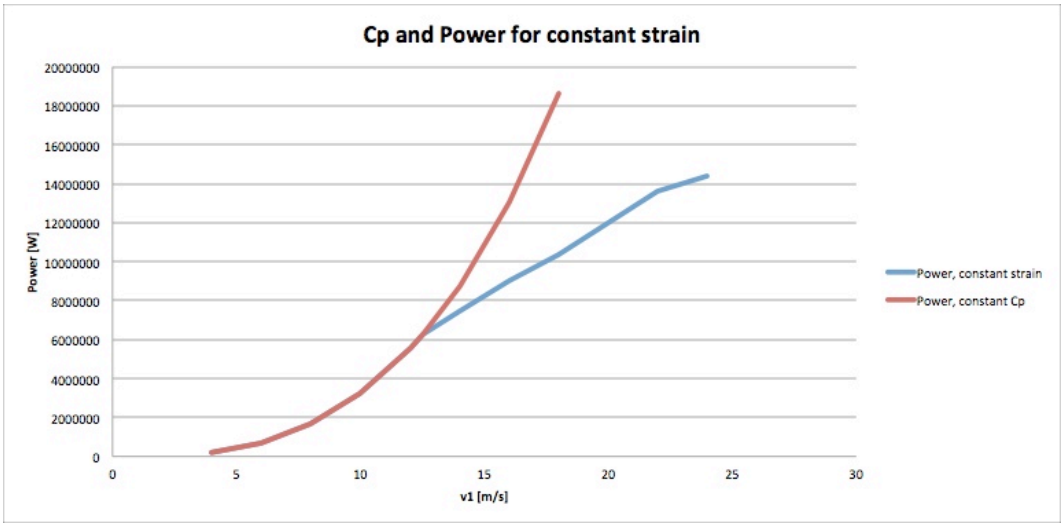

Figure 5.10: Developed power curve, constant strain

6 The developed power curve in context

The fields of engineering that would need attention, in the case that the developed power curve for this rotor actually was to be implemented, will now be discussed. In that connection is it assumed that the political decision has been made to grant floating offshore wind turbines permission to exceed todays' current noise limits, due to their remote locations.

Up until now have only the primarily loads from a steady-state airflow on the wind turbine been considered, and the final results for maximum comparative stresses are only from a static point of view. As this diploma thesis aims to generate results for the preliminary phase, this is sufficient for this scope of work. The results will now, however, be seen in a broader context, and the necessary precautions that would have had to be taken in the case that the developed power curve actually were to be used, highlighted. First, the dynamic stability of the rotor blades will be looked at.

6.1 Secondary loads due to aeroelasticity and wind conditions

Because the rotor blades experience displacement and twisting under the loads in operation, secondary loads due to aeroelasticity occur. Aeroelasticity is an interaction of aerodynamic loads, elasticity and inertia, and the result of which may lead to aerodynamic instability [24]. The two main categories of aerodynamic instability are flutter and divergence, and the most important factors, which determine when and how aerodynamic instability occur on a wind turbine rotor blade are:

Blade structure:

- Material
- Material shaping/arrangement (For composites and hybrid materials)
- Blade shape and dimensions
- Internal structure and rigidity

Loads:

- Wind speed
- Rotational speed
- Degree of turbulence in the air
- Momentarily efficiency of the rotor and AoA

The result of flutter and divergence can be sudden increase in loading and strain on the blades, which are particularly critical if the rotor operate under near maximum strain before the aerodynamic instabilities occur. Flutter is the effect when fluctuations in the aerodynamic loads interact with the elastic deformations, and a resonant condition occurs [24]. Every aerodynamic body has a flutter boundary, and the conditions in which the body is to operate will

therefore have to be checked for a satisfying safety factor with regard to this phenomenon. Divergence is a quasi-static condition where the blade is twisted due to the aerodynamic loads, and the twisting of the blade further increases the load until this load exceeds the blades' ability to resist the load [24]. These two effects are boundaries, which never should be crossed by the rotor blades' operational range. An example of the regions of stability and instability for a wind turbine blade is displayed in Figure 6.1:

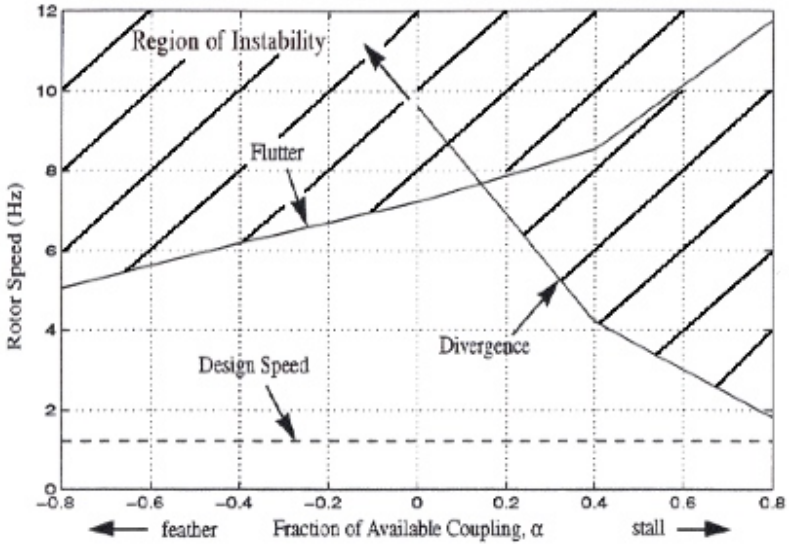

Figure 6.1: Operational region limited by dynamic instability [24]

The x-axis in Figure 6.1 is the range of possible AoA's, normed to a scale from -1< α < 1, with the range [-80%; 80%] is evaluated here. As can be seen in Figure 6.1, is the boundary from flutter almost a horizontal limit, mostly affected by the rotational speed Ω, and this is also the most important factor to monitor with regards to rotor blade flutter. For the divergence, one can observe that this effect is more prone to happen at high AoA's.

The foundation for the calculations of aerodynamic stability/instability, is given by the following matrix [24]:

$$\begin{bmatrix} EI & -g \\ -g & GK \end{bmatrix} \begin{Bmatrix} \varepsilon_b \\ \varepsilon_t \end{Bmatrix} = \begin{Bmatrix} M_b \\ M_t \end{Bmatrix} \tag{6.1}$$

EI Blade bending rigidity [Nmm^2]
g Coupling coefficient, [Nmm^2]
GK Blade torsional rigidity [Nmm^2]
ε_b Bending strain [mm^{-1}]
ε_t Torsion strain [mm^{-1}]
M_b Bending moment [Nmm]
M_t Torsion moment [Nmm]

The coupling coefficient is further calculated as:

$$g = \alpha \cdot \sqrt{EIGK} \qquad \textbf{(6.2)}$$

Without going further into detail about the flutter and divergence calculations, it is obvious that the new results for the bending moments from torque and thrust, as well as the torsion moment would have had to be put to the test in (6.1), and the sizes ε_b and ε_t calculated correspondingly. As mentioned under 5.2.1 sinks the value of the bending moment due to thrust considerably with the new power curve at higher wind speeds, whereas the torque bending moment increases steadily. Summarized sinks the value of the combined bending moment, and the resulting direction of the bending moment turn in the direction of the torque in the rotational plane.

The most critical load in this regard is probably the increased torsional moment. As derived under 5.2.1, increases the torsional moment at 24m/s to almost twice the value at rated wind speed, and this would hence challenge the torsional rigidity of the blade in terms of avoiding aerodynamic instability.

Another significant load factor, which must be accounted for when the dynamic loads are taken into consideration, is that from uneven wind velocities due to turbulence and wind gusts. These are loads that have to be determined particularly for each wind turbine site, and the most important influences are:

- Wind turbine layout (E.g. upwind/downwind rotor, tower dimensions etc.)
- Mean wind velocity
- Site topography and surface roughness

For an offshore wind turbine is normally the turbulence lower than the case is for wind turbines on land, as the surface of the sea disturbs the wind less. Naturally, the turbulence level will increase parallel with increasing wave height. In order to evaluate how these loads will affect the rotor during operation with the newly developed power curve, it must be studied how turbulence and wind gusts are related to the wind speed. In Figure 6.2 can the relationship between the significance of wind gusts and the site mean wind speed, for three cases of occurrence probabilities:

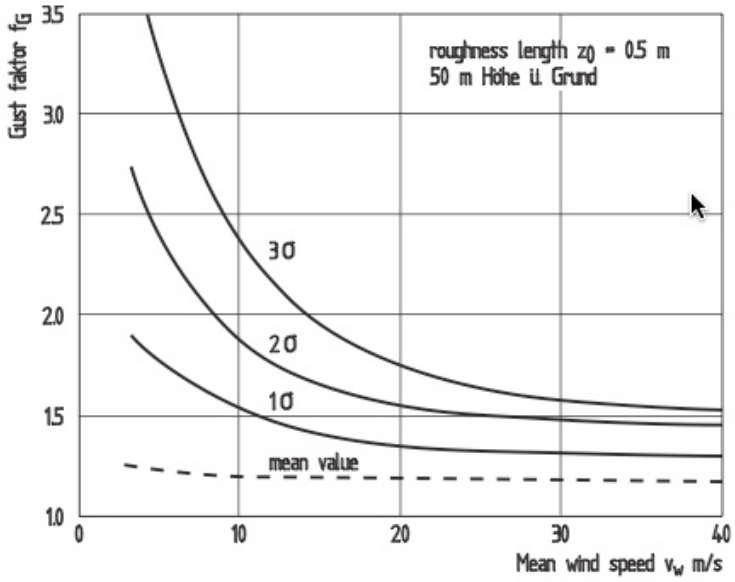

Figure 6.2: Wind gusts and mean wind speed [6]

As can be recognized from Figure 6.2 is actually the factor of wind gusts decreasing with increasing wind, which would indicate that the danger of overloads due to wind gusts are not more likely to occur during the wind speeds above the rated wind speed. Nevertheless is the rotor loaded to a higher degree under these wind speeds than with the flat rated power curve, and the safety factor would therefor have had to be checked. Even though the gust factor decreases at higher wind speeds, the factor coupled with the higher wind speeds could cause the actual dynamic loading from a wind gust to be greater than that of a lower wind speed with higher gust factor.

6.2 Fatigue strength

A very important field of engineering, that would have had to be investigated for the newly developed power curve, is the new load spectrums' influences on the fatigue strength. The fatigue strength is in fact the designing criteria for wind turbine rotor blades [6]. With the assumption that the maximum comparative stress values obtained with the calculation tool are allowable values for the fatigue strength for the rotor when the flat rated power curve is followed, there are two things that will cause the life span for the rotor to drop by use of the new power curve:

1. The rotor will operate with higher rotational speed at higher wind speed, which means a higher number of load cycles from gravity.
2. The stress values are higher at wind speed above the rated wind speed because of the improved C_P value, which leads to far more cycles/time under higher stress than with the flat rated power curve.

Large modern wind turbine rotor blades are almost exclusively made from composites materials like GRP or CRP. These materials have excellent fatigue strength, and can also withstand partly damage, as e.g. cracks, much better than metals [25]. Nevertheless is it necessary also for these materials to calculate the maximum life span, and to make sure that the fatigue strength for the material and the applicable numbers of cycles is not exceeded. The load spectrum for a load on the rotor blade can look like the example in Figure 6.3:

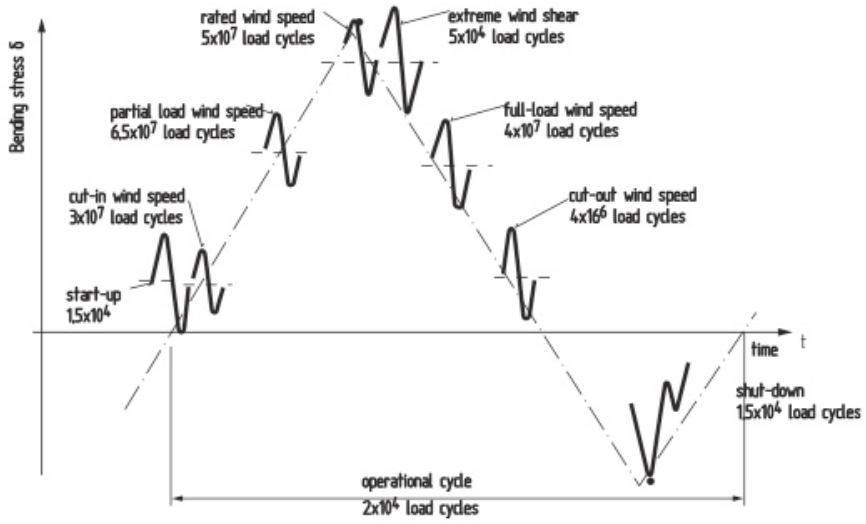

Figure 6.3: Load spectrum for the flap-wise bending moment [6]

For this chart, the number of cycles under full load would be increased. With the new load spectrum identified, the number of allowable cycles, or life span, has to be calculated based on the maximum occurring stress values. The chart in Figure 6.4 visualizes the basis for such a decision:

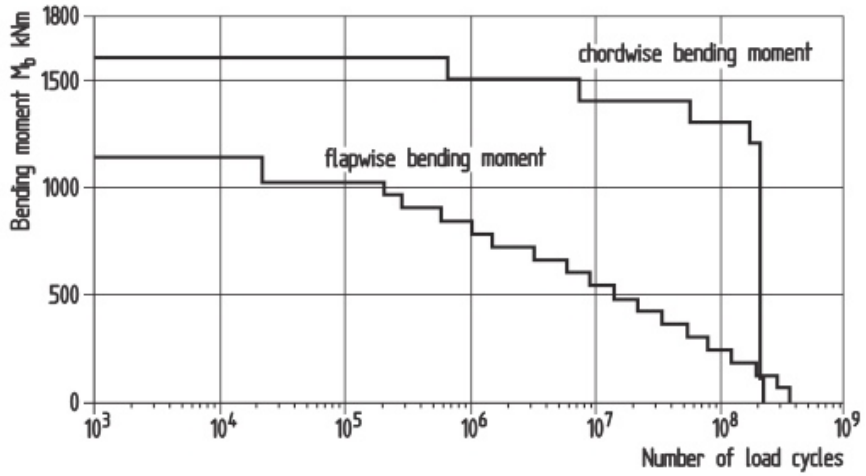

Figure 6.4: Allowable load with respect to number of cycles [6]

Ultimately, the case for an existing rotor to be used with the developed power curve in this work, would be:

- Shorter life span
- Shorter service intervals

Two examples of allowable stress for a limit of 10^7 cycles compared to static strength limit is given here [6]:

- Fibre Glass/epoxy* composite: σ_b = 420MPa, σ_F = 35MPa
- Carbon fibre/epoxy* composite: σ_b = 550MPa, σ_F = 100MPa

*EP-matrix 40-vol.%

The changed fatigue prerequisite would naturally also affect all the other components in the wind turbine, which are designed after this criterion. For example would the *Dynamic Load Rating C* for the roller bearings of the rotor/hub attachment change, and these too would get a shorter life span.

6.3 Matching Gearbox and Generator with the Rotor

Now, the challenges of matching the rotor with a gearbox and generator for the new power curve will be looked at.

First of all, one has to determine the maximum wanted power output, and choose a generator accordingly. In this case, if the full potential of the rotor were to be utilized, a generator with the power capacity of the rotor power at 24m/s multiplied with the gearbox efficiency would be needed. This would be the rated *input* power for the generator, but a certain safety margin has to be guarantied. This power multiplied with the generators' efficiency would be the rated power for the generator. If the rotor power output from let say 16m/s were to be defined as maximum, that power would dictate the rated generator power in the same manner, and the power output would have had to be flat rated at higher wind speeds in the same manner as the original power curve above rated wind speed.

Second, the maximum chosen power output from the rotor, would determine the maximum *input* torque for the gearbox. The now known generator has a rated working rpm, and this would give the constraint for the gearbox transmission ratio. The design and finally determination of the gearbox and generator is an iterative process, by which one optimizes the variable parameters until the end results come as close to the wanted, optimum values as possible. In this process would it also be strived to maintain the constant for the load torque function, c_{gen}, so that the full potential of the rotor efficiency and torque would be utilized.

The whole project would be dictated by the site wind-resources. Based upon the costs for the project would it be determined if the best option would be to uprate an existing wind turbine in the way pursued in this diploma thesis, or to design a new, larger wind turbine with a conventional power curve.

The final, real power curve for an existing wind turbine that was to be uprated as strived for in this work could be similar to the power curve displayed in Figure 6.5. The actual safety margin would be calculated during the detail design phase.

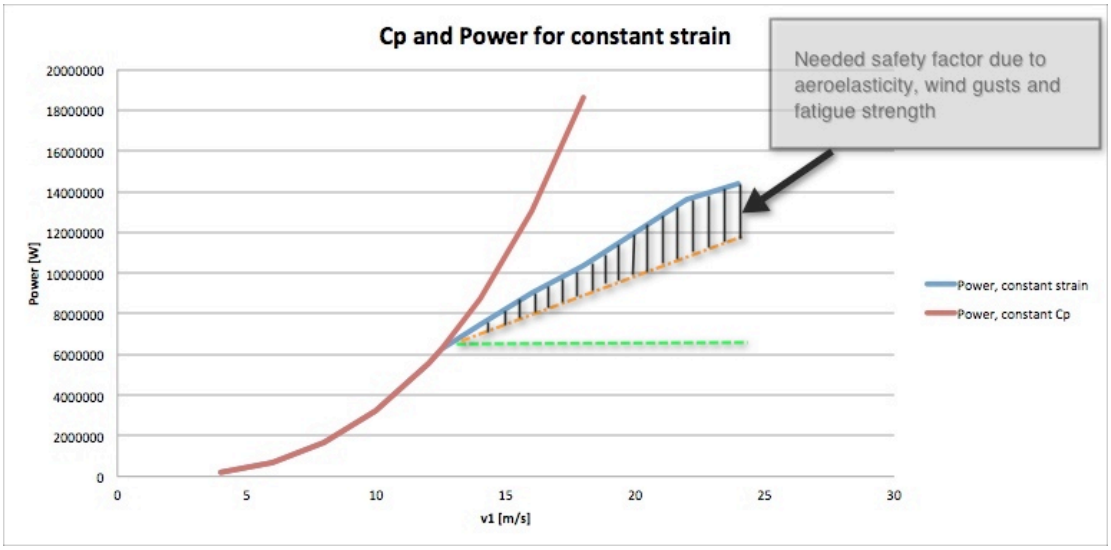

Figure 6.5: Final power curve

7 Summary and Overview

It was in this diploma thesis looked upon the potential to extract more power from existing wind turbine rotors at wind speeds above the reference value, without exceeding their limitation of solidity. This was based upon the scenario that todays' regulatory limitations of noise emissions were revoked for floating offshore wind turbines, once this concept has been realized, as such wind turbines not would come in conflict with the public due to their remote locations. The basis for this study was a HAWT equipped with a blade variable pitch system. The calculations of performance and loads were to be preliminary, and a calculation tool for this task was to be developed.

After elaborating about the theme and bringing it in context of the wind turbine industry, the theory for the energy capture, by which wind turbines work, the BEM theory, and the theory for the structural calculations were shown and derived. The BEM theory provided the foundation for the calculations of both performance and loads, and it was shown how these results, in combination with a subsequent numerical integration, in addition to the whole blade also could provide results for sections of the blade. These methods and equations were to be used in the exact same manner by the calculation tool. Further was the chosen NACA 4410 airfoil together with the calculation method of its coordinates presented. The coordinates were needed to obtain the dimensions of the torque box, upon which the structural calculations applied to. It was then shown how the aerodynamic properties were obtained, by the use of the program XFOIL. The results were further linked to a spreadsheet in Excel where approximate functions for the aerodynamic coefficients dependent on AoA were created.

Next the calculation tool was presented. The input values needed from the user were listed, and how the blade geometry was structured in the program was shown and explained. The structure and philosophy of the program was then explained in detail, and how the scope of the work had to be based on three different main parts in the program: Part 1 was intended for the initialization of the input values, the design of the twist of the blade, the determination of the load function, and the calculations of performance and loads at the rated wind speed. The results of part 1 for the solidity of the rotor would further be used as the reference/maximum allowable values, by which the other values would be evaluated and decided if they were below or above the limit. For further calculations of the same wind turbine at wind speeds lower than the rated wind speed, part 2 of the program was executed. Here, the already known twist of the blade and the load function were utilized, and the peak performance at the submitted wind speed was obtained by imaginary utilizing the variable pitch system, and calculate the applicable pitch. Part 3 of the program was the most important part of the program in terms of reaching the goal of the solidity-optimized power curve. In this part were wind speeds higher than the rated wind speed submitted, along with the wanted power output. The wanted power output must naturally be equal to or less than the maximum possible, and this

was thus the only part of the program where the BEM calculations were executed with the goal of not achieving optimum results. As under part 2 were also here the variable pitch system imaginary utilized, but here in a more sophisticated way. A big part of this solution was to first obtain the correct rotational speed.

At this point was the example wind turbine presented, that would serve as foundation for comparing and validating the results of power output and efficiency from the program. The wind turbine was an Areva Wind M5000, 5MW wind turbine designed especially for offshore use. This is in other words a wind turbine, which would be relevant for the strived power curve of this diploma thesis.

The results of part 1 were presented next, after the information regarding the example wind turbine had been submitted into the program, together with guesses for the unknown parameters. Compared to the example wind turbine, the results for power output and efficiency turned out to be slightly better, but even so, plausible. To produce the rotor-strength optimized power curve, the program was now executed over the whole wind speed range of the wind turbine. For the wind speeds above the rated wind speeds, were values for power output submitted through trial, until the stress values were within the limits set by part 1 of the program.

With all of the results now generated, the results for performance and loads were presented, and discussed. The structural values could not be validated with the example wind turbine, and these results were hence closely studied, and evaluated based on logical assumptions – including in view of the rotor angles and wall positions of occurrence for the maximum stresses over the wind speed range.

Finally, the now produced and discussed preliminary results were seen in context with the case if the developed power curve actually were to be implemented for an existing wind turbine. Thereby were the necessary fields of engineering highlighted, which eventually would turn the produced preliminary results into results for an actual sizing of the wind turbine. These categories included aeroelasticity/dynamic instability, airflow disturbances due to turbulence and wind gusts, fatigue strength and the matching of rotor, gearbox and generator.

Based on the results achieved through this work, it is reason to believe that this subject could be put into practice in the future. When the floating offshore wind turbine concept has completed the testing phase and is available for use, it would be in all parties' interest to exploit it for its full potential – not least because these wind turbines will be expensive to purchase and operate. Based on their remote locations and their total isolation from the public, it would not make any sense to limit the rotational speed based on noise levels any more. After seeing how much reserves of solidity a wind turbine rotor has when the C_P value drops, this is at least something the operating energy companies probably would like to investigate. When initializing a new project consisting of a floating wind-turbine park, the decision of which wind turbine to choose will ultimately be constrained by the existing wind resources on the site, and decided by the costs and the profitability of the energy production. In this connection would it in no

doubt be interesting if a smaller wind turbine rotor could achieve the same power output as a larger one. The blade production costs would be lower, and the onshore and offshore transport would be cheaper. Shorter life span and service intervals for the smaller rotor could however tip the scale in the larger rotors' favor. When it comes to matching the rotor with a new gearbox and generator rated for the new power output, this should not be new to the wind turbine producers. It is not uncommon to offer two or more wind turbine systems consisting of the same rotor, but different gearboxes and generators. The greatest challenge in this matter would maybe be to prove that the variable pitch system in all scenarios would be able to adjust the pitch satisfactory, and thus keep the loading of the blades within limits.

8 Literature

[1]	WORLD WIND ENERGY ASSOCIATION (WWEA): *World Wind Energy Report 2009 [*.pdf]:* Copyright: WWEA: Version: March 2010: Available in internet [13.06.2011] under http://www.wwindea.org/home/images/stories/ worldwindenergyreport2009_s.pdf
[2]	BAUHAUS LUFTFAHRT, DR. ANDREAS KUHLMANN: *Präsentation – Luftfahrt und Klimawandel: Vorlesungsreihe von VDI, DGLR, RAeS 25.06.2009, Hamburg, HAW:* Copyright: Bauhaus Luftfahrt
[3]	GLOBAL WIND ENERGY COUNCIL (GWEC): *Global Wind Report – Annual Market Update 2010 [*.pdf]:* Copyright: GWEC: Version: March 2011: Available in internet [13.06.2011] under http://www.gwec.net/fileadmin/documents/Publications/ Global_Wind_2007_report/GWEC%20Global %20Wind%20Report%202010%20low%20res.pdf
[4]	ENVIRONMENTAL AND ENERGY INSTITUTE (EESI): *Fact sheet Offshore Wind Energy [*.pdf]*: Copyright: EESI: Version: October 2010: Available in internet [13.06.2011] under http://www.eesi.org/files/offshore_wind_101310.pdf
[5]	SWAY AS, AREVA WIND GMBH: Press release - *Areva and Sway announce partnership on deep water floating wind turbine solutions* [*.pdf]: Copyright: Sway AS, Areva Wind GmbH: August 5. 2009: Available in internet [30.05.2011] under http://sway.no/publish_files/Press_release_09.pdf
[6]	HAU ERIC: *Wind Turbines – Fundamentals, Technologies, Application, Economics:* 2nd edition, ISBN 3-540-24240-6: Springer Verlag Berlin, Heidelberg 2006
[7]	INGRAM GRANT: *Wind Turbine Blade Analysis using the Blade Element Momentum Method [*.pdf]*: Copyright: Ingram Grant: Version 1.0: December 13th 2005: Available in internet [13.06.2011] under http://www.dur.ac.uk/g.l.ingram/download/wind_turbine_design.pdf
[8]	SWITZER ERIC R.: *Energy devices – the wind (Lecture 4) [*.pdf]*: Copyright: Switzer Eric R.: Version: 24.10.2009: Available in internet [13.06.2011] under http://kicp.uchicago.edu/~switzer/compton/lecture4_notes.pdf
[9]	MORIARTY PATRICK J., HANSEN CRAIG A.: *Aerodyn Theory Manual [*.pdf]*: Copyright: National Renewable Energy Laboratory, Golden Colorado / Windward Engineering, Salt Lake City Utah: Version: December 2005: Available in internet [13.06.2011] under: http://wind.nrel.gov/designcodes/simulators/aerodyn/AD_Theory.pdf

[10]	PAPULA, LOTHAR: *Mathematische Formelsammlung für Ingenieure und Wissenschaftler*: 8. Auflage, ISBN 3-528-74442-1: Verlag: Vieweg, Wiesbaden Juni 2003
[11]	GHOSE, J. P., GOKARN, R. P.: *Basic Ship Propulsion*: ISBN 81-7764-606-0, Publisher: Allied Publishers Pvt. Limited, New Dehli 2004
[12]	SCHULZE D.: *Vorlesungsskript – Strömungslehre*: Hochschule für Angewandte Wissenschaften Hamburg, Studiendepartment Fahrzeugtechnik und Flugzeugbau, Auflage Sommersemester 2006
[13]	LAGING G.: *Vorlesungsskript - Festigkeit im Leichtbau I*: Hochschule für Angewandte Wissenschaften Hamburg, Studiendepartment Fahrzeugtechnik und Flugzeugbau, Auflage Sommersemester 2007
[14]	FLÜH HANS J.: *Vorlesungsskript – Festigkeit im Leichtbau II*: Hochschule für Angewandte Wissenschaften Hamburg, Studiendepartment Fahrzeugbau und Flugzeugbau, Auflage Sommersemester 2007
[15]	SEIBEL M.: *Strukturkonstruktion – Eine Vorlesung zur Gestaltung und Auslegung von Flugzeugzellen*: Hochschule für Angewandte Wissenschaften Hamburg, Studiendepartment Fahrzeugtechnik und Flugzeugbau, Auflage Januar 2005
[16]	LÄPPLE VOLKER: *Einführung in die Festigkeitslehre: Lehr- und Übungsbuch*: 2. Auflage, ISBN 978-3-8348-0426-6: Verlag: Vieweg + Teubner Verlag I GWV Fachverlag, Wiesbaden, 2008
[17]	NATIONAL AERONAUTICS AND SPACE ADMINISTRATION (NASA): *Computer Program To Obtain Ordinates for NACA Airfoils [*.pdf]*: Copyright: NASA: Version: NASA technical Memorandum 4741, December 1996: Available in internet [13.06.2011] under: http://www.unibw.de/lrt13_1/lehre/xtras/profildaten/nasa-tm-4741.pdf
[18]	DRELA MARK, YOUNGREN HAROLD: *XFOIL*: *Interactive program for the design and analysis of subsonic airfoils [*.tar.gz]*: Copyright: Drela Mark and Youngren Harold, under the GNU General Public Licence: Version 6.9: 30.11.2001: Available in internet [02.06.2011] under *http://web.mit.edu/drela/Public/web/xfoil/*
[19]	DRELA MARK, YOUNGREN HAROLD: *Excerpts from information regarding XFOIL: User Guide in plain text [*.txt]:* Copyright: Drela Mark and Youngren Harold, under GNU General Public Licence. Available in internet [02.06.2011] under *http://web.mit.edu/drela/Public/web/xfoil/*
[20]	REH STEPHAN: *Informatik 1 Programmieren mit C*: Hochschule für Angewandte Wissenschaften Hamburg, Studiendepartment Fahrzeugbau und Flugzeugbau, Auflage 1. Märtz 2007
[21]	ZINGEL HARTMUT: *Vorlesungsskript – Flugmechanik 1*: Hochschule für Angewandte Wissenschaften Hamburg, Studiendepartment Fahrzeugtechnik und Flugzeugbau: Auflage Märtz 2006

[22]	JOHNSON GARY L.: *Wind Energy Systems [*.pdf]*: Copyright: Johnson Gary L.: Electronic Edition, Manhattan, KS, 19.05.2005: Available in internet [13.06.2011] under http://www.eece.ksu.edu/~gjohnson/Windbook.pdf
[23]	AREWA WIND GMBH: *Photos and technical information regarding the Areva Wind M5000 wind turbine [online]*: Copyright: Areva Wind GmbH: Available in internet [15.06.2011] under http://www.areva-wind.com/1/m5000/technical-data/
[24]	VEERS PAUL, BIR GUNJIT, LOBITZT DONALD: *Aeroelastic Tailoring In Wind-Turbine Blade Applications [*.pdf]*: Presented at *Windpower ’98*, American Wind Energy Association Meeting and Exhibition, Bakersfield, California, April 28 – May 1, 1998: Available online [20.06.2011] under: http://windpower.sandia.gov/other/AWEA4-98.pdf
[25]	WAGNER M.: *Vorlesungsskript – Betriebsfestigkeit*: Hochschule für Angewandte Wissenschaften Hamburg, Studiendepartment Fahrzeugtechnik und Flugzeugbau, Auflage Wintersemester ´07/´08

Appendix A

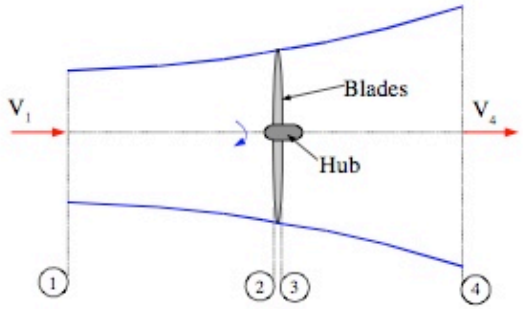

Figure 1: Axial Stream tube around a Wind Turbine

1 Introduction

This short document describes a calculation method for wind turbine blades, this method can be used for either analysis of existing machines or the design of new ones. More sophisticated treatments are available but this method has the advantage of being simple and easy to understand.

This design method uses blade element momentum (or BEM) theory to complete the design and can be carried out using a spreadsheet and lift and drag curves for the chosen aerofoil.

The latest version of this document should be available from the author's website[1] Any comments on the document would be gratefully received. Further details on Wind Turbine Design can be found in Manwell et al. (2002) which provides compreshensive coverage of all aspects of wind energy. Walker and Jenkins (1997) also provide a comprehensive but much briefer overview of Wind Energy.

2 Blade Element Momentum Theory

Blade Element Momentum Theory equates two methods of examining how a wind turbine operates. The first method is to use a momentum balance on a rotating annular stream tube passing through a turbine. The second is to examine the forces generated by the aerofoil lift and drag coefficients at various sections along the blade. These two methods then give a series of equations that can be solved iteratively.

3 Momentum Theory

3.1 Axial Force

Consider the stream tube around a wind turbine shown in Figure 1. Four stations are shown in the diagram 1, some way upstream of the turbine, 2 just before the

[1] http://www.dur.ac.uk/g.l.ingram

blades, 3 just after the blades and 4 some way downstream of the blades. Between 2 and 3 energy is extracted from the wind and there is a change in pressure as a result.

Assume $p_1 = p_4$ and that $V_2 = V_3$. We can also assume that between 1 and 2 and between 3 and 4 the flow is frictionless so we can apply Bernoulli's equation. After some algebra:

$$p_2 - p_3 = \frac{1}{2}\rho(V_1^2 - V_4^2) \tag{1}$$

Noting that force is pressure times area we find that:

$$dF_x = (p_2 - p_3)dA \tag{2}$$

$$\Rightarrow dF_x = \frac{1}{2}\rho(V_1^2 - V_4^2)dA \tag{3}$$

Define a the axial induction factor as:

$$a = \frac{V_1 - V_2}{V_1} \tag{4}$$

It can also be shown that:

$$V_2 = V_1(1-a) \tag{5}$$

$$V_4 = V_1(1-2a) \tag{6}$$

Substituting yields:

$$dF_x = \frac{1}{2}\rho V_1^2[4a(1-a)]2\pi r dr \tag{7}$$

3.2 Rotating Annular Stream tube

Consider the rotating annular stream tube shown in Figure 2. Four stations are shown in the diagram 1, some way upstream of the turbine, 2 just before the blades, 3 just after the blades and 4 some way downstream of the blades. Between 2 and 3 the rotation of the turbine imparts a rotation onto the blade wake.

Consider the conservation of angular momentum in this annular stream tube. An "end-on" view is shown in Figure 3. The blade wake rotates with an angular velocity ω and the blades rotate with an angular velocity of Ω. Recall from basic physics that:

$$\text{Moment of Inertia of an annulus}, I = mr^2 \tag{8}$$

$$\text{Angular Moment}, L = I\omega \tag{9}$$

$$\text{Torque}, T = \frac{dL}{dt} \tag{10}$$

$$\Rightarrow T = \frac{dI\omega}{dt} = \frac{d(mr^2\omega)}{dt} = \frac{dm}{dt}r^2\omega \tag{11}$$

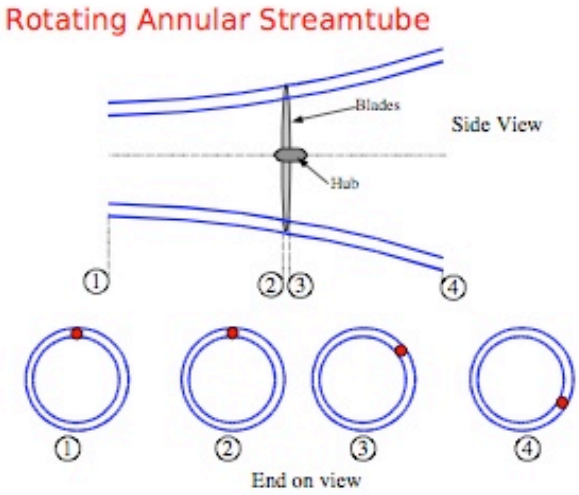

Figure 2: Rotating Annular Stream tube

So for a small element the corresponding torque will be:

$$dT = d\dot{m}\omega r^2 \tag{12}$$

For the rotating annular element

$$d\dot{m} = \rho A V_2 \tag{13}$$

$$d\dot{m} = \rho 2\pi r dr V_2 \tag{14}$$

$$\Rightarrow dT = \rho 2\pi r dr V_2 \omega r^2 = \rho V_2 \omega r^2 2\pi r dr \tag{15}$$

Define angular induction factor a':

$$a' = \frac{\omega}{2\Omega} \tag{16}$$

Recall that $V_2 = V(1-a)$ so:

$$dT = 4a'(1-a)\rho V \Omega r^3 \pi dr \tag{17}$$

Momentum theory has therefore yielded equations for the axial (Equation 7) and tangential force (Equation 17) on an annular element of fluid.

4 Blade Element Theory

Blade element theory relies on two key assumptions:

- There are no aerodynamic interactions between different blade elements
- The forces on the blade elements are solely determined by the lift and drag coefficients

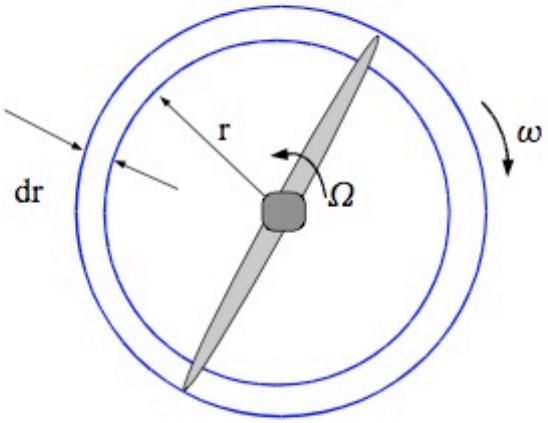

Figure 3: Rotating Annular Stream tube: notation.

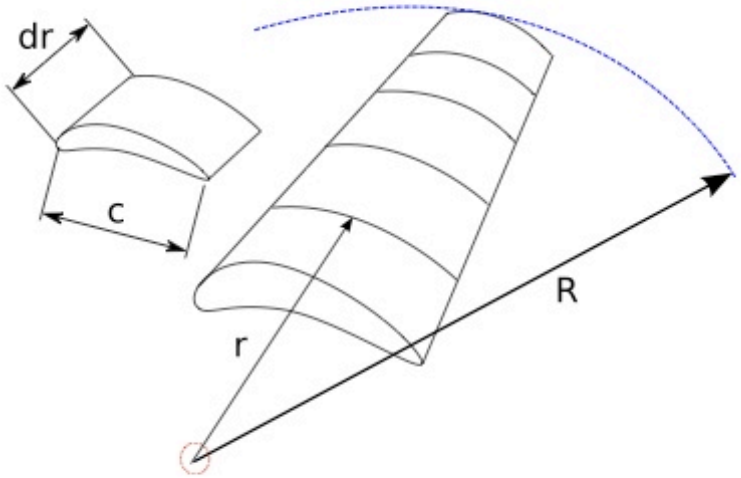

Figure 4: The Blade Element Model

Consider a blade divided up into N elements as shown in Figure 4. Each of the blade elements will experience a slightly different flow as they have a different rotational speed (Ωr), a different chord length (c) and a different twist angle (γ). Blade element theory involves dividing up the blade into a sufficient number (usually between ten and twenty) of elements and calculating the flow at each one. Overall performance characteristics are determined by numerical integration along the blade span.

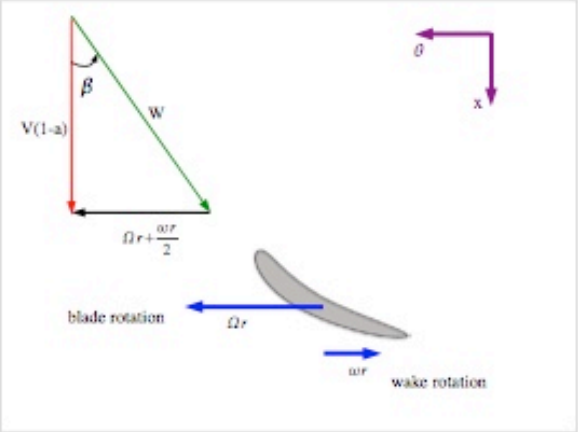

Figure 5: Flow onto the turbine blade

4.1 Relative Flow

Lift and drag coefficient data area available for a variety of aerofoils from wind tunnel data. Since most wind tunnel testing is done with the aerofoil stationary we need to relate the flow over the moving aerofoil to that of the stationary test. To do this we use the relative velocity over the aerofoil. More details on the aerodynamics of wind turbines and aerofoil selection can be found in Hansen and Butterfield (1993).

In practice the flow is turned slightly as it passes over the aerofoil so in order to obtain a more accurate estimate of aerofoil performance an average of inlet and exit flow conditions is used to estimate performance.

The flow around the blades starts at station 2 in Figures 2 and 1 and ends at station 3. At inlet to the blade the flow is not rotating, at exit from the blade row the flow rotates at rotational speed ω. That is over the blade row wake rotation has been introduced. The average rotational flow over the blade due to wake rotation is therefore $\omega/2$. The blade is rotating with speed Ω. The average tangential velocity that the blade experiences is therefore $\Omega r + \frac{1}{2}\omega r$. This is shown in Figure 5.

Examining Figure 5 we can immediately note that:

$$\Omega r + \frac{\omega r}{2} = \Omega r(1+a') \tag{18}$$

Recall that (Equation 5): $V_2 = V_1(1-a)$ and so:

$$\tan\beta = \frac{\Omega r(1+a')}{V(1-a)} \tag{19}$$

Where V is used to represent the incoming flow velocity V_1. The value of β will vary from blade element to blade element. The local tip speed ratio λ_r is defined as:

$$\lambda_r = \frac{\Omega r}{V} \tag{20}$$

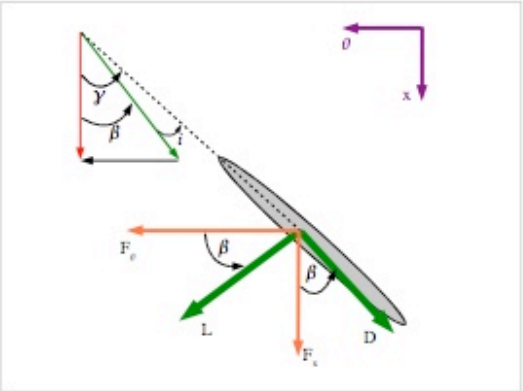

Figure 6: Forces on the turbine blade.

So the expression for $\tan\beta$ can be further simplified:

$$\tan\beta = \frac{\lambda_r(1+a')}{(1-a)} \tag{21}$$

From Figure 5 the following relation is apparent:

$$W = \frac{V(1-a)}{\cos\beta} \tag{22}$$

4.2 Blade Elements

The forces on the blade element are shown in Figure 6, note that by definition the lift and drag forces are perpendicular and parallel to the incoming flow. For each blade element one can see:

$$dF_\theta = dL\cos\beta - dD\sin\beta \tag{23}$$

$$dF_x = dL\sin\beta + dD\cos\beta \tag{24}$$

where dL and dD are the lift and drag forces on the blade element respectively. dL and dD can be found from the definition of the lift and drag coefficients as follows:

$$dL = C_L\frac{1}{2}\rho W^2 c dr \tag{25}$$

$$dD = C_D\frac{1}{2}\rho W^2 c dr \tag{26}$$

Lift and Drag coefficients for a NACA 0012 aerofoil are shown in Figure 7, this graph shows that for low values of incidence the aerofoil successfully produces a

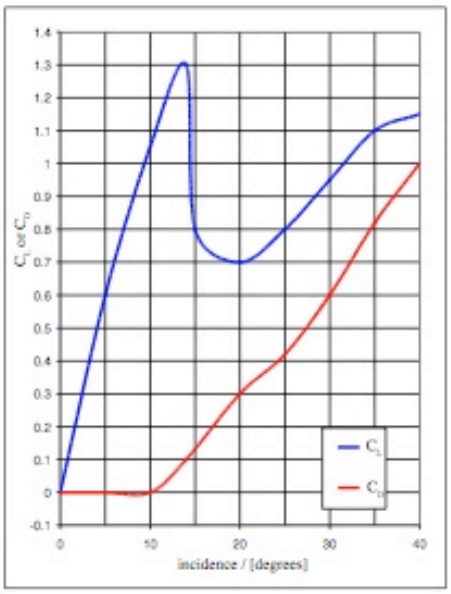

Figure 7: Lift and Drag Coefficients for a NACA 0012 Aerofoil

large amount of lift with little drag. At around $i = 14^\circ$ a phenomenon known as stall occurs where there is a massive increase in drag and a sharp reduction in lift.

If there are B blades, combining Equation 23 and equation 25 it can be shown that:

$$dF_x = B\frac{1}{2}\rho W^2(C_L\sin\beta + C_D\cos\beta)cdr \tag{27}$$

$$dF_\theta = B\frac{1}{2}\rho W^2(C_L\cos\beta - C_D\sin\beta)cdr \tag{28}$$

The Torque on an element, dT is simply the tangential force multiplied by the radius.

$$dT = B\frac{1}{2}\rho W^2(C_L\cos\beta - C_D\sin\beta)crdr \tag{29}$$

The effect of the drag force is clearly seen in the equations, an increase in thrust force on the machine and a decrease in torque (and power output).

These equations can be made more useful by noting that β and W can be expressed in terms of induction factors etc. (Equations 21 and 22). Substituting and carrying out some algebra yields:

$$dF_x = \sigma'\pi\rho\frac{V^2(1-a)^2}{\cos^2\beta}(C_L\sin\beta + C_D\cos\beta)rdr \tag{30}$$

$$dT = \sigma'\pi\rho\frac{V^2(1-a)^2}{\cos^2\beta}(C_L\cos\beta - C_D\sin\beta)r^2dr \tag{31}$$

To calculate rotor performance Equations 35 and 34 from a momentum balance are equated with Equations 30 and 31. Once this is done the following useful relationships arise:

$$\frac{a}{1-a} = \frac{\sigma'[C_L \sin\beta + C_D \cos\beta]}{4Q\cos^2\beta} \tag{40}$$

$$\frac{a'}{1-a} = \frac{\sigma'[C_L \cos\beta - C_D \sin\beta]}{4Q\lambda_r cos^2\beta} \tag{41}$$

Equation 40 and 41 are used in the blade design procedure.

Appendix B

Abstract

Computer programs to produce the ordinates for airfoils of any thickness, thickness distribution, or camber in the NACA airfoil series were developed in the early 1970's and are published as NASA TM X-3069 and TM X-3284. For analytic airfoils, the ordinates are exact. For the 6-series and all but the leading edge of the 6A-series airfoils, agreement between the ordinates obtained from the program and previously published ordinates is generally within 5×10^{-5} chord. Since the publication of these programs, the use of personal computers and individual workstations has proliferated. This report describes a computer program that combines the capabilities of the previously published versions. This program is written in ANSI FORTRAN 77 and can be compiled to run on DOS, UNIX, and VMS based personal computers and workstations as well as mainframes. An effort was made to make all inputs to the program as simple as possible to use and to lead the user through the process by means of a menu.

Introduction

Although modern high-speed aircraft generally make use of advanced NASA supercritical airfoil sections, there is still a demand for information on the NACA series of airfoil sections, which were developed over 50 years ago. Computer programs were developed in the early 1970's to produce the ordinates for airfoils of any thickness, thickness distribution, or camber in the NACA airfoil series. These programs are published in references 1 and 2. These programs, however, were written in the Langley Research Center version of FORTRAN IV and are not easily portable to other computers. The purpose of this paper is to describe an updated version of these programs. The goal was to combine both programs into a single program that could be executed on a wide variety of personal computers and workstations as well as mainframes. The analytical design equations for both symmetrical and cambered airfoils in the NACA 4-digit-series, 4-digit-modified-series, 5-digit-series, 5-digit-modified-series, 16-series, 6-series, and 6A-series airfoil families have been implemented. The camber-line designations available are the 2-digit, 3-digit, 3-digit-reflex, 6-series, and 6A-series. The program achieves portability by limiting machine-specific code. An effort was made to make all inputs to the program as simple as possible to use and to lead the user through the process by means of a menu.

Symbols

The symbols in parentheses are the ones used in the computer program and in the computer-generated listings (.rpt file).

A	camber-line designation, fraction of chord from leading edge over which design load is uniform
a_i	constants in airfoil equation, $i = 0, 1, ..., 4$
b_i	constants in camber-line equation, $i = 0, 1, 2$
c (C, CHD)	airfoil chord
$c_{l,i}$ (CLI)	design section lift coefficient
d_i	constants in airfoil equation, $i = 0, 1, 2, 3$
dx	derivative of x; also basic selectable interval in profile generation
$d(x/c)$, dy, $d\delta$	derivatives of x/c, y, and δ
I	leading-edge radius index number
k_1, k_2	constants
m	chordwise location for maximum ordinate of airfoil or camber line
p	maximum ordinate of 2-digit camber line
R	radius of curvature
R_{le} (RLE)	leading-edge radius
r	chordwise location for zero value of second derivative of 3-digit or 3-digit-reflex camber-line equation
t	thickness
x (X)	distance along chord
y (Y)	airfoil ordinate normal to chord, positive above chord
z	complex variable in circle plane
z'	complex variable in near-circle plane
δ	local inclination of camber line
ϵ	airfoil parameter, $\phi - \theta$
ζ	complex variable in airfoil plane
θ	angular coordinate of z'
ϕ	angular coordinate of z
ψ	airfoil parameter determining radial coordinate of z'

ψ_0	average value of ψ, $\frac{1}{2\pi}\int_0^{2\pi} \psi \, d\phi$

Subscripts:

cam	cambered
l (L)	lower surface
N	forward portion of camber line
T	aft portion of camber line
t	thickness
u (U)	upper surface
x	derivative with respect to *x*

Computer Listing Symbols

For reasons having to do with code portability, the computer-generated listing (.rpt file) will always have the alphabetic characters in upper case. The following list is intended to eliminate any confusion.

A	camber-line designation, fraction of chord from leading edge over which design load is uniform
A0,...,A4	constants in airfoil equation
CHD, C	airfoil chord
CLI	design section lift coefficient
CMB	maximum camber in chord length, $p = \frac{y(m)}{c}$
CMBNMR	number of camber lines to be combined in 6- and 6A-series multiple camber-line option
CMY	*m*, location of maximum camber
CRAT	cumulative scaling of EPS, PSI, Π RAT(I), I = 1 → IT
D0,...,D3	constants in airfoil equation
DX	basic selectable interval in profile generation
DY/DX	first derivative of *y* with respect to *x*, $\frac{dy}{dx}$
D2Y/DX2	second derivative of *y* with respect to *x*, $\frac{d^2y}{dx^2}$
EPS	airfoil parameter, $\varepsilon = \phi - \theta$
IT	number of iterations to converge 6-series profile
K1, K2	3-digit-reflex camber parameters, k_1 and k_2
PHI	ϕ, angular coordinate of *z*
PSI	ψ, airfoil parameter determining radial coordinate of z'
RAT(I)	*i*th iterative scaling of ε, ψ
RC	radius of curvature at maximum thickness for 4-digit modified profile
RK2OK1	3-digit reflex camber parameter ratio, $\frac{k_2}{k_1}$
RLE	leading-edge radius
RNP	radius of curvature at origin
SF	ratio of input *t/c* to converged *t/c* after scaling
TOC	thickness-chord ratio
X	distance along chord
XMT	*m*, location of maximum thickness for 4-digit modified profile
XT(12), YT(12), YTP(12)	location and slope of ellipse nose fairing for 6- and 6A-series thickness profiles
XU, XL	upper and lower surface locations of *x*
XTP	*x/c* location of slope sign change for 6- and 6A-series thickness profile
XYM	*m*, location of maximum thickness for 6- and 6A-series profiles or chordwise location for maximum ordinate of airfoil or camber line
Y	airfoil ordinate normal to chord, positive above chord
YM	*y/c* location of slope sign change for 6- and 6A-series thickness profile
YMAX	*y*(*m*), maximum ordinate of thickness distribution
YU, YL	upper and lower surface *y* ordinate

Analysis

Thickness Distribution Equations for Analytic Airfoils

The design equations for the analytic NACA airfoils and camber lines have been presented in references 3 to 7. They are repeated herein to provide a better understanding of the computer program and indicate the use of different design variables. A summary of some of the design equations and ordinates for many airfoils from these families is also presented in references 8 to 10.

The traditional NACA airfoil designations are shorthand codes representing the essential elements (such as thickness-chord ratio, camber, design lift coefficient) controlling the shape of a profile generated within a given airfoil type. Thus, for example the NACA 4-digit-series airfoil is specified by a 4-digit code of the form *pm*xx, where *p* and *m* represent positions reserved for

specification of the camber and xx allows for specification of the thickness-chord ratio as a percentage, that is, "*pm*12" designates a 12-percent-thick ($t/c = 0.12$) 4-digit airfoil.

NACA 4-digit-series airfoils. Symmetric airfoils in the 4-digit-series family are designated by a 4-digit number of the form NACA 00xx. The first two digits indicate a symmetric airfoil; the second two, the thickness-chord ratio. Ordinates for the NACA 4-digit airfoil family (ref. 2) are described by an equation of the form:

$$\frac{y}{c} = a_0\left(\frac{x}{c}\right)^{1/2} + a_1\left(\frac{x}{c}\right) + a_2\left(\frac{x}{c}\right)^2 + a_3\left(\frac{x}{c}\right)^3 + a_4\left(\frac{x}{c}\right)^4$$

The constants in the equation (for $t/c = 0.20$) were determined from the following boundary conditions:

Maximum ordinate:

$$\frac{x}{c} = 0.30 \qquad \frac{y}{c} = 0.10 \qquad \frac{dy}{dx} = 0$$

Ordinate at trailing edge:

$$\frac{x}{c} = 1.0 \qquad \frac{y}{c} = 0.002$$

Magnitude of trailing-edge angle:

$$\frac{x}{c} = 1.0 \qquad \left|\frac{dy}{dx}\right| = 0.234$$

Nose shape:

$$\frac{x}{c} = 0.10 \qquad \frac{y}{c} = 0.078$$

The following coefficients were determined to meet these constraints very closely:

$$a_0 = 0.2969 \qquad a_1 = -0.1260$$

$$a_2 = -0.3516 \qquad a_3 = 0.2843$$

$$a_4 = -0.1015$$

To obtain ordinates for airfoils in the family with a thickness other than 20 percent, the ordinates for the model with a thickness-chord ratio of 0.20 are multiplied by the ratio $(t/c)/0.20$. The leading-edge radius of this family is defined as the radius of curvature of the basic equation evaluated at $x/c = 0$. Because of the term $a_0(x/c)^{1/2}$ in the equation, the radius of curvature is finite at $x/c = 0$ and can be shown to be (see appendix)

$$R_{le} = \frac{a_0^2}{2}\left(\frac{t/c}{0.20}\right)^2$$

by taking the limit as x approaches zero of the standard expression for radius of curvature:

$$R = \frac{\left[1 + (dy/dx)^2\right]^{3/2}}{d^2y/dx^2}$$

To define an airfoil in this family, the only input necessary to the computer program is the desired thickness-chord ratio.

One might expect that this leading-edge radius $R(0)$, found in the limit as $x \to 0$ to depend only on the a_0 term of the defining equation, would also be the minimum radius on the profile curve. This is not true in general; for the NACA 0020 airfoil, for example, a slightly smaller radius ($R = 0.0435$ as compared to $R(0) = 0.044075$) is found in the vicinity of $x = 0.00025$.

NACA 4-digit-modified-series airfoils. The 4-digit-modified-series airfoils are designated by a 4-digit number followed by a dash and a 2-digit number (such as NACA 0012-63). The first two digits are zero for a symmetrical airfoil and the second two digits indicate the thickness-chord ratio. The first digit after the dash is a leading-edge-radius index number, and the second is the location of maximum thickness in tenths of chord aft of the leading edge.

The design equation for the 4-digit-series airfoil family was modified (ref. 4) so that the same basic shape was retained but variations in leading-edge radius and chordwise location of maximum thickness could be made. Ordinates for these airfoils are determined from the following equations:

$$\frac{y}{c} = a_0\left(\frac{x}{c}\right)^{1/2} + a_1\left(\frac{x}{c}\right) + a_2\left(\frac{x}{c}\right)^2 + a_3\left(\frac{x}{c}\right)^3$$

from leading edge to maximum thickness, and

$$\frac{y}{c} = d_0 + d_1\left(1 - \frac{x}{c}\right) + d_2\left(1 - \frac{x}{c}\right)^2 + d_3\left(1 - \frac{x}{c}\right)^3$$

from maximum thickness to trailing edge.

The constants in these equations (for $t/c = 0.20$) can be determined from the following boundary conditions:

Maximum ordinate:

$$\frac{x}{c} = m \qquad \frac{y}{c} = 0.10 \qquad \frac{dy}{dx} = 0$$

Leading-edge radius:

$$\frac{x}{c} = 0 \qquad R = \frac{a_0^2}{2}$$

Appendix C

```
#include <math.h>
#include <stdio.h>
#define Arrowlength 65 /* Number of blade elements */

void main(void)
{
    /* PART 1 */
    for(iNumber_of_Elements == 0 ; iNumber_of_Elements < Arrowlength ; iNumber_of_Elements ++)
    {
        /*Here are the initial geometric values for the blades determined.*/
        iOuterCouter = 0;
        iTest = 1;
        do
        {
            dTorque_aerodynamic[iNumber_of_Elements] = dTorque_old;
            /*In this loop is the optimum pitch found, and thereby also defining the twist of the blades.
            The pitch alterations are here executed based on the results from the evaluation
            from the last run, and the variables "iOuterCounter, "iFortegn" and "iTest".

            Before entering the inner do-while loop are the initial aerodynamic parameters calculated.*/
            iCounter = 0;
            do
            {
                dAxial_Induced[iNumber_of_Elements] = dAxial_Induced_old;
                dTangential_Induced[iNumber_of_Elements] = dTangential_Induced_old;

                /* In this loop is the pitch angle considered fixed, and the flow parameters
                accrordingly iterativ calculated, based on the BEM Tehory.*/

                ddiff1 = dAxial_Induced[iNumber_of_Elements] - dAxial_Induced_old;
                ddiff2 = dTangential_Induced[iNumber_of_Elements] - dTangential_Induced_old;
                iCounter =+ 1;
            }while(ddiff1 > dAccuracy || ddiff2 > dAccuracy);
            /*Following the BEM calculations are the torque for this pitch angle evaluated.*/

            ddiff = dTorque_aerodynamic[iNumber_of_Elements] - dTorque_old;

            /*Based on the result from "ddiff", number of iOuterCounter, and value of
            "iFortegn" are the correct pitch command assigned*/

            if(iTest != 0)
            {
                /*Pitch mode 1, 2, 3 or 4 is chosen*/
            }
            iOuterCounter =+ 1;
        }while(iTest != 0);
    }

    for(iNumber_of_Elements == 0 ; iNumber_of_Elements < Arrowlength ; iNumber_of_Elements ++)
    {

        iVariable2 = iNumber_of_Elements;

        for(iVariable2 == iNumber_of_Elements; iVariable2 < Arrowlength ; iVariable2)
        {
            /* Here are the numeric integration that are the foundation for the load calculations
               executed, for the current blade element.
               Also the CoG for each blade segment is determined here through numeric integration.

               The calculations are carried out as described under 2.5.2, for the applicable

            blade segment*/
    }

    /*Here are the completed numeric integrations utilized, and the load cases that are independent
      from rotor angle carried out. These include torque, torque force, thrust, thrust moment,
      inertia, and torsion.The results are thereafter printed to the file "Loads_and_Zentroids1.txt"*/

    for(iRotor_Angle_Position == 0; iRotor_Angle_Position < Arrowlength2; iRotor_Angle_Position++)
    {
        /* In this loop are the loads generated by gravity included, dependent on the current
        rotor angle. These loads are shear force from gravity, normal force from gravity, and
        the bending moment generated by the shear force and the current blade segments' CoG.

        The normal force from gravity is therafter added to the inertia, to describe the total
        normal force. The shear force from gravity is added to that of the torque force, to
        describe the total shear force in the rotor plane. Finally are the bending moments from
        gravity and torque added, to identify the total bending moment in the rotor plane.

        These results are now added to "Loads_and_Zentroids1.txt"*/
    }
}

for(iNumber_of_Elements == 0 ; iNumber_of_Elements < Arrowlength ; iNumber_of_Elements ++)
{
    /*Here are the geometric dimensions and properties for the torque box calculated for the
    current blade element, ref. 2.5.3, equations (2.59) - (2.86)*/

    for(iRotor_Angle_Position == 0; iRotor_Angle_Position < Arrowlength2; iRotor_Angle_Position++)
    {

        for(iTorsionBox_Var == 0; iTorsionBox_Var < Arrowlength3 ; iTorsionBox_Var ++)
        {

            /*In this loop is the shear flow "q1" calculated for each side in the torque box.
            Ref. 2.5.3, equations (2.88) - (2.92).
            They are not connected to each other at this point, and start on zero at the
            beginning of each side.

            Following the calculations for q1, are the complete normal flows determined next,
            and these are hence completed at this point. Ref. 2.5.3, equations (2.100) - (2.105)*/

            /*The results for the normal flow are here printed to the file "ny_1.txt"*/

            if(iTorsionBox_Var == Arrowlength -1)
            {

                for(iTorsionBox_Var == 0; iTorsionBox_Var < Arrowlength3 ; iTorsionBox_Var ++)
                {
                    /*At this point are the results from "q1" for each side added to each
                    other, to deliver a continuous "q1" counter clockwise, starting at
                    the upper flange, on top of the rear spar. This means that the starting
                    value for the rear spar is added to the end value for the upper flange, and
                    so forth.*/

                    /*The now completed values for "q1" are now being stored in the file "q1_1.txt"*/
                }
            }
        }
    }
}
```

```
    /*In this sequence are the SC for each blade element, and q0 for each rotor angle
    calculated*/

for(iNumber_of_Elements == 0 ; iNumber_of_Elements < Arrowlength ; iNumber_of_Elements ++)
{
    for(iRotor_Angle_Position == 0; iRotor_Angle_Position < Arrowlength2; iRotor_Angle_Position++)
    {
        for(iTorsionBox_Var == 0; iTorsionBox_Var < Arrowlength3 ; iTorsionBox_Var ++)
        {
            /*In this loop are the calculation of q0 prepared, through numeric integration
            of q1, ref. 2.5.3, equation (2.93)*/
        }

        /* At this point is the completed numeric integration utilized, and equation (2.93)
        executed. q0 for the current rotor angle has now been determined.*/

        if(iRotor_Angle_Position == 0)
        {
            /* For the first rotor angle of each blade element are the distance in x direction
            between the torque box CoG and the SC calculated, ref. 2.5.3, equation (2.97)*/
        }

        /*Here are the value for the current q0 printed to the file "q0_1.txt"*/

    }
}

/* Now are the final, complete shear flows calculated. This sequence is repeated for
   each of the sides of the torque box*/

for(iNumber_of_Elements == 0 ; iNumber_of_Elements < Arrowlength ; iNumber_of_Elements ++)
{
    /* Here are the deviations between the 0.5c point of the current blade element to the
    0.5c point of the effective arms for the bending moments from gravity and thrust calculated.
    Ref 2.5.3, equation (2.95) and Figures 2.14 and 2.15.*/

    for(iRotor_Angle_Position == 0; iRotor_Angle_Position < Arrowlength2; iRotor_Angle_Position++)
    {
        for(iTorsionBox_Var == 0; iTorsionBox_Var < Arrowlength3 ; iTorsionBox_Var ++)
        {
            /* At this point are the complete shear flows for the given positions in the
            torque box determined. Ref, 2.5.3, equation (2.98).
            These include the allready calculated q1 and q0, and are now being added with
            the shear flow from torsion caused by the aerodynamic torsion of "cm", and the
            resulting torsion from the shear forces.

            For the shear flow from torsion, ref. 2.5.3, equations (2.94)-(2.97)*/

            /* Now, both the complete normal-, and shear flow are known, and out of this are
            the resulting normal, shear and overall stresses calculated.
            The comparative stresses are executed according to 2.5.3.4, equations (2.107)-(2.109)*/

            /*The last part in this sequence is a screening of the resulting normal, shear and
            three types of comparative stresses. Here are the largest contributions from shear
            stress, tensional and compressive normal stress, and the three types of comparative
            stresses screened for each of the walls. The results include in addition to the stress
            value, also wich blade element, at which rotor angle, and at which position of the wall
            they occur.*/


        }
    }
}

/* Here are the results from the screening of the stresses printed to "Stress_analysis1.txt"*/


/* PART 2*/
do
{
    /*Here is the rotational speed adjusted, based on the evaluation of the total torque from
    the rotor, and the values of "iTest_Energy" and "iFortegn_Energy".*/
    do
    {
        /*At this point is the rotational speed from the outer do-while loop assigned to the blade element
        with the largest torque contribution from program part 1 (ref.4.3.3 and equation (4.40) ). The pitch
        alteration follows the same pattern as under Part 1, and screens the values of "iTest" and "iFortegn"
        Further are  preparations made for the BEM calculations.
        In this do-while loop is the pitch angle iterativ improved, based on the pitch command given at the bottom
        of the loop. For the first run is an initial value for the pitch angle given, and the alteration section bypassed.*/
        iCounter = 0;
        do
        {
        /*In this loop are the BEM calculations for the blade element with the highest torque contribution iterativ calculated.*/
        iCounter += 1;
        }
        while(dDiff > dAccuracy || dDiff2 > dAccuracy);
        /*Here are the results for the torque from the blade element with the highest torque
        contribution evaluated, and assigned eiter pitch command 1, 2, 3 or 4*/
        iOuterCounter += 1;
    }
    while(iTest != 0);
    /*When the program has reached this point, does that mean that the optimum pitch has been found
    for the blade element with the highest torque contribution, and the BEM calculations can be executed
    for the whole rotor. The calculated twist is now used to determine the pitch for the other bøade elements.*/
    for(iNumber_of_Elements == 0 ; iNumber_of_Elements < Arrowlength ; iNumber_of_Elements ++)
    {
        /*Here are both the rotational speed and the pitch of the blade known values, and the
        BEM calculations are now carried out for all the blade elements.*/
        iCounter = 0;
        do
        {
            /*In this loop are the BEM calculations for all the blade elements iterativ calculated.*/
            iCounter += 1;
        }
        while(dDiff > dAccuracy || dDiff2 > dAccuracy);
    }
    /*At this point is the total torque from the rotor evaluated agianst the load torque from the
    gear and generator. The decision if the rotational speed has to be altered, is made upon the
    equation of the current rotor torque and the magnitude of the load torque. If these have the
    same value, the correct rotor speed has been found. Also here are either alteration command 1, 2, 3 or 4 made.*/
    iEnergyCounter += 1;
}
while(iTestEnergy != 0);


/* PART 3 */
do
{
```

```
        /*In this loop is it pursued to find the equivalent full-rate wind speed. In that connection
        is the energy output from the rotor monitored, and the wind speed altered accordingly. The
        control variables are iWindCounter, iFortegnEnergy_2 and iTestEnergy2.*/
        do
        {   /*Here is the rotational speed adjusted, based on the evaluation of the total torque from
            the rotor, and the values of "iEnergyCounter" "iTorque_control" and "iFortegn_Energy".*/
            do
            {
                /*Here is the torque of the blade element with the highest torque contribution from part 1
                screened, and the pitch angle altered accordingly, to find the optimium pitch angle at
                the current wind speed and rotational speed. The control variables are "iOuterCounter",
                "iFortegn" and "test"*/
                do
                {
                    /*BEM calculations for the blade element with the highest torque contribution*/
                }
                while(dDiff > dAccuracy || dDiff2 > dAccuracy);
                /*Here is the torque under the current conditions monitored for the blade element with
                the highest torque contribution, and the appropriate command of alteration given,
                until a peak has been found*/
                }
            }
            while(itest != 0);
            /*At this point are the wind speed, rotational speed and pitch constraints, and the
            calculations can be carried out for the whole rotor.*/
            for(iNumber_of_Elements = 0; iNumber_of_Elements < Arrowlength; iNumber_of_Elements++)
            {
                do
                {
                    /*In this loop are the BEM calculations for all the blade elements iterativ calculated.*/
                }
                while(dDiff > dAccuracy || dDiff2 > dAccuracy);
                /*Now is the total torque from the rotor evaluated agianst the load torque from the gear and
                generator. The decision if the rotational speed has to be altered, is made upon the equation
                of the current rotor torque and the magnitude of the load torque. If these have the same value,
                the correct rotor speed has been found. Also here are either alteration command 1, 2, 3 or 4 made.*/
        }
        while(iTorque_control !=0);
        /*Here is the total power output from the rotor evaluated, and compared to the submittet power output from the
        user. Based on this comparison is the appropriate command given to alter the wind speed, and thus iterativ
        close in on the equivalent full-rate wind speed.*/
    }
    while(iTestEnergy2 !=0);



    /*Now has the equivalent full-rate wind speed and the corresponding rotational speed been found, and the only
    variable left to calculate is the blade pitch*/

    do
    {
        /*Here is the pitch of the rotor continous altered to lower the efficiency of the rotor. The submitted
        wind speed is used, and the obtained rotational speed from the previous sequence. The control variables
        are: "iOuterCounter", "iFortegn" and "itest"*/

        for(iNumber_of_Elements = 0; iNumber_of_Elements < Arrowlength; iNumber_of_Elements++)
        {
            do
            {

            {
                /*BEM iteration for all the blade elements*/
            }
            while(dDiff > dAccuracy || dDiff2 > dAccuracy);
      }

      /*Now is the total torque from the rotor evaluated agianst the load torque from the gear and
      generator. The decision if the rotational speed has to be altered, is made upon the equation
      of the current rotor torque and the magnitude of the load torque. If these have the same value,
      the correct rotor speed has been found. Also here are either alteration command 1, 2, 3 or 4 made.*/

    }
    while(itest != 0);
}
```